Tesis Doctoral

Molecular determinants of K_v7.2 surface expression

Unidad de Biofísica (CSIC-UPV/EHU)

Departamento de Bioquímica y Biología Molecular

Facultad de Ciencia y Tecnología

Universidad del País Vasco

Memoria presentada por **Dña. Juncal Fernández Orth**
para optar al grado de Doctora en Ciencias por la
Universidad del País Vasco (UPV/EHU)

Director: Dr. Alvaro Villarroel Muñoz

Este trabajo se ha desarrollado en la Unidad de Biofísica UPV-EHU/CSIC, con el apoyo de una beca de Formación de Personal Investigador (FPI) asociada al proyecto de investigación SAF2006-13450 y contratos de investigación de la Fundación Biofísica Bizkaia.

Por fin llega el momento de escribir esto… y es que cuando empiezas a escribir la tesis no ves el momento de llegar al final y escribir los agradecimientos, y cuando la acabas… ya no sabes por donde empezar a agradecer…

En primer lugar quería dedicar esta tesis a mis padres, sin duda soy lo que soy gracias a ellos, por el cariño y el apoyo incondicional que me han dado a lo largo de toda mi vida, y también a Dietmar, por ser ese hermano con el que puedes contar cuando lo necesitas, muchas gracias.

Parte de esta tesis es de toda la gente de Biofísica, amigos y compañeros con los que he compartido todo este tiempo, tanto de los que se han ido como de los que quedan. Quisiera dar un agradecimiento especial a Paloma. Qué puedo decir de la mejor persona que he conocido nunca! Gracias por enseñarme todo lo que sé hoy, nunca cambies! A Teresa, por tu amistad y por saber, que aún en la distancia, tengo una hermana mayor muy lista con la que puedo contar cuando lo necesito. Y por supuesto… como olvidarme de las risas que nos hemos echado con Txellita, qué buenos momentos pasamos! Muchas gracias, nunca lo olvidaré. A Rosa, que aunque no fue muy largo el camino juntas me inyectaste la esencia del labo Villarroeliano, y a Patri, por tus consejos telefónicos tan importantes. A Aless, por enseñarme esas cosillas de última hora sobre fluorescencia y proteínas y hacerme reír y como no, adentrarme en el mundo numismático…jeje. A Carol, quién nos iba a decir en Soria que un día trabajaríamos juntas y que congeniaríamos tan bien! A Camilo por tus batallitas, porque nunca nos aburríamos en la poyata. A Araitz por tu incondicional ayuda en momentos de crisis y tu permanente sonrisa en los labios. A Ganeko, Natalia y Cova… GRACIAS a TOD@S.

Al resto de la familia Biofísica, a los que ya no están y se fueron: Urko, Igor, Benoit, Sergi, Paloma, Bego, Ariel… ojalá un día coincidamos de nuevo. Y a los que aún andan por aquí, en concreto a toda la gente de becarios, escribir la tesis se hubiera hecho más cuesta arriba sin vuestra compañía diaria. Gracias. Por supuesto a los compañeros de café, batallitas y salidas nocturnas: Marián, Bea, Pitzi, Ane, Fernan,

Jorge, Ruth, Txus… A Artur por su ayuda técnica y a todos aquellos que de alguna manera han hecho que estos años en la Unidad hayan sido muy especiales. No me olvido de Marije, Ana y Agur, mis otras tres madres que tantas veces me han sacado de marrones... MUCHISIMAS GRACIAS A TOD@S de corazón.

A Alvaro, por confiar en mi para trabajar en su laboratorio durante estos años e iniciarme en este gran mundo de la ciencia. Se que a veces no ha sido fácil, mi carácter y el tuyo de vez en cuando han sido un poco difíciles, pero al final siempre nos hemos arreglado, gracias.

A la kuadri, tengo que deciros por una vez y dejarlo por escrito, que os quiero un montón y agradeceros haber estado ahí SIEMPRE que lo he necesitado, sobre todo en esta última época txunga de mi vida (y en alguna otra). ESKERRIK ASKO NESKAS. [Pa´que luego digáis que soy una "rusa sosa" ;-)]

Y sobre todo a Jon, por ser como eres y tu paciencia todo este tiempo, aún nos queda un largo camino por recorrer juntos, GRACIAS.

A mis padres

CSIC

eman ta zabal zazu
Universidad del Pais Vasco
Euskal Herriko Unibertsitatea

CSIC-UPV/EHU

Doctoral Thesis

Molecular determinants of $K_v7.2$ surface expression

Candidate:

Juncal Fernández Orth

Supervisor: **Dr. Alvaro Villarroel Muñoz**

INDEX

ABBREVIATIONS

CHAPTER 1. GENERAL INTRODUCTION

1.1 Ion channels as functional units 4

1.2 Cell signaling is based on changes on the membrane potential mediated by ion channels 4

1.3 Nowadays, around 200 genes have been found to codify for ion channels 8

1.3.1 Ligand-gated ion channels

1.3.1.1 Cys-loop receptors

1.3.1.2 Ionotropic glutamate receptors

1.3.1.3 ATP-sensitive potassium channels (P2X receptors)

1.3.2 Voltage-dependent ion channels

1.3.2.1 Voltage-dependent calcium channels (Ca_v)

1.3.2.2 Voltage-gated sodium channels (Na_v)

1.3.2.3 Transient Receptor Potential ion channel (TRP channels)

1.3.2.4 Cyclic Nucleotide-Gated ion channels (CNG)

1.4 Potassium channel genes are known to be mutated in human diseases, four of them being encoded by the KCNQ gene family 11

1.5 Potassium channel related diseases 13

1.6 K_v7 channels and the M-current 14

1.7 Neuronal K_v7 channels 16

1.7.1 Structural characteristics of K_v7 channels

1.7.2 Helices A and B: Calmodulin binding module and PIP_2 interaction

1.7.3 Calmodulin and its role in channel trafficking

1.7.4 Helices C and D: tetramerization and trafficking domain

1.7.5 The end of the channel

1.8 $K_v7.1$ is part of the cardiac K_v current **24**

1.9 Mutations on $K_v7.2$ and $K_v7.3$ channels lead to a rare neonatal epilepsy **25**

1.10 Mutations on $K_v7.4$ lead to an accumulation of potassium in the inner ear producing deafness **28**

1.11 The role of $K_v7.5$ is still uncertain **29**

1.12 Drugs related to K_v7 channels **29**

1.13 BFNC-linked mutations **30**

1.14 M-channel regulation **32**

1.14.1 M-current inhibition

1.14.1.1 Inhibition by PIP_2 hydrolysis

1.14.1.2 Inhibition by Ca^{2+}/CaM

1.14.1.3 Inhibition by phosphorylation

1.14.2 M-current activation

1.15 The birth of a channel: from the nascent protein to its place at the plasma membrane **36**

1.15.1 The beginning

1.15.2 Folding and trafficking in a correct way

1.15.3 ER machinery to ensure proper protein folding

1.15.4 ER retention/retrieval motifs

1.15.4.1 Arg-based ER-localization signals

1.15.4.2 Di-lysine motifs/KKXX

1.15.4.3 ER export signals

1.15.5 Do you want to coassemble with me?

1.16 Human disorders caused by defects in protein folding, oligomerization and targeting to the cell surface **45**

OBJECTIVES **47**

CHAPTER 2. EXPERIMENTAL PROCEDURES

2.1 Molecular biology **51**

2.1.1 Mutations and deletions of K_v7.2 channels

2.1.1.1 DNA constructs

2.1.1.2 PCR technique

2.1.1.3 Fragment digestion, purification and ligation

2.1.1.4 Bacterial transformation

2.1.1.5 DNA extraction and quantification

2.1.2 Tags and fluorophores

2.1.3 Vector expression

2.1.4 Chimeras

2.1.4.1 CD25/Tac-K_v7.2

2.1.4.2 K_v7.5/K_v7.2

2.1.4.3 CD4/K_v7.2

2.2 Mammal cell experimentation techniques **60**

2.2.1 HEK293T cell maintenance

2.2.2 Cell counting

2.2.3 Cell preservation

2.2.4 Cell transfection

2.2.4.1 Calcium phosphate transfection method

2.2.4.2. Lipofectamine transfection method

2.2.5 Protein extraction

2.2.6 Western blot

2.2.7 Flow citometry

2.2.8 Immunoprecipitation (IP)

2.2.9 Immunofluorescence

2.2.10 Electrophysiological recordings

2.2.11 Xenopus oocyte experimentation techniques

2.2.11.1 cRNA synthesis

2.2.11.2 Oocyte preparation and RNA injection

2.2.11.3 Two-electrode voltage clamp recordings

2.2.11.4 Luminescence assay

2.2.12 Drug treatments for degradation assays

2.3 Protein purification and fluorescence assays **81**

2.3.1 GST fusion protein purification

2.3.2 Calmodulin purification

2.3.3 Calmodulin dansylation

2.3.4 Fluorescence spectroscopy assays

2.4 Antibodies **87**

2.5 Solutions and reactives **88**

RESULTS

CHAPTER 3. SURFACE EXPRESSION AND SUBUNIT SPECIFIC CONTROL OF STEADY-STATE PROTEIN LEVELS BY THE K_V7.2 HELIX A-B LINKER

3.1 Introduction **93**

3.2 Results **95**

3.2.1 The linker between helices A and B increases protein yield

3.2.2 There is a correlation between CaM binding and channel function

3.2.3 Removal of the A-B linker increases protein yield in mammalian cells

3.2.4 The presence of the A-B loop does not augment the rate of protein degradation

3.2.5 Removing the linker between helices A-B is compatible with channel function in HEK293T

3.2.6 PIP_2 sensitivity is not reduced after A-B loop removal

3.2.7 There is a significant increase in the number of cells displaying surface staining when transfected with Del6

3.2.8 The K_v7.2 A-B linker does not have a major impact on the steady-state protein levels of K_v7.3 subunits

CHAPTER 4. EFFECT OF TETRAMERIZATION IN CALMODULIN BINDING AND SURFACE EXPRESSION

4.1 Introduction **119**

4.2 Results **120**

4.2.1 Del2 mutant does not prevent channel function

4.2.2 Del2 mutant retains the ability of binding calmodulin

4.2.3 K_v7.2 helices A-B Del2 fused to Tac do not bind CaM and present reduced glycosylation levels

4.2.4 Trafficking and CaM binding

4.2.5 Tetramerization and trafficking

4.2.6 Is tetramerization playing a role in CaM binding?

4.2.7 Identification of relevant residues in the Del2 construct

4.2.8 CD4 and its artificial tetramerization domain as a new tool

CHAPTER 5: DISCUSSION **141**

5.3.1 Tetramerization and trafficking are connected

5.3.2 BFNC-linked mutations

CONCLUSIONS **151**

BIBLIOGRAPHY **155**

PUBLICATIONS **181**

APPENDIX **185**

Abbreviations

aa	Aminoacid
Ab	Antibody
AKAP	A-kinase anchor proteins
ATP	Adenosine 5'-triphosphate
BFNC	Benign familial neonatal convulsions
BN-PAGE	Blue native page
BSA	Bovine serum albumin
BR	Breakage buffer
CaM	Calmodulin
Ca_v	Voltage dependent calcium channels
cDNA	Complementary DNA
CFP	Cyan fluorescent protein
CHX	Cycloheximide
CNG	Cyclic nucleotide-gated channels
COP	Coat protein complex
CQ	Chloroquine
DAG	Diacylglycerol
DNA	Deoxyribonucleic acid
DMSO	Dimethyl sulfoxide

DTT	Dithiothreitol
EDTA	Ethylenediaminetetraacetic acid
EGTA	Ethylene glycol tetraacetic acid
ER	Endoplasmic reticulum
ERAD	ER associated degradation
FBS	Fetal bovine serum
FSC	Forward scatter
GHK	Goldman-Hodgkin-Katz equation
GST	Glutathione S-transferase
H	Hour
HEK293T	Human embryonic kidney
IQ	Calmodulin binding domain
IP	Immunoprecipitation
IP_3	Inositol tri-phosphate
IPTG	Isopropyl-beta-thio galactopyranoside
JNLS	Jervell and Lange-Nielsen syndrome
kDa	Kilodaltons
K_v	Voltage-dependent potassium channel
Kir	Potassium inward rectifier channel
LB	Luria Bertani Broth
LGIC	Ligand-gated ion channels
LQT	Long QT-syndrome
M1	Muscarinic receptor

MHC	Major histocompatibility complex
Min	Minutes
mRNA	Messenger RNA
ms	Milliseconds
Na_v	Voltage-gated sodium channel
PBS	Phosphate buffer saline
PCR	Polymerase chain reaction
PIP_2	Phosphatidylinositol 4,5-bisphosphate
PKC	Protein kinase C
PLC	Phospholipase C
PFA	Paraformaldehyde
PTC	Peptidil transferase centre
RNA	Ribonucleic acid
RPM	Revolutions per minute
RT	Room temperature
RTG	Retigabine
SEC	Seconds
SDS	Sodium dodecyl sulphate
SDS-PAGE	Sodium dodecyl sulphate polyacrylamide gel electrophoresis
SRP	Signal recognition particle
SSC	Side scatter

SUR	Sulfonylurea receptor
TEA	Tetraethylammonium
TM	Transmembrane domain
Tris	Hydroxymethylaminomethane
TRP	Transient receptor potential ion channel
UPR	Unfolded protein response
WB	Western blot
YFP	Yellow fluorescent protein

INDEX OF EXPERIMENTAL PROTOCOLS

Mutations and deletions

- P1. PCR protocol

- P2. Fragment digest protocol

- P3. Purification protocol

- P4. Ligation protocol

- P5. Transformation protocol

- P6. DNA extraction protocol

Mammal cell experimentation techniques

- P7. Cell passage protocol

- P8. Cell preservation: freezing

- P9. Cell preservation: thawing

-P10. Calcium phosphate transfection protocol (T25 flask)

-P11. Lipofectamine transfection protocol

-P12. Protein extraction protocol

-P13. Western blot protocol

-P14. Flow cytometry protocol

-P15. Immunoprecipitation protocol

-P16. Immunofluorescence protocol

-P17. cRNA synthesis protocol

-P18. Oocyte preparation protocol

* Times exposed in the protocols are estimated.

CHAPTER 1

GENERAL INTRODUCTION

General Introduction

How can a scientific area give so many Nobel Prizes?

In 1963 John C. Eccles, Alan L. Hodgkin and Andrew F. Huxley obtained the Nobel Prize in Physiology and Medicine "for their discoveries concerning the ionic mechanisms involved in excitation and inhibition in the peripheral and central portions of the nerve cell membrane". In 1991, the Nobel Prize in Physiology and Medicine was awarded jointly to Erwin Neher and Bert Sakmann "for their discoveries concerning the function of single ion channels in cells" and in 2003 the Nobel Prize in Chemistry was awarded "for discoveries concerning channels in cell membranes" jointly between Peter Agre "for the discovery of water channels" and Roderick MacKinnon "for structural and mechanistic studies of ion channels".

Given that ion channels developed early in evolution and are involved in every thought, perception and heartbeat, it is easy to understand why is so important to know how do they work (Hille *et al.*, 1999). There are many diseases where ion channels are implicated, most of them arise from mutations in genes encoding channel proteins. In 1989, cystic fibrosis, the first myasthenia gravis related to ion channels was identified (Tsui, 1992). Since then, the list of diseases related to ion channels keeps growing, including epilepsy, episodic ataxia, Alzheimer's disease, schizophrenia, etc.

1.1 Ion channels as functional units

Ion channels form the basic electric units at the membrane of excitable cells as well as in intracellular organelles, such as nucleus, mitochondria, endoplasmic reticulum, Golgi apparatus and so on. They form pores across the membrane that allow the passive diffusion of different ions down their electrochemical gradient, leading to changes in the membrane potential. All ion channels undergo conformational changes from closed to open states, and once open, channels allow the passage of thousand of ions. That distinguishes ion channels from transporters and pumps, which can also transport ions but only one or as much few at the same time (Jentsch *et al.*, 2004).

The rapid propagation of these voltage changes is the basis for the electrical signaling in brain and other tissues. The main types of perturbations that are known to cause ion channels to open are a change in the voltage across the membrane (**voltage-gated channels**), mechanical stimulation (**mechanically-gated channels**), or the binding of a signaling molecule (**ligand-gated channels**). The signal ligand can be either an extracellular mediator, called neurotransmitter (**transmitter-gated channels**), or an intracellular mediator, such as an ion (**ion-gated channels**), a nucleotide (**nucleotide-gated channels**) or a GTP-binding regulatory protein (**G-protein-gated channels**).

1.2 Cell signaling is based on changes on the membrane potential mediated by ion channels

The plasma membrane is composed by a lipid bilayer, which is formed by glicerophospholipids, sphingolipids, sterols, and many proteins embedded in it.

This plasma membrane confers the isolation and the impermeable conditions necessary to maintain the homeostasis of the cell. The fluid surrounding both sides of the membrane is rich on mobile ions, being sodium (Na^+), potassium (K^+), chloride (Cl^-) and calcium (Ca^{2+}) the most important. The ion channels and ion pumps embedded in the membrane maintain different ion concentrations on the intracellular and extracellular sides of the membrane. This creates a voltage difference between the inner and the outer cellular spaces, which is called **membrane potential**. In neurons and in many other cell types, the membrane potential is important because it transmits signals between different parts of the cell and also could play a role in signal transduction. The equilibrium condition is reached when no net flow of electric current across the membrane is occurring, defined as the **resting membrane potential,** being the inner cell negative with respect to the exterior, which depends on different variables such as the ion concentration, the type of cells, etc.

Therefore, ions flow across the membrane thanks to their electrochemical gradient. This gradient is composed by two factors: the voltage gradient and the concentration gradient for this ion across the membrane. When these two factors balanced each other, the electrochemical gradient for the ion is zero and there is no net ion flow through the channel. The membrane potential at which this equilibrium is reached is called the **equilibrium potential**. The **Goldman-Hodgkin-Katz equation** (GHK equation) expresses the equilibrium potential across the cell membrane, taking into account all the ions that are permeant through that membrane. The GHK equation is defined as follows:

$$V_m = \frac{RT}{V} \ln \frac{P_K [K^+]_o + P_{Na} [Na^+]_o + P_{Cl} [Cl^-]_i}{P_K [K^+]_i + P_{Na} [Na^+]_i + P_{Cl} [Cl^-]_o}$$

where,

V = equilibrium potential in volts

P_0 / P_1 = outside/inside ion concentration

R = gas constant (1,9872 cal. mol^{-1}. K^{-1})

T = absolute temperature (K)

When ion channels become open, they allow passing passively thousands of ions through them, being the membrane potential modulate. The **reversal potential** (also known as Nernst potential, E_n) of an ion, is the membrane potential at which there is no net (overall) ion flow from one side of the membrane to the other. When a potassium channel is opened, the membrane potential reaches the K^+ reversal potential (for a typical cell is about -88 mV) what means that K^+ is hyperpolarizing the cell, making the cell more negative. In the same way, the increase of Na^+ conductance depolarizes the cell carrying the potential to +69 mV.

For neurons, typical values of resting potential range from -70 to -80 mV. In excitable cells, a sufficiently large depolarization can evoke a short-lasting all-or-nothing event called an **action potential,** where the membrane potential very rapidly undergoes a large change, often briefly reversing its sign (Fig. 1.1).

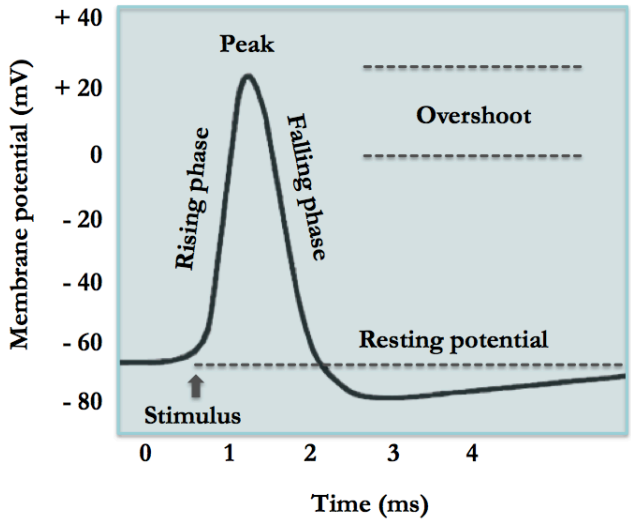

Figure 1.1. Action potential steps.
1.- Voltage sensing Na_v channels become open and an inward flow of Na^+ ions come in to the cell (depolarization step). **2.-** The rapid influx of Na^+ ions causes the polarity of the plasma membrane to reverse, and the ion channels then rapidly inactivate. **3.-** As the Na^+ channels close, Na^+ ions can no longer enter the neuron, and they are actively transported out of the plasma membrane. **4.-** K^+ channels are then activated, and there is an outward current of K^+ ions, returning the electrochemical gradient to the resting state.

The rapid propagation of these voltage changes is the basis for the electrical signaling in the brain and other tissues. Ion channels regulate also the concentration of second messengers such as calcium, and the ionic homeostasis of the cytoplasm, intracellular organelles and extracellular compartments.

1.3 Nowadays, around 200 genes have been found to codify for ion channels

Ion channels are pore-forming proteins composed by transmembrane segments and extra membrane loops/domains. They are ion selective, which means that they can discriminate between size and charge of the permeant ion leading to changes in the membrane voltage.

Ion channels can be classified according to which chemical or physical modulator controls their gating activity:

- Ligand-gated channels (neurotransmitters)
- Voltage-gated channels (transmembrane potential, electric field)
- Second-messenger-gated channels nucleotides, G-proteins
- Mechanosensitivity-channels (osmotic pressure, membrane curvature)
- Gap junctions, non gated porins

1.3.1 Ligand-gated ion channels

Ligand-gated ion channels (LGICs) are a group of transmembrane ion channels that are opened or closed in response to the binding of a chemical messenger, i.e., ligand, in the extracellular domain of the channel. The ligand could be an ion, an organic molecule or a peptide. In general, they are less selective than voltage-gated channels and are able to transport two or more types of ions, playing an important role in the central nervous system, where they form important neurotransmitters receptors for the synaptic transmission and cellular signaling.

LGICs can be divided into three families:

1.3.1.1 Cys-loop receptors: generally pentamerics (composed of five protein subunits that form a pentameric arrangement around a central pore), they contain a loop formed by a disulfide bond between two cysteine residues. Cys-loop receptors are subdivided into the type of ion that the corresponding channel conducts (anionic or cationic) and further into families defined by the endogenous ligand. This family is composed by nicotinic acetylcholine, GABAA, GABAA-ρ, glycine and 5-HT3 receptors.

1.3.1.2 Ionotropic glutamate receptors: composed by four homologous subunits, each subunit contains an extra-cellular amino-terminal domain, two transmembrane segments separated by a "P-loop" that takes part in the formation of the pore and a third transmembrane domain. The ionotropic glutamate receptors bind the neurotransmitter glutamate. All known glutamate receptor subunits include the AMPA, kainate and NMDA receptors, which differ in the glutamate analogue that activates the channel.

1.3.1.3 ATP-sensitive potassium channels (P2X receptors): forming trimers, these channels are gated in response to the binding of extracellular adenosine 5'-triphosphate (ATP). All subunits share a common topology of two plasma membrane domains, a large extracellular loop and an intracellular carboxyl and amino termini. These channels are composed by $K_{ir}6.x$-type subunits and sulfonylurea receptor (SUR) subunits with additional components.

1.3.2 Voltage-dependent ion channels

More than 140 ion channels are activated or inactivated by voltage. The name given to the channels makes reference to the ion that is permeated (K^+, Na^+, Ca^{2+}, Cl^-), followed by a "v" which means voltage. In general, the main subunit that

forms the pore of the voltage dependent channels, the alpha (α) subunit, is composed by six transmembrane domains (6TM, S1-S6) that are assemble to form tetramers (Doyle *et al.*, 1998; Li *et al.*, 1992). The S1-S4 segments confer the voltage-dependence, and its characteristic is the presence of positively charged aminoacids. The filter region forms the extracellular end of the pore (S5 and S6 segments), an important structure that decides which ion will pass or will not. The intracellular N- and C- terminals are structural domains that could generally interact with ligands and also take part in processes like inactivation.

Apart from voltage-gated potassium channels (K_v channels), the main voltage-dependent ion channels are the following:

1.3.2.1 Voltage-dependent calcium channels (Ca_v): present in the membrane of most excitable cells, those channels mediate the Ca^{2+} influx in response to depolarization. Ca_v channels are formed as a complex of several different subunits: α_1, $\alpha_2\delta$, β_{1-4}, and γ. The α_1 subunit (190-250 kDa) forms the ion conducting pore and the sensor voltage, and is organized in four homologous motifs (I-IV) with six transmembrane domains (6TM) each. They regulate important intracellular processes such as contraction, secretion, neurotransmission and gene expression. They are divided into three subfamilies: Ca_v1, Ca_v2 and Ca_v3.

1.3.2.2 Voltage-gated sodium channels (Na_v): consisting of a large α subunit that associates with other proteins such as β subunits, those channels conduct Na^+ ions through their pores. The entry of Na^+ always has depolarized effects. In excitable cells such as neurons, myocytes, and certain types of glia, Na_v channels are responsible for the rising phase of action potentials. Nine are the genes that codify to Na_v channels, which structurally, are quite similar to Ca_v.

1.3.2.3 Transient receptor potential ion channel (TRP channels): TRP channels were first described in 1969 in mutant *Drosophila* photoreceptors and were given their name because this mutant lacked sustained photoreceptor activity and showed only transient changes in receptor potential (Cosens and Manning, 1969). These channels share certain homology with K^+ channels. Each subunit has six transmembrane domains and functional channels are likely composed of tetramers (Benham, 2003). TRP channels play a role in pain and sensorial sensations. Mammalian TRP channels are classified into six subfamilies: TRPC (canonical), TRPV (vanilloid), TRPM (melastatin), TRPP (polycystin), TRPML (mucolipin), and TRPA (ankyrin) (Clapham, 2003).

1.3.2.4 Cyclic nucleotide-gated ion channels (CNG): activated by cyclic nucleotides, their discovery was intimately tied with the quest for the intracellular messenger that mediates the photoresponse in retinal photoreceptors. CNG channels are non selective cation channels that poorly discriminate between alkali ions and even allow the passage of divalent cations, in particular Ca^{2+} (Kaupp and Seifert, 2002). Like TRP channels, CNG form tetramers and have the typical structure of 6TM.

1.4 Potassium channel genes are known to be mutated in human diseases, being four of them encoded by the KCNQ gene family

It is known that more than 140 genes codify for human ion channels, which almost 90 are K^+ channels. It is one of the biggest protein families known, highlighting the variety of functions that they carry out as the action potential, insulin secretion, cell proliferation, cell differentiation, immune response, pH

regulation, apoptosis, etc. (Hille *et al.*, 1999). K^+ channel diversity is enhanced by splice variants and by the formation of heteromeric channels, which complicates the study of their function in the organism. The first cloned potassium channel gene was the *Drosophila* voltage gated Shaker channel (Papazian *et al.*, 1987), and this was rapidly followed by the identification of other voltage- and ligand-gated potassium channel genes in flies, mammals, and many other organisms. In the last few years, genetic linkage analysis has greatly facilitated the identification of many diseases produced by mutated loci, four of them being encoded by the K_v7 family (Gutman *et al.*, 2005; Jentsch, 2000; Shieh *et al.*, 2000).

The diversity of K_v channels arises from several factors (Gutman *et al.*, 2005):

- ***Heteromultimerization***: K_v genes encode one peptide subunit, and four of them form a functional channel. K_v channels may be homotetramers when four subunits of the same K_v gene coassemble together, but may also be heterotetramers, when different subunits within the same family form a functional channel (K_v1, K_v7 and K_v10 families). The heteromeric channels express different properties from those of any homotetramers.

- ***Modifier subunits:*** K_v5, K_v6, K_v8 and K_v9, encode subunits that act as modifiers, and although by their own do not produce functional channels, they form heterotetramers with K_v2 family subunits, increasing the functional diversity within this family.

- ***Accessory proteins:*** the presence of accessory subunits such as AKAP and Calmodulin (CaM) modify their properties.

- ***Alternate mRNA splicing:*** although one gene can produce only a protein

subunit, various members of the K_v3, K_v4, K_v6, K_v7, K_v9, K_v10, and K_v11 gene families have coding regions made up of several exons that are alternatively spliced, giving rise to another source of functional diversity.

- ***Post-translational modification:*** it has been described that K_v channels could suffer post-translational modifications, such as phosphorylation (Jerng *et al.*, 2004), ubiquitinylation (Henke *et al.*, 2004) and palmitoylation (Gubitosi-Klug *et al.*, 2005), which at the end modify channel function.

1.5 Potassium channel related diseases

Why organisms need such a variety of potassium channels with the same basic function of conducting ions is a major challenge to be elucidated. The discovery of gene disruptions that encode for potassium channels has shown the diverse roles of ion channels. Most of the anomalies giving rise to diseases are due to mutations present in K_v channels, however, have been shown autoimmune failures or changes in the expression levels. Mutations usually affect the folding or the trafficking of the channel, and not very often, channel function. As mentioned before, ion channels are important for excitable cells such as neurons, cardiac and skeletal muscle. Several channelopathies affect these tissues. Action potentials are initiated by the opening of voltage-dependent Na^+ channels. This leads to a depolarizing influx of Na^+, which is stopped by an intrinsic inactivation of Na^+ channels, being the membrane repolarized to its normal values thanks to a K^+ efflux and sometimes also by a Cl^- influx. Concomitantly, it is easy to understand why so many diseases are related to defects in the electric activity. In table 1 are reported mutations found in potassium channels involved in several channelopathies.

Protein	Gene	Disease
$K_v1.1$	KCNA1	episodic ataxia myokymia
Kv7.1	KCNQ1	autosomal-dominant long-QT syndrome with deafness autosomal-reccessive long-QT syndrome
Kv7.2	KCNQ2	benign familial neonatal convulsions (BFNC), also with myokymia
Kv7.3	KCNQ3	benign familial neonatal convulsions
Kv7.4	KCNQ4	autosomal-dominant deafness
KCNH2	KCNH2	long-QT syndrome
Kir1.1/ROMK	KCNJ1	bartter syndrome
Kir2.1	KCNJ2	long-QT syndrome with dysmorphic features
Kir6.2	KCNJ11	persistant hyperinsulinaemic hypoglycaemia of infancy diabetes mellitus
SUR1	SUR1	persistant hyperinsulinaemic hypoglycaemia of infancy
SUR2	SUR2	dilated cardiomyopathy
KCNE1	KCNE1	autosomal-dominant long-QT syndrome with deafness autosomal-dominant long-QT syndrome
KCNE2	KCNE2	long-QT syndrome
KCNE3	KCNE3	hypokalaemic periodic paralysis

Table 1. Potassium channels involved in human diseases. In the table are represented the genes with the proteins that encode for, and the diseases that could be developed in case of mutations.

1.6 K_v7 channels and the M-current

The M-current was first reported by Brown and Adams in 1980, and discovered in bullfrog sympathetic ganglion neurons and subsequently in a variety of mammalian peripheral and central neurons (Brown and Adams, 1980; Delmas and Brown, 2005; Marrion, 1997) (Fig. 1.2).

Across the cell membranes of neurons, there is an ionic gradient established by pumps and co-transporter proteins that extrude Ca^{2+} and Na^{+} ions and take in K^{+}

ions. When Ca^{2+} ions flow through ion channels, the inner cell becomes more positive and depolarizes the membrane towards the threshold for action potential firing. On the other hand, when K^+ selective channels become opened, K^+ ions flow from the inner to the outer, becoming the cell to the back toward rest and, subsequently, reducing membrane excitability. The M-current possesses the unique characteristic of sustained activation. The M-current is modulated by a variety of receptor types, and the modulation can occur by suppression or enhancement. Modulation of the M-current has dramatic effects on the excitability of central and peripheral neurons (Adams *et al.*, 1982; Brown *et al.*, 1981; Brown *et al.*, 2007; Cooper *et al.*, 2000; Delmas and Brown, 2005; Marrion, 1997).

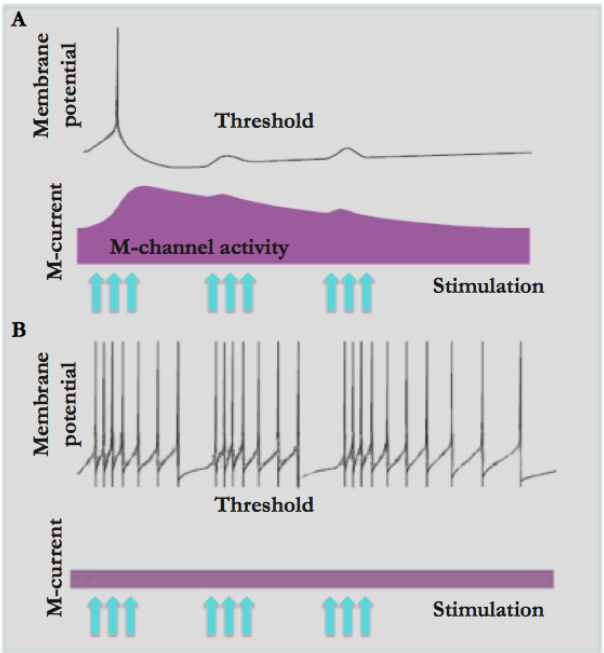

Figure 1.2. Role of neuronal M-channels in response to a specific stimulus. **A.-** Excitatory inputs (blue arrows) cause membrane depolarization and a single

action potential. Afterwards, an increased activation of M-channels hyperpolarizes the membrane potential, preventing spiking in response to recurrent excitation.
B.- When M-channel activity is reduced, excitatory inputs lead to multiple action potentials. Adapted from (Cooper and Jan, 2003).

1.7 Neuronal K_v7 channels

The term KCNQ gene, recently named K_v7 protein, is a genomic shorthand with K representing potassium, CN, channel, and Q, long QT syndrome. The K_v7 family of voltage-gated K^+ channels comprises five members ($K_v7.1$-5 – KCNQ1-5) and plays a prominent role in brain and cardiac excitability (Schwake *et al.*, 2006). Mark Keating discovered in 1996 the K_vLQT1 gene, nowadays called $K_v7.1$, as the ion channel involved in the Long-QT-syndrome (LQTS), the most common cardiac inherited disease (Wang *et al.*, 1996). Later, the other four related genes were discovered ($K_v7.2$ - $K_v7.5$).

Mutations in K_v7 channels give rise to diverse diseases such as severe cardiovascular and neurological disorders.

1.7.1 Structural characteristics of K_v7 channels

K_v7 ion channels have six transmembrane domains with a voltage-sensing segment (S1-S4) and a single P-loop that forms the selectivity filter of the pore (S5-S6). In contrast to other potassium channels, the K_v7 family presents a large C-terminus (300-500 residues) domain that plays a crucial role in channel gating, assembling and trafficking, as well as scaffolding the channel with signaling proteins (Haitin and Attali, 2008) (Fig. 1.3).

The secondary structure analysis of the C-terminus of K_v7 channels revealed four helical regions (helices A-D) conserved in all family members. While helices A and

B are highly conserved between several members of this family, helices C and D are more divergent regions (Yus-Najera *et al.*, 2002).

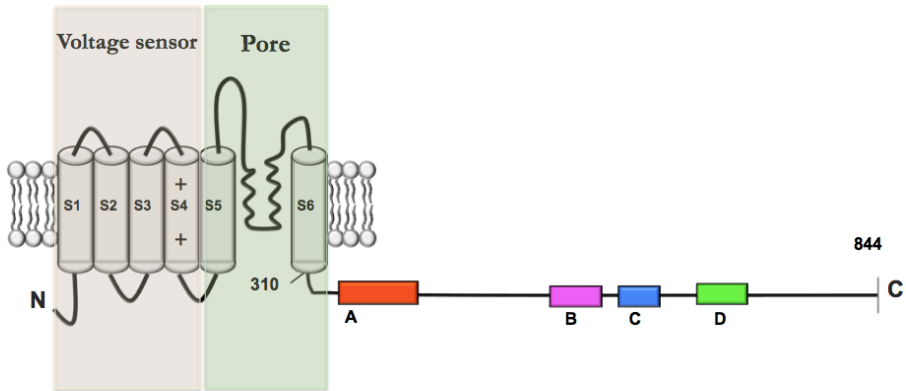

Figure 1.3. Schematic representation of a K_v7 channel subunit. The N-terminal is composed by six transmembrane domains where S5 and S6 form the pore domain and S4 is the voltage sensor. The C-terminal is supposed to form four helical regions called helices A-D.

Helices C and D are thought to form coiled coil assemblies (Wiener *et al.*, 2008), which are characterized by two or three strongly amphipathic parallel α helices. They display a pattern of hydrophilic and hydrophobic residues repeated every seven residues $(abcdefg)_n$ (Lupas, 1996) and frequently found in ion channels (Jenke *et al.*, 2003).

Helix A has an IQ-like CaM-binding motif and two overlapping consensus 1-5-10 CaM binding motifs in helix B (Yus-Najera *et al.*, 2002). Both helices also play a role in the interaction with accessory proteins, such as the A-kinase anchoring protein (AKAP) or KCNE subunits. A work by Howard and collaborators in 2007 provided the high resolution structure (2 Å) of the $K_v7.4$ helix D, and the results showed that this helix is a self assembling, parallel, four-stranded coiled

coil that is conserved among the K_v7 channel subtypes, thereby providing a critical module for K_v7 tetrameric assembly (Howard *et al.*, 2007; Wiener *et al.*, 2008) (Fig. 1.4).

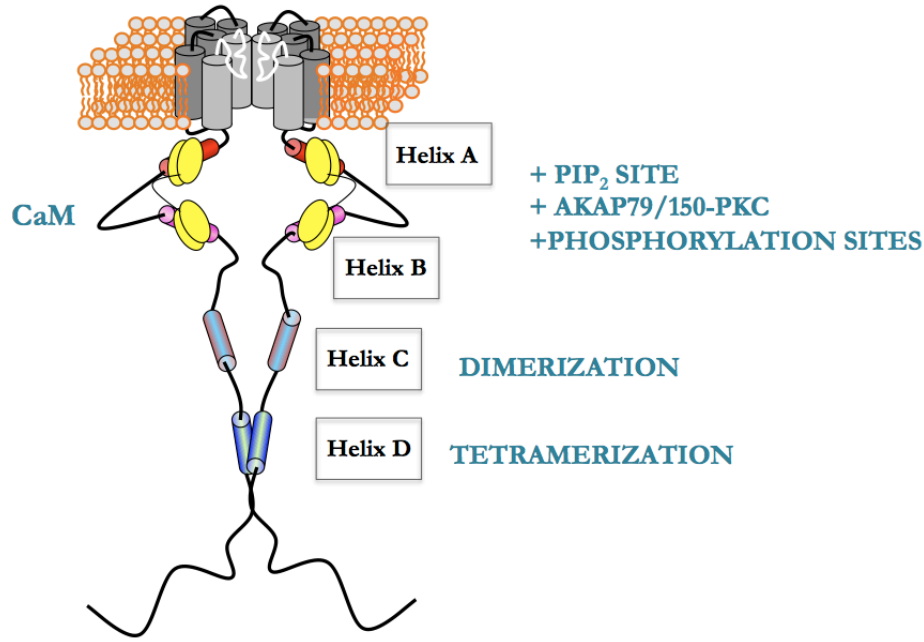

Figure 1.4. Structure of K_v7 channels and the interaction sites on the carboxy-terminal tail. In the image only two subunits are shown.

1.7.2 Helices A and B: Calmodulin binding module and PIP_2 interaction

CaM is an abbreviation for calcium-modulated protein (Harper *et al.*, 1980). It is a Ca^{2+} binding protein expressed in all eukaryotic cells. Small and acidic, it is 148 aminoacids long (16.706 Dalton), with two lobes that comprises two homologous domains consisting of two helix-loop-helix Ca^{2+} binding sites, called EF-hands (Fig. 1.5). This small Ca^{2+} sensing molecule binds to a wide variety of target

proteins and acts as a trigger to modify their functions (Houdusse *et al.*, 1996). The crystallographic structure shows that the N-terminal lobe (aa 1-77) contains EF hands 1 and 2, and the C-terminal lobe (aa 82-148) contains EF hands 3 and 4, being the two lobes connected by a flexible central helix (aa 78-81) (Jurado *et al.*, 1999; Saimi and Kung, 2002; Yus-Najera *et al.*, 2002). Ca^{2+} binds to the four EF hand motifs in a highly cooperative manner, being first associated with the EF hands 4 and 3, and afterwards with EF 2 and 1.

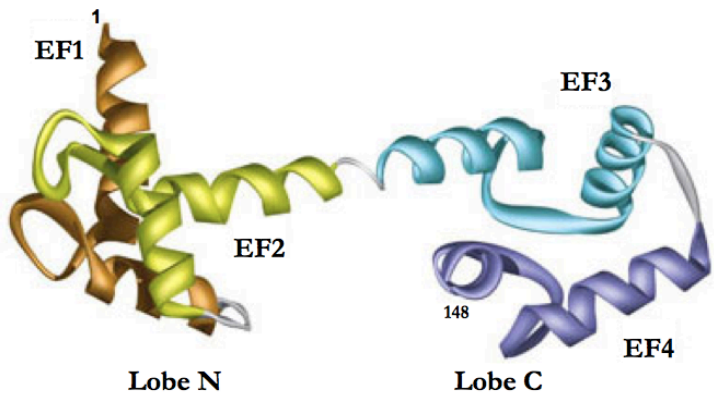

Figure 1.5. **Structure of CaM.** The N-terminal and the C-terminal lobes with their respective EF hands. In white the hinge linker between the two lobes.

Every member of the K_v7 channel family is capable of interacting with CaM. A closer analysis of the helix A region revealed an IQ-like binding motif (IQ*XXX*R*XXXX*R) that mediates apo-CaM binding and contains positively charged residues at positions 6 and 11 (Yus-Najera *et al.*, 2002). Generally, the initial portion of this motif (IQXXXR) is the most critical part (Houdusse and Cohen, 1995), as this region is specifically recognized by the loop between EF

hands 3 and 4 determining a semi-open lobe conformation (Houdusse *et al.*, 1996; Yus-Najera *et al.*, 2002). When point mutations are introduced, the interactions of K_v7.2 with CaM become destabilized (Etxeberria *et al.*, 2008; Yus-Najera *et al.*, 2002).

Although K_v7 channels interact better with apo-CaM, it has been found that both helices can also be associated with Ca^{2+}-CaM, (Gamper and Shapiro, 2003; Ghosh *et al.*, 2006; Shamgar *et al.*, 2006; Wen and Levitan, 2002; Yus-Najera *et al.*, 2002). This issue has generated some controversy, as the role of CaM in K_v7 channel function is not clear. At the beginning, CaM was considered an essential auxiliary subunit for the correct functioning of K_v7.2 and K_v7.3 channels, because K_v7.2 mutants deficient in CaM binding were unable to generate currents when co-expressed with K_v7.3 subunits (Wen and Levitan, 2002). Something widely accepted is that interaction with CaM is essential for the K_v7.2 surface expression. Indeed, QT mutations close to the IQ motif of the K_v7.1 C-terminus impair CaM binding and markedly decrease the current density (Ghosh *et al.*, 2006). Similarly, mutations in helices A and B of K_v7.2 channels exhibit weaker CaM binding and produce smaller K^+ currents (Etxeberria *et al.*, 2008; Haitin and Attali, 2008; Richards *et al.*, 2004).

Phosphatidylinositol 4,5-biphosphate (PIP_2) is a phospholipid from the family of phosphoinositides that is at the cellular plasma membrane (Fig. 1.6). Representing less than 1 % of plasma membrane phospholipids, it plays an important role on a remarkable number of crucial cellular processes such as cellular signaling, regulation of both endocytosis and exocytosis, formation of microvilli and membrane attachment to the cytoskeleton (Czech, 2000).

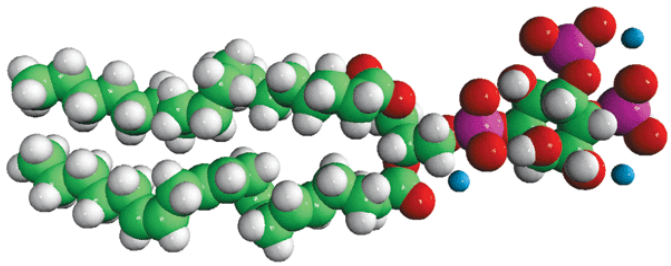

Figure 1.6. Structure of PIP_2. Representative structure of brain porcine L-α-phosphatidylinositol-4,5-bisphosphate, (Adapted from Avanti polar lipids, Alabaster, USA).

PIP_2 is cleaved by phospholipase C (PLC) resulting in diacylglycerol (DAG) and inositol triphosphate (IP_3). It is known that many ion channel family members are activated by PIP_2, including the K_v7 family. PIP_2 may serve the role of the elusive second messenger accounting for M-current inhibition. Indeed, PIP_2 is a direct modulator of the M-current activity and its hydrolysis causes current inhibition (Suh and Hille, 2002; Telezhkin *et al.*, 2012). A recent work has shown that M-channels might be activated by a range of lipid phosphates, being the minimal requirements a phosphate group attached to an appropriate acyl chain, with a potency and efficacy that increases with increasing the number of phosphates (Telezhkin *et al.*, 2012). Although it is known that PIP_2 binds to the C-terminal of K_v7 channels, the exact site is still unknown (Haitin and Attali, 2008). It has been described that some mutations associated to the Long QT syndrome in $K_v7.1$ channels reduce its affinity their PIP_2 (Park *et al.*, 2005).

1.7.3 Calmodulin and its role in channel trafficking

CaM is not only required in gating processes but it may be also important in other

processes such as the assembly and trafficking of ion channels to the plasma membrane, regulating its exit from the ER by a mechanism that is independent of subunit heteromerization. CaM was suggested to be important for the assembly and trafficking of ion channels like SK4/IK1 Ca^{2+}-activated K^+ channels (Etxeberria *et al.*, 2008; Gao *et al.*, 2000; Joiner *et al.*, 2001).

1.7.4 Helices C and D: tetramerization and trafficking domain

The molecular mechanisms that determine the K_v7 subunit assembly selectivity remain imperfectly understood. Although helices A and B encode the CaM-binding domain and other auxiliary proteins, these seem to be unable to support multimerization by their own. However, helices C and D also form coiled-coil assemblies functioning as the tetramerization domain (Howard *et al.*, 2007; Maljevic *et al.*, 2003; Schmitt *et al.*, 2000; Schwake *et al.*, 2006; Schwake *et al.*, 2003). Hence, the two coiled-coil domains appear to act as a module for the channel assembly and trafficking as well as a platform for the interaction with other auxiliary proteins.

Helix D shows several sequence differences sequence among the K_v7 channel family, this suggested to be the primary determinant of channel assembly (Haitin and Attali, 2008; Maljevic *et al.*, 2003; Schwake *et al.*, 2006; Schwake *et al.*, 2003). In this regard, the differences could explain the distinct assembly preferences within the K_v7 family (Howard *et al.*, 2007).

The subunit $K_v7.1$ does not co-assemble with the other K_v7 subunits but, however, it associates with the β-subunit of KCNE1 and KCNE3 (Jentsch, 2000; Wiener *et al.*, 2008). As $K_v7.1$ helix D is about two helix longer than the other family members, this additional heptad repeat may prefer to assemble with a

partner of equal length and sequence in order to fully accomplish its folding potential (Wiener *et al.*, 2008).

The other family members, $K_v7.2$, $K_v7.4$ and $K_v7.5$ can form functional homotetramers and functional heterotetramers with $K_v7.3$ (Kubisch *et al.*, 1999; Yus-Najera *et al.*, 2002). Different combinations of K_v7 subunits display different biophysical properties that produce a functional diversity underlying the M-current (Hadley *et al.*, 2000; Kubisch *et al.*, 1999; Schwake *et al.*, 2000; Selyanko *et al.*, 2000; Wang *et al.*, 1998).

The crystal structure of helix D resolved for $K_v7.1$ and $K_v7.4$ channels showed a four-stranded parallel coiled-coil as well as a self-assembling capacity (Howard *et al.*, 2007; Wiener *et al.*, 2008). In addition, helix D has not only an important role in the assembly between $K_v7.2$ and $K_v7.3$, it is also important in cell surface trafficking as well as underlying the M-current (Schwake *et al.*, 2006).

It is worth mentioning that, the same as helix D in $K_v7.1$ channels mediates the interaction with the A-kinase anchoring protein (AKAP) yotiao, KCNE1 and KCNE3 subunits (Haitin and Attali, 2008; Howard *et al.*, 2007; Marx *et al.*, 2002; Shamgar *et al.*, 2006), helix D in other subunits such as $K_v7.2/K_v7.3$ could act as the binding site for other auxiliary proteins. Moreover, KCNE2 (substantially expressed in human brain) has been shown to regulate the $K_v7.2$ and/or the $K_v7.3$ channel activities by modulating their deactivation kinetics (Tinel *et al.*, 2000).

Mutations in the C-terminal of $K_v7.2$ channels when assembled with $K_v7.3$ may have important consequences causing neonatal convulsions; an impaired assembly could explain why these mutations reduce the K^+ current, and in this regard,

tetramerization could be probably required for the channel proteins to reach the plasma membrane (Biervert and Steinlein, 1999; Papazian, 1999).

1.7.5 The end of the channel

As mentioned before, while helices A and B contain the binding sites for CaM and PIP_2, helices C and D contain important sequences for tetramerization and subunit interaction. What happens then with the distal C-terminal domain?

A more distal 80 aminoacids section that contains a putative ankyrin-G binding loop after helix D has been found. It is highly conserved in $K_v7.2$ and $K_v7.3$, but completely absent in other K_v7 family members (Pan *et al.*, 2006). Ankyrin-G is the first component that becomes clustered at nodes and initial segments during development. There it binds multiple integral membrane proteins such as Na_v channels, neurofascin or Nr-CAM (neuronal cell adhesion molecule) to the actin-spectrin cortical cytoskeleton (Garrido *et al.*, 2001; Garrido *et al.*, 2003; Jenkins and Bennett, 2001; Srinivasan *et al.*, 1992). Indeed, the ankyrin-G membrane binding domain is responsible for the localization of $K_v7.2$ and $K_v7.3$ at the AIS and Ranvier nodes (Pan *et al.*, 2006).

1.8 $K_v7.1$ is part of the cardiac K_v current

$K_v7.1$ was the first K_v7 gene identified using a positional cloning approach on chromosome 11p15.5 in families with long QT syndrome type 1 (LQT1). Expressed mainly in the heart, it has been observed to be mutated in about half of the hereditary cases of the long QT syndrome. They are also expressed in the *stria vascularis* of the inner ear, the small intestine, the pancreas, the thyroid gland, the forebrain neuronal networks and the brainstem nuclei, the lung, the

gastrointestinal tract and the ovaries. When associated with the KCNE ß-subunit, the cardiac action potentials are repolarized, resulting in a slow activation and in an increase macroscopic current amplitude (Shamgar *et al.*, 2006), whereas homomeric K_v7.1 channels give rise to fast-activating potassium currents (Jentsch, 2000). Mutations on K_v7.1 or KCNE1 can lead to cardiac arrhythmia in the dominant LQTS, also called Romano-Ward syndrome (RWS). They can also provoke a more severe loss of function, leading to the recessive Jervell and Lange-Nielsen syndrome (JNLS), in which cardiac arrhythmia is associated with congenital deafness (Schmitt *et al.*, 2000). Other function of K_v7.1 channels is to recycle potassium at the basolateral membrane of intestinal crypt cells, a process that is required for intestinal chloride secretion (Jespersen *et al.*, 2005).

It has been as well found that this channel is functionally expressed in pancreatic ß-cells, being actually under study the possible implications of the K_v7.1 channel in the regulation of the insulin secretion and type 2 diabetes (Ullrich *et al.*, 2005; Unoki *et al.*, 2008).

1.9 Mutations on K_v7.2 and K_v7.3 channels lead to a rare neonatal epilepsy

K_v7.2 as well as K_v7.3 were identified by screening and positional cloning in families affected with Benign Familiar Neonatal Epilepsy Convulsions (BFNC) (Biervert *et al.*, 1998; Singh *et al.*, 1998). Both subunits are found in most of the brain regions as the cortex, the cerebellum, the basal ganglia and the hippocampus, being as well in rat cervical superior ganglion cells (Maljevic *et al.*, 2010). K_v7.2 and K_v7.3 in both homomeric and heteromeric conformation revealed that those channels carry noninactivating potassium currents that slowly activate upon depolarization. K_v7.2 co-assembles with K_v7.3 with different

stoichiometries leading to large currents predominantly followed by an increase in surface expression of both heteromers (Jentsch, 2000; Schroeder *et al.*, 1998; Schwake *et al.*, 2000; Wang *et al.*, 1998; Yang *et al.*, 1998) (Fig. 1.7). Furthermore, it has been demonstrated that heteromeric $K_v7.2$-$K_v7.5$, and specially $K_v7.2/K_v7.3$ channels give rise to the M-current.

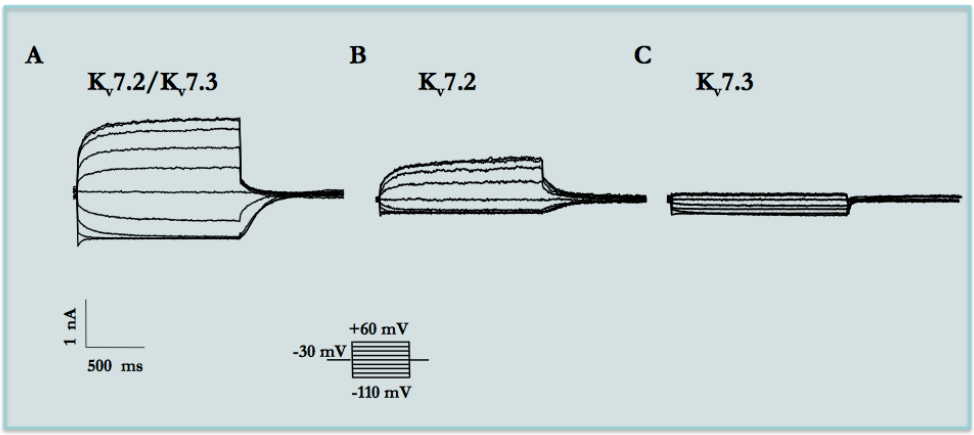

Figure 1.7. Two-electrode voltage-clamp traces co-injected at a 1:1 ratio $K_v7.2/K_v7.3$ (**A**), homomeric $K_v7.2$ (**B**) and homomeric $K_v7.3$ (**C**). The voltage-clamp protocol is shown in the figure. Note the large current increase observed when both subunits are coexpressed.

Mutations in $K_v7.2$ and $K_v7.3$ channels (more than 30 and 4 respectively) cause BFNC (Maljevic *et al.*, 2010). This is a rare autosomal dominant epilepsy syndrome mapped to be located on chromosomes 20 and 8 (Biervert *et al.*, 1998; Charlier *et al.*, 1998; Hirose *et al.*, 2000; Leppert *et al.*, 1989; Maljevic *et al.*, 2010; Singh *et al.*, 1998). It starts the first days of life with frequent partial and secondary generalized seizures and disappear after several weeks or months. The risk of recurring seizures later in life is of about 15% (Castaldo *et al.*, 2002; Ronen *et al.*, 1993). Rarely, there are some cases of patients with mental retardation and

difficult to treat epilepsies (Borgatti *et al.*, 2004; Maljevic *et al.*, 2010; Robbins, 2001). Some cases in which the patients are successively affected by BFNC and myokymia have also been described, characterized by spontaneous involuntary contraction of muscle fiber groups that can be observed as vermiform movement of the overlying skin (Dedek *et al.*, 2001; Wuttke *et al.*, 2007). Pharmacologists discovered that the biological activities of 3 classes of compounds in the development as in the treatment for Alzheimer disease, epilepsy, and stroke were mediated in part by effects on brain K_v7 channels (Cooper and Jan, 2003).

It has also been observed that the KCNQ2 gene can produce multiple spliced transcripts that differ in their cytoplasmic C-terminal tail (Nakamura *et al.*, 1998; Pan *et al.*, 2001; Tinel *et al.*, 1998). To date, only 5 splice variants have been reported but it these are expected to increase (Fig. 1.8). They present differences in their expression during neuronal development and also reveal important implications for the regulation of the M-current function (Smith *et al.*, 2001).

```
331 KRRNPAAGLIQSAWRFYATNLSRTDLHSTW kcnq2-1      451 AAKGKGSPQAQTVRRSPSADQSLEDSPSKV kcnq2-1
331 KRRNPAAGLIQSAWRFYATNLSRTDLHSTW kcnq2-2      433 AAKGKGSPQAQTVRRSPSADQSLEDSPSKV kcnq2-2
331 KRRNPAAGLIQSAWRFYATNLSRTDLHSTW kcnq2-3      423 AAKGKGSPQAQTVRRSPSADQSLEDSPSKV kcnq2-3
331 KRRNPAAGLIQSAWRFYATNLSRTDLHSTW kcnq2-4      421 AAKGKGSPQAQTVRRSPSADQSLEDSPSKV kcnq2-4
331 KRRNPAAGLIQSAWRFYATNLSRTDLHSTW kcnq2-5      376 -------------RRAPATKQ--------- kcnq2-5


361 QYYERTVTVPMYSSQTQTYGASRLIPPLNQ kcnq2-1      481 PKSWSFGDRSRARQAFRIKGAASRQNSEEA kcnq2-1
361 QYYERTVTVPMYSSQTQTYGASRLIPPLNQ kcnq2-2      463 PKSWSFGDRSRARQAFRIKGAASRQNSEEA kcnq2-2
361 QYYERTVTVPMY----------RLIPPLNQ kcnq2-3      453 PKSWSFGDRSRARQAFRIKGAASRQNSEEA kcnq2-3
361 QYYERTVTVPMYSSQTQTYGASRLIPPLNQ kcnq2-4      451 PKSWSFGDRSRARQAFRIKGAASRQNSE-A kcnq2-4
361 QYYERTVTVPMYR----------------- kcnq2-5      384 ------------------------------ kcnq2-5


391 LELLRNLKSKSGLAFRKDPPPEPSPSKGSP kcnq2-1      511 SLPGEDIVDDKSCPCEFVTEDLTPGLKVSI kcnq2-1
391 LELLRNLKSKSGLAFRKDPPPEPSPS---- kcnq2-2      493 SLPGEDIVDDKSCPCEFVTEDLTPGLKVSI kcnq2-2
391 LELLRNLKSKSGLAFRKDPPPEPSPS---- kcnq2-3      483 SLPGEDIVDDKSCPCEFVTEDLTPGLKVSI kcnq2-3
391 LELLRNLKSKSGLAFRKDPPPEPSPS---- kcnq2-4      480 SLPGEDIVDDKSCPCEFVTEDLTPGLKVSI kcnq2-4
374 -------------YR-------------- kcnq2-5      384 ------------------------------ kcnq2-5


421 CRGPLCGCCPGRSSQKVSLKDRVFSSPRGV kcnq2-1      541 SLPGEDIVDDKSCPCEFVTEDLTPGLKVSI kcnq2-1
417 --------------QKVSLKDRVFSSPRGV kcnq2-2      523 SLPGEDIVDDKSCPCEFVTEDLTPGLKVSI kcnq2-2
407 --------------QKVSLKDRVFSSPRGV kcnq2-3      513 SLPGEDIVDDKSCPCEFVTEDLTPGLKVSI kcnq2-3
417 -------------------------PRGV kcnq2-4      510 SLPGEDIVDDKSCPCEFVTEDLTPGLKVSI kcnq2-4
376 ------------------------------ kcnq2-5      384 ----LFHFL--------------------- kcnq2-5
```

Figure 1.8. Alignment of the different $K_v7.2$ alternative splicing aminoacidic sequences.

$K_v7.2$ expression appears earlier than that of $K_v7.3$ in mice and rapidly increases during the first week of life (Nakamura *et al.*, 1998; Tinel *et al.*, 1998). At birth, $K_v7.3$ is expressed in very low amount whereas $K_v7.2$ is already expressed at a significant level. It is not already known how and where $K_v7.2$ and $K_v7.3$ appear in human brain during development, and how differences in expression might be related to the age-dependent seizure remission of BFNC. This seizure remission is probably due to a compensation mechanism of the levels of $K_v7.2$ and $K_v7.3$ respectively (Tinel *et al.*, 1998).

1.10 Mutations on $K_v7.4$ lead to an accumulation of potassium in the inner ear producing deafness

$K_v7.4$ channel was cloned by homology to $K_v7.3$ and localized in the inner ear, certain nuclei and tracts of the brainstem. It forms homomeric K^+ channels that slowly activate upon depolarization and that can also form heteromeric channels with $K_v7.3$, which present a slightly faster activation (Kubisch *et al.*, 1999). As other K_v7 channels, $K_v7.4$ is classified as an M-type channel, being inhibited by the stimulation of muscarine. $K_v7.4$ was mapped at the same locus as a deafness provoking dominant disease. It is thought that the role of $K_v7.4$ is related with the expulsion of K^+ from the cochlear sensory hair cells, and that mutations on this channel provoke the accumulation of potassium in those cells slowly unleashing a progressive loss of hearing. It has recently been discovered that $K_v7.4$ does also

modulate the mechanosensitivity in the cutaneous sensory system, resulting in an increased touch of sensitivity (Heidenreich *et al.*, 2012; Munns and Caterina, 2012).

1.11 The role of $K_v7.5$ is still uncertain

$K_v7.5$ channel was the last member of the family to be discovered (Lerche *et al.*, 2000) and is nowadays the less characterized (Schroeder *et al.*, 2000). The gene was cloned by homology with $K_v7.3$, and is mainly expressed in the brain and in the skeletal muscle, being regulated during myoblast proliferation (Lerche *et al.*, 2000). $K_v7.5$ was also found in colon, lungs and uterus. As $K_v7.5$ channels could be inhibited by muscarine receptors, this member of the K_v7 family could be included within the M-channel family. They can also form heteromultimers with $K_v7.2$ and $K_v7.3$ channels, which are expressed in the nervous central system and peripheral ganglions. The assembly with $K_v7.3$ produces an increase on the current and provokes small changes on the activation kinetics. Up to know, no $K_v7.5$-related diseases have been found. It has also been demonstrated that $K_v7.5$ could interact with KCNE peptides (KCNE1, KCNE3), increasing the diversity of K^+ currents (Roura-Ferrer *et al.*, 2008).

1.12 Drugs related to K_v7 channels

Actually, common diseases such as cardiac arrhythmia and epilepsy, that are known to be related to K_v7 mutations, require important therapic improvements. Epilepsy affects more than 0.5% of the world's population and has a large genetic component (Schroeder *et al.*, 1998). Neuronal K_v7 channels offer an attractive pharmacological target for diseases going along with an intrinsic neuronal hyperexcitability such as epilepsy or peripheral nerve hyperexcitability, (PHN)

(Maljevic *et al.*, 2010).

The first selective blocking agent, **linopirdine,** was originally introduced as a cognition enhancer for potential application in Alzheimer's disease (Zaczek *et al.*, 1998). However, it did not prove very effective in clinical trials mostly due to pro-epileptic side effects such as tremors. Another problem with linopirdine (and its successor XE991) is that they are not selective for neural K_v7 channels and that they can also block cardiac $K_v7.1$ channels.

Retigabine (RTG), first discovered in the early 80s, was effective in preventing seizures induced by electrical shock or by a broad range of chemical convulsants (Cooper and Jan, 2003). Several groups showed that retigabine was a potent opener of channels formed by $K_v7.2$ and $K_v7.3$ subunits. RTG caused the channels to open with hyperpolarized membrane potentials, increased the rate of channel opening, and slowed the rate of channel closing. RTG has been investigated in phase III clinical trials for adjunctive treatment of epilepsy with partial-onset seizures. Retigabine has as well analgesic activity, especially in animal models of chronic inflammatory and neuropathic pain (Brown and Passmore, 2009).

1.13 BFNC-linked mutations

Most of the BFNC-linked mutations, both in $K_v7.2$ and $K_v7.3$, do not abolish channel function at all, with a surprisingly small reduction (Dedek *et al.*, 2001; Lerche *et al.*, 1999; Schroeder *et al.*, 1998; Wuttke *et al.*, 2008). Expression in *Xenopus* oocytes indicates that a 25% loss of heteromeric $K_v7.2/K_v7.3$ channel function is enough to cause the electrical hyperexcitability in BFNC (Schroeder *et al.*, 1998). Probably, increases in the loss of function will lead to severe

consequences or even death. By generating $K_v7.2$ knockout mice, it has been shown that homozygous mutants developed normally in utero but died after the first postnatal day. Indeed, although heterozygous mice showed normal behaviour compared to the wild type, they showed increase sensitivity to an epileptic seizure (Watanabe *et al.*, 2000).

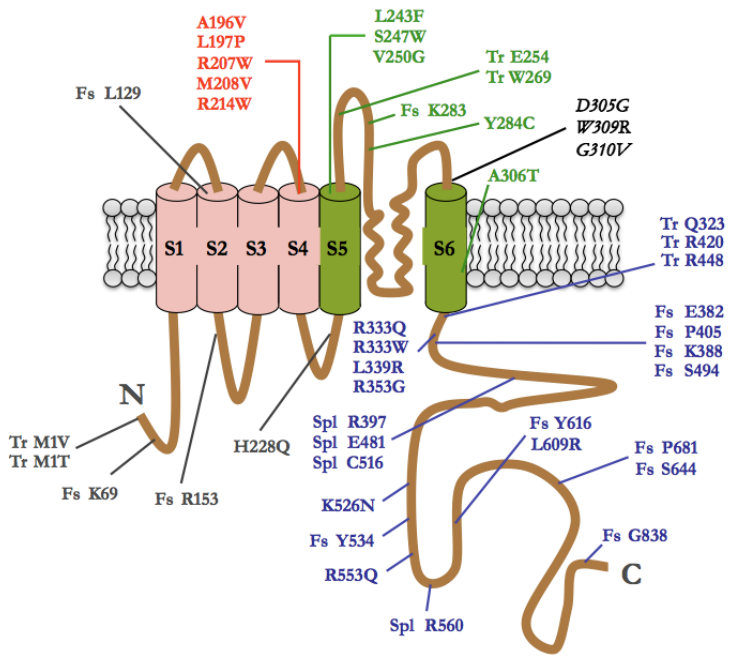

Figure 1.9. BFNC-linked mutations. Fs abbreviation corresponds to mutations that provoke a frameshift mutation. Spl, mutations related to splicing processes, and Tr, is linked to truncated proteins. In italics, mutations corresponding to the $K_v7.3$ subunit and related to BFNC.

The M-current depends on the number of M-channels at the plasma membrane (N), their open probability (P_o) and the unitary conductance (I). Any alteration in whatever of these parameters could underlie BFNC disease. Interestingly, most of

the mutations are located at the C-terminus, at the pore domain and at the voltage sensor of the $K_v7.2$ subunit (Fig. 1.9). Whereas pore mutations presumably decrease single channel conductance, mutations at the C-terminus probably decrease surface expression of the protein (Gomez-Posada *et al.*, 2011; Maljevic *et al.*, 2003; Schwake *et al.*, 2000; Shamgar *et al.*, 2006), although it has been shown that R214W mutation induced gating alterations of the M-current, giving rise to epilepsy in neonates (Castaldo *et al.*, 2002).
Overall, many of the mutations that give rise to BFNC play an important role on channel trafficking.

1.14 M-channel regulation

1.14.1 M-current inhibition

Although the transduction mechanism between the receptors and the channels is not well understood, some studies have shown that membrane-transducing microdomains play a key role in spatio-temporal coding of IP_3 signals, enabling the cell to discriminate between identical signaling pathways that are triggered by different membrane receptors (Delmas *et al.*, 2002). Some other works hypothesized local production or degradation of intracellular messengers that resulted in local concentrations gradients (Gamper and Shapiro, 2007; Zaika *et al.*, 2006).

M-channels are inhibited by a variety of neurotransmitters and hormones acting on G-protein-coupled receptors. In superior cervical ganglion sympathetic neurons, muscarinic M1 (Brown and Adams, 1980), angiotensin II AT1 (Zaika *et al.*, 2006), bradykinin B2 (Cruzblanca *et al.*, 1998) and purinergic P2Y agonists

(Filippov *et al.*, 1998) suppress the M current (I_M) (Hernandez *et al.*, 2008). All of these receptors are coupled to a G-protein (principally Gq and/or G11), stimulate PLC and catalyze PIP_2 hydrolysis (Marrion, 1997). All these four receptors have been grouped into two related modes of action. The first one involves PIP_2 depletion at the membrane (muscarinic and angiotensin receptors) (Delmas and Brown, 2005; Suh and Hille, 2002; Zhang *et al.*, 2003), while the second mode (bradykinin and purinergic receptors) involves IP_3–mediated intracellular Ca^{2+} signals that stimulate PIP_2 re-synthesis, preventing its depletion and suppressing the M-current via CaM (Hernandez *et al.*, 2008) (Fig. 1.10).

1.14.1.1 Inhibition by PIP_2 hydrolysis

As mentioned before (see 1.6.2), PIP_2 is the precursor of the second messengers IP_3 and DAG. This mechanism is used by muscarinic and angiotensin II agonists and principally involves PIP_2depletion. Due to the lack of spatial colocalization with IP_3 receptors, stimulation of these receptors does not elicit $[Ca^{2+}]_I$ rises. Instead, membrane PIP_2 abundance is allowed to fall and the M-channels are inhibited (Hernandez *et al.*, 2008; Suh and Hille, 2007; Zaika *et al.*, 2006).

1.14.1.2 Inhibition by Ca^{2+}/CaM

The second mechanism is based on the IP_3-mediated rises of intracellular Ca^{2+} induced by B2 and P2Y agonists (Bofill-Cardona *et al.*, 2000; Cruzblanca *et al.*, 1998; Delmas *et al.*, 2002; Zaika *et al.*, 2006), with a subsequent Ca^{2+} binding to CaM that acts on the channels (Gamper and Shapiro, 2003; Zaika *et al.*, 2006). The hydrolysis of PIP_2 produces IP_3, which triggers Ca^{2+} release from the endoplasmic reticulum (Berridge, 1993; Loew, 2007). The $[Ca^{2+}]_I$ signals produced by these receptors also augment PI4-kinase activity via NCS-1, thereby stabilizing PIP_2 levels. The Ca^{2+}/CaM action could involve a reduction of the channel's affinity

for PIP_2, which would then unbind from the channel proteins (Hernandez *et al.*, 2008).

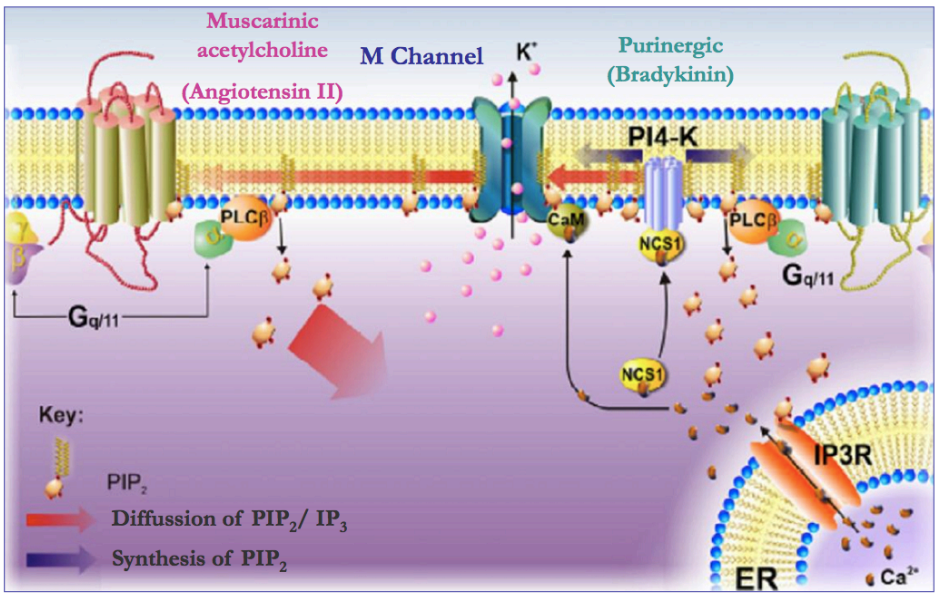

Figure 1.10. **M-current inhibition.** Shown are the mechanisms of inhibition of M-channels used by two types of Gq/11-coupled receptors in the SCG. Both types activate PLC*β*, which in turn hydrolyses PIP_2 to IP_3 and DAG. The first is used by M1 muscarinic acetylcholine and AT1 angiotensin II receptors (left). These agonists are ineffective in producing cytoplasmic Ca^{2+} signals, probably because the receptors are too far away from ER IP_3 receptors, and the produced IP_3dissipates away (thick red arrow). Thus, much PIP_2 is consumed, PIP_2 unbinds from M-channels down the [PIP_2] gradient and M-channels are suppressed. The second mechanism is used by bradykinin B_2 and purinergic $P2Y_6$ receptors (right). Due to the spatial colocalization of these receptors with ER IP_3 receptors, cytoplasmic Ca^{2+} signals are elicited. The released Ca^{2+} binds to neuronal Ca^{2+} sensor-1 (NCS-1) and to CaM. NCS-1 promotes PIP_2 synthesis via acceleration of PI4-kinase, providing PIP_2 to the membrane (purple arrows) and stabilizing PIP_2 levels of the PLC activity. CaM binds to carboxy-terminal domains of the channel and likely acts by reducing its affinity for PIP_2, which then unbinds from the channel since tonic [PIP_2] is now insufficient to maintain its association with the channel and thus the M-current is suppressed (Hernandez *et al.*, 2008).

1.14.1.3 Inhibition by phosphorylation

Another mechanism that mediates the inhibition of the M-current is the phosphorylation of some K_v7 subunit residues. The epidermal growth factor receptor (EGF) induces phosphorylation of both $K_v7.2$ and $K_v7.3$, and also a slow $K_v7.2/3$ current inhibition as a result of the combined $K_v7.2$ and $K_v7.3$ phosphorylations (Jia *et al.*, 2007). On the other hand, the Src family kinases regulate several different K^+ channels of the K_v1 family. Thus, the effect of Src on K_v7 channels involves tyrosine phosphorylation, being inhibited by the phosphotyrosine $K_v7.3$, $K_v7.4$ and $K_v7.5$ but not by $K_v7.1$ and $K_v7.2$ (Gamper *et al.*, 2003).

1.14.2 M-current activation

Somatostatin is reported to be the second or third most abundant neuropeptide in most mammalian brain regions. Somatostatin is predominantly an inhibitory transmitter in the hippocampus. The inhibition of spike discharge is accompanied by a hyperpolarization associated with an increase in the conductance to K^+ ions, at least in part via augmentation of the M-current (Moore *et al.*, 1988; Schweitzer *et al.*, 1993; Schweitzer *et al.*, 1990).

The cytoplasmic N-terminus of the $K_v7.2$ subunit contains a consensus site for cAMP-dependent phosphorylation that promotes an increase of the M-current (Schroeder *et al.*, 1998). It has also been demonstrated an enhancement of the M-current of $K_v7.2$, $K_v7.4$ and $K_v7.5$ K^+ currents induced by physiological concentrations of H_2O_2. The enhancement is due to the oxidative modification of cysteines in a triple cysteine pocket within the cytosolic S2–S3 linker (Gamper *et al.*, 2006).

1.15 The birth of a channel: from the nascent protein to its final destination at the plasma membrane

Ion channels begin their life in the same way as other proteins do. They start as a nascent peptide inside a ribosome that then moves to the endoplasmic reticulum (ER) where its synthesis continues. Being the inside of the ER equivalent to the extracellular space, it contains a unique group of proteins and factors that modify the nascent channel peptide. Once modified, the peptide becomes integrated into the lipid bilayer laterally, oligomerizes, folds and associates with auxiliary proteins. In this regard, ion channel expression is determined by the correct functioning of all these steps, as well as those involved in the trafficking. Any failure or interruption of any of these events will prevent the surface expression of the channel, making impossible its function as ion conductors in a well-regulated fashion (Deutsch, 2002; 2003).

1.15.1 The beginning

Once the mRNA chain is generated by transcription, it associates with the ribosomes where the tRNA undergoes the translation. Multiple copies of the channel protein are generated after a polysome is formed (many ribosomes on a single tRNA). Ribosomes are composed by two subunits: the small and the large subunit. The small subunit is engaged in decoding mRNA, while the large subunit is responsible for protein elongation and release (Tenson and Ehrenberg, 2002) via the peptidil transferase centre (PTC) located at the interface of the two subunits. The PTC is composed of RNA and is supposed to play a role as a ribozyme, catalyzing peptide bond formation. A tunnel starts close to the PTC, passing through the large ribosomal subunit and emerging on its back side (Nissen

et al., 2000). The ribosomal tunnel has a length of around 100 Å from the PTC to the exit site and an average diameter of around 15 Å (Deutsch, 2003). Its role is to host protein synthesis as well as being the normal exit from the ribosome for the nascent proteins. The tunnel walls consist of hydrophilic non-charged groups to facilitate the passage of all kind of peptide sequences (Nissen *et al.*, 2000). However, there are other proteins that could leave the PTC via the interface between the ribosomal subunits (Tenson and Ehrenberg, 2002).

A signal sequence in the N-terminus of the nascent protein/ribosome complex is recognized by a signal recognition particle (SRP), which subsequently binds to a receptor at the ER membrane. The whole complex is targeted to the ER where the synthesis continues (Deutsch, 2003).

The mechanisms underlying protein synthesis regulation in eukaryotes are poorly understood. However, some studies on $K_v1.3$ potassium channels have demonstrated that the T1-recognition domain (located at the NH_2-terminus) confers a subfamily specificity for intersubunit assembly, and that forms a tetramer while the nascent channel peptides are still attached to the ribosomes, perhaps before the monomer is fully synthesized. Thus, folding of the T1 domain and the intersubunit T1-T1 interaction may represent the first assembly event in channel formation (Lu *et al.*, 2001).

1.15.2 Folding and trafficking in a correct way

The journey from a nascent protein chain to a mature protein passes through several stages of folding and oligomerization, being retained at the ER if the protein cannot achieve its correct secondary, tertiary and quaternary structure (Kosolapov and Deutsch, 2003). Both translocon and ribosome impose some

restrictions along the folding process and could act in a chaperone-like fashion (Das *et al.*, 1996). Folding is not a single step but it is presumably undertaken during all the stages of the biogenesis. Given that the folding process is a complex issue for ion channels that are composed by functional domains, it is easy to understand that their rapid and efficient folding will depend on a sequential folding during synthesis (Netzer and Hartl, 1997). It is thought that the pore, as well as the voltage sensors, folds later than it is inserted, tetramerized and associated with the auxiliary subunits. This may suggest that some domains fold before targeting to the ER while others do it at a later stage of the biogenesis, perhaps requiring oligomerization (Deutsch, 2003).

The first secretory pathway is the ER, where ion channels (as most membrane proteins) are synthesized, folded and assembled using the translocon for their translocation and integration into the lipid bilayer (Heusser and Schwappach, 2005). As part of a cellular quality control, a variety of ER resident proteins exert their function preventing the exit of unassembled subunits or partially assembled complexes (Yuan *et al.*, 2003). Several peptide trafficking motifs (mostly recognize by vesicle coat proteins) or larger domains that influence or govern protein movement along the secretory pathway have been recognized (Heusser and Schwappach, 2005).

1.15.3 ER machinery to ensure proper protein folding

Cell function and viability are dependent upon an efficient protein folding. There are more than 100 disorders linked to bad protein conformations in which misfolded ER substrates are prematurely degraded or accumulated as toxic aggregates, highlighting the importance of an effective quality control machinery (Brodsky and Skach, 2011; McClellan *et al.*, 2005).

By preventing the premature exit of folding and incompletely assembled proteins intermediates from the ER, the folding machinery of the ER lumen has a chance to improve the correct maturation. Indeed, the ER machinery ensures that proteins are not delivered to their terminal compartments if they are still not folded, which could damage the cell (cystic fibrosis) (Ellgaard and Helenius, 2003).

The main function of the ER is to allow the newly synthesized proteins their access to a correctly folded conformation by using resident folding enzymes and molecular chaperones. If this process stalls, the ER responds by activating the machinery to up-regulate the expression of molecular chaperones and to down-regulate the overall protein expression, and finally by triggering a process that destroys incorrectly-folded-proteins to prevent their accumulation (Chevet *et al.*, 2001). Two pathways are involved in the process: the unfolded protein response (UPR) and the ER-associated degradation (ERAD) (Brodsky and Skach, 2011).

When secreted proteins enter the ER, a network of chaperones comes face, minimizing the aggregation, facilitating the native structure formation and ensuring the oligomeric assembly. The molecular chaperone family includes non-covalent interactions with Hsp40 (DnaJ), Hsp70 (Grp78/BiP/Kar2) and Hsp90 (Grp94), with the lectin based chaperones (calnexin (CNX) and calreticulin (CRT) and with protein disulfide isomerases (PDIs) (Brodsky and Skach, 2011; Kleizen and Braakman, 2004). These chaperones are involved in binding unfolded proteins, and probably participate in their degradation as well as in the activation of signaling pathways (Chevet *et al.*, 2001; Ellgaard *et al.*, 1999). The exit from the ER to the Golgi complex is limited to those proteins that have reached the native conformation, whereas the misfolded subunits become retro-translocated and

degraded in the cytosol (Ellgaard and Helenius, 2003). The ER-associated degradation is mainly performed by the 26S proteasome, which is located in the cytosol. The process occurs in several steps, being before the proteasomal degradation, deglycosylated and polyubiquitinated. Although the exact mechanisms have not been yet described, what is sure is that the responsible machinery for protein folding plays again a role in the selection and preparation of aberrant products for disposal (Ellgaard *et al.*, 1999) (Fig. 1.11).

1.15.4 ER retention/retrieval motifs

Proper ion channel function requires more than a simple manufacture and assembly of channel building proteins. The cell must provide the mechanisms to ensure proper ER exit, targeting, localization, abundance and turnover to control surface expression levels as well as the distribution of ion channel conductance (Deutsch, 2003). Otherwise, improper unfolding and defects in the trafficking could give rise to severe diseases as cystic fibrosis, epilepsy or schizophrenia among others.

1.15.4.1 Arg-based ER-localization signals

First discovered in the oligomeric transmembrane protein formed by the major histocompatibility complex (MHC) class II by deleting the invariant chain (Ii) (Bakke and Dobberstein, 1990), these signals are mainly present in membrane complexes destined to leave the ER (Michelsen *et al.*, 2005). The presence of these motifs, that can function both at the independently at the N- or C- terminus of a membrane protein as well as in an intracellular loop, being not required a specific distance to the distal termini, maintain the improper assembly channels in the ER until a heteromultimeric assembly is done. During that these motifs are masked,

allowing the protein the to be transported to the cell surface (Michelsen *et al.*, 2005). These motifs are positional dependent, and when mutated, the effect can be reversed. Furthermore, when transferred to another protein, it keeps then at the ER. Something interesting about that is the role of the 14-3-3 proteins: When a multimeric state of the protein is reached, 14-3-3 proteins bind to the exposed Arg-based signals, allowing the complex its transport to the cell surface. In the other hand, a monomeric state of the protein leaves the Arg-based signals exposed, being them retrieved by the coat protein complex I (COP I) (Michelsen *et al.*, 2006). In some cases as in K_v1 channels, the ER retention is not due to a canonical ER retention or retrieval signal like R*X*R(R) or KDEL. In contrast, it appears more likely that the ER retention of a given subunit is due to an inefficient folding or an insufficient stability caused by chaperone-mediated partial retention (Zhu *et al.*, 2001). Due to their flexibility, more and more of these motifs are being discovered. Some examples of these motifs are the RKR sequence that, when present, prevent K_{ATP}-channel surface expression (Zerangue, 1999). The RxR(R) motif (related to the RKR sequence), shielded in $GABA_BR1$ by the interaction of GB1 and GB2 through their coiled-coil domains and allowing the assembled heterodimeric complex to traffic to the cell surface (Margeta-Mitrovic, 1999) and the RRR motif that, when expressed alone in heterologous cells, NR1 and NR2 subunits of the NMDA receptor, are retained at the ER and do not efficiently reach the plasma membrane (Scott *et al.*, 2001).

1.15.4.2 di-lysine motifs/KKXX

The di-lysine motif appears to be conserved among eukaryotes, and mutagenesis studies show remarkable conservation of the functional motif between yeast and humans (Teasdale and Jackson, 1996). In this well characterized ER-localization signal, the two lysine residues cannot be substituted by other basic amino acids

and must be in either the -3, -4 or the -3, -5 positions relative to the COOH terminus to function efficiently as a retrieval motif. This motif suggests a role for non-clathrin-coated vesicles in dilysine-mediated Golgi-to-ER recycling (Scott *et al.*, 2004).

Nevertheless, there are more mechanisms apart from these previously described that could affect the folding, the oligomerization, and the stability of homomeric or heteromeric protein complexes such as the phosphorylation state, the association of the channel with scaffolding/anchoring proteins (Scott *et al.*, 2001) and the subunit composition underlying the stoichiometry (Ma and Jan, 2002). Moreover, it has been demonstrated that the C-terminal coiled-coil forming structures in some K^+ channels (K_v7 and HERG) as well as in Ca^{2+}-activated channels (IK and SK) function as specific domains for multimeric assembly and surface expression. The tetramerising coiled-coils seem to be important for the global structure of the multimeric ion channel complex (Heusser and Schwappach, 2005).

1.15.4.3 ER export signals

Proteins, once folded and assembled, are able to exit the ER. It has been shown that some membrane proteins become concentrated during the process of ER export, suggesting that selective enrichment of export signals could mediate the membrane protein ER export.

Studies on the inward-rectifier K^+ ion channel Kir2.1 revealed an ER export signal (FCYENE) that, when fused to unrelated proteins, promotes the ER export and subsequently the steady-state surface expression of these membrane proteins (Ma and Jan, 2002). Similar but distinct ER export signals are shown in other members of the Kir family like Kir1.1, Kir3.2 and Kir3.4. The three subunits coassemble to

form heterotetrameric channels, being retained at the ER when only one subunit is expressed, meaning that the ER export signals are also useful to verify the subunit composition of membrane complexes. Two other motifs present in $K_v1.4$ and SUR1 are also involved in the transport from the ER to the Golgi apparatus. When one of these motifs is mutated, a decrease on the number of channels with mature glycosylation is observed. The glycosylation status shows the steady-state subcellular distribution of the channels, suggesting a defect in their ER-to-Golgi transport resulting from a defective folding or a removal of a traffic signal or, by contrast, a rapid degradation after acquiring mature glycosylation at the Golgi (Ma and Jan, 2002).

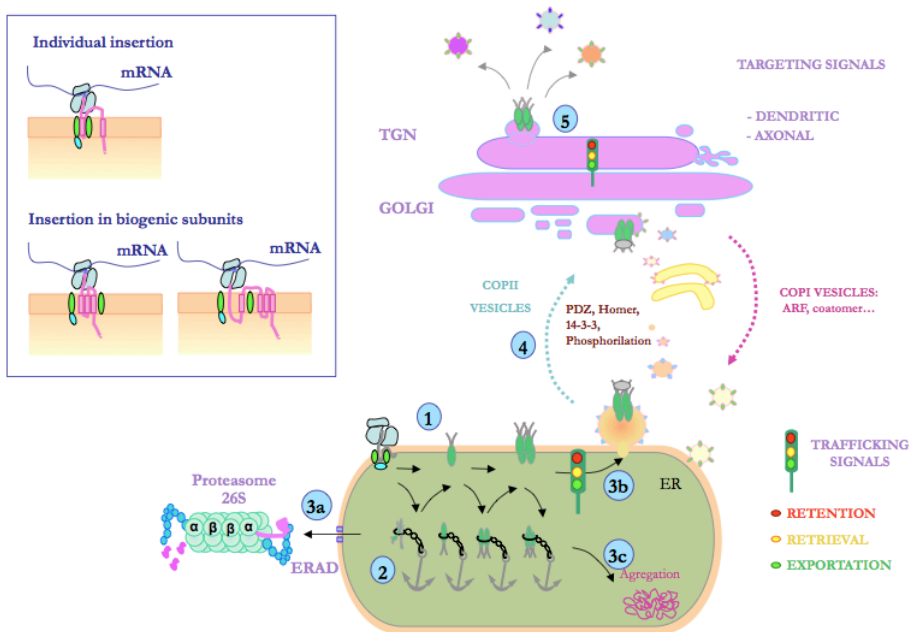

Figure 1.11 Schematic overview of the transport pathway of a transmembrane protein. Proteins are synthesized at the ER (1). At the ER, most proteins are retained until correctly folded and assembled (2). Persistently, misfolded proteins are retrotranslocated to the cytosol and degraded by the proteasome 26S (3a). Also, incompletely folded proteins are prone to aggregation (3c). Once folded, proteins leave the ER and enter the so-called "exit sites" (3b), where the COPII associate

with the cytosolic surface of the membrane (4) to export them to the Golgi complex (5). Once the COPII vesicles have detached from the ER, the COPII coat is replaced by the COPI coat, which mediates the formation of return vesicles that bring some of the membrane contents back to the ER.

1.15.5 Do you want to coassemble with me?

There is a vast repertory of ion channels formed by a combination of different subunits. Through the recognition domains, different subunits coassemble together in their right stoichiometry provided by the sufficient stabilization energy for a stable structure to be formed. The ER is the place for that (unless in some exceptions like the gap junction channels). What happens when two different monomers of the same family coassemble together? When this occurs, it gives an extensively variety of channels formed by homomers and tetramers, with a crucial composition for the normal function of most tissues such as the brain and heart. Little is known about this regulation *in vivo*, although some theories point out that different mRNAs are bound in a translational unit via RNA binding proteins and are coordinately translated (Deutsch, 2003). Two types of domains are involved in the assembly of K^+ channels. In Shaker K^+ channel family (K_v1), the cytoplasmic T1 domain is a highly conserved N-terminal sequence responsible for subfamily-specific subunit coassembly (Kosolapov and Deutsch, 2003; Schwake *et al.*, 2006). In contrast, in other K^+ channels such as the inward rectifier IRK1/Kir2.1 and K_v7 channels, a specific part of the C-terminal domain is required for the assembly, which exhibit high probability for coiled-coil formation (Wehling *et al.*, 2007).

As mentioned before, the carboxy-terminal of K_v7 channels shows a bipartite coiled-coil motif separated by an about 30-aminoacid linker. The first coiled-coil region is required to form functional homomeric or heteromeric $K_v7.2/K_v7.3$

channels, whereas the second coiled-coil domain assist the transport of heteromeric $K_v7.2/K_v7.3$ channels (Wehling *et al.*, 2007). Although the mechanism by which K^+ channels as oligomeric structures are form is still unknown, what is certainly sure is that tetramers are formed at the ER and reside within the plasma membrane as irreversibly-formed channels (Tu and Deutsch, 1999). Furthermore, the dominant pathway in K_v tetramer formation is the formation of dimers. These conformational changes that accompany the dimer formation create new interaction sites that could be used as a previous step for tetramer formation (Deutsch, 2003).

1.16 Human disorders caused by defects in protein folding, oligomerization and targeting to the cell surface

The development of some diseases is sometimes associated to failures where the trafficking steps are affected. Advances in molecular biology have shown that a punctual mutation in the cystic fibrosis transmembrane conductance regulator gene (CTFR) gives rise to an immature protein not fully glycosylated, that indeed, becomes ubiquitinated and targeted at the ER for subsequent proteolytic degradation (Powell and Zeitlin, 2002). Other example is shown in K_{ATP} channels, which play a central role in glucose-stimulated insulin secretion by the pancreatic beta-cell. The mutation E282K prevents the surface expression of K_{ATP} channels due to its retention at the ER. The simplest explanation of this effect would be that the mutation inhibits the ability of Kir6.2 to assemble with SUR1. Two mutations, Y330C and F333I, reported in patients with neonatal diabetes mellitus (NDM), disrupted an endocytic traffic signal thereby impairing clathrin-coated vesicle (CCV) formation and endocytosis. The consequent increase in the density

of K_{ATP} channels, together with an attenuated sensitivity to ATP previously reported, may account for the severe form of NDM (Sivaprasadarao *et al.*, 2007). GABA receptors are the main receptors involved in the synaptic inhibition in mammalian brain. Deficits in the functional expression of GABA due to alterations on the trafficking, are critical in epilepsy, anxiety disorders, cognitive deficits, schizophrenia, depression and substance abuse (Jacob *et al.*, 2008). In K_v7 channels, a LQT mutant minK alters K_vLQT1 trafficking, which is responsible for the hereditary LQT syndrome (Krumerman *et al.*, 2004). On the other hand, perturbation of CaM binding leads to ER retention of $K_v7.2$, reducing the number of channels that reach the plasma membrane (Etxeberria *et al.*, 2008).

Objectives

The aims of the present Doctoral Thesis are:

1) **To identify intrinsic determinants regulating K_v7.2 surface expression**

2) **To ascertain the role of calmodulin in K_v7.2 channel assembly**

CHAPTER 2

EXPERIMENTAL PROCEDURES

Experimental procedures

2.1 Molecular biology

2.1.1 Mutations and deletions of K_v7.2 channels

2.1.1.1 DNA constructs

The human cDNA of K_v7.2 (UniProtKB/Swiss-Prot: 043526) and K_v7.3 (UniProtKB/Swiss-Prot: 043525) channels were provided by:

-K_v7.2 splice 1/K2KL: Dr. Marc Borsotto (Institut de Pharmacologie Moléculaire et Cellulaire, Valbonne, France) (Tinel *et al.*, 1998).

-K_v7.2 splice 2/K2ΔL: generated in the laboratory with PCR techniques, by the combination of the templates of the 3 and 4 splices.

-K_v7.2 splice 3 and K_v7.3 channel: Prof. Thomas J. Jentsch (Max-Delbrück-Centrum für Molekulare Medizin, Berlin, Germany) (Biervert *et al.*, 1998)

-K_v7.2 splice 4: Prof. David Mckinnon (Stony Brook State University of New York, Stony Brook, New York, NY, USA) (Wang *et al.*, 1998).

Constructs of the present work have been generated following different cloning strategies:

2.1.1.2 PCR technique

The polymerase chain reaction (PCR) is a technique to amplify a single or few copies of a piece of DNA across several orders of magnitude, generating thousands to million copies of a particular DNA sequence. The method relies on

thermal cycling, consisting on cycles of repeated heating and cooling of the reaction for DNA melting and enzymatic replication of the DNA (T100™ Thermal Cycler, Bio-Rad, Hercules, CA, USA). Different PCR assays were done:

- *Simple PCRs*: to amplify sequences not longer than 700 bp that allows adding new restriction sites, needed to produce not only deletions, but also to mutate residues close to the restriction sites that already exist. The Taq polymerase used was the one provided by Roche, the Expand High Fidelity polymerase (Ref.: 03300242001, Roche Applied Science, Penzberg, Germany) that introduces deoxiadenosines in the 3´extrems of the amplified product.

- *Assembly PCRs*: useful to mutate residues located in the inner part of a fragment that is flanked by restriction sites. First, two simple PCRs using the Pfu Turbo polymerase (Ref.: 600250, Agilent Tech., Santa Clara, CA, USA) are done. Each PCR corresponds to half of the fragment where we want to introduce the mutations. The primers from each PCR are specifically designed to hybridise between them at least in one extreme. Next step is to make a third PCR with the Expand polymerase to amplify the whole fragment with the deoxiadenosines at the extremes.

Primers were designed manually and synthesised by Sigma-Aldrich (Sigma-Aldrich Co., St. Louis, MO, USA) and IDT (Integrated DNA Technologies Inc., Coralville, IA, USA). All PCR fragments were first subcloned in the pGEM-EasyT vector (Ref.: A1360, Promega Corp., Fitchburg, WI, USA). This is a linear vector that has a 3´terminal thymidine in both ends. These single 3´-T overhangs at the insertion site greatly improves the ligation efficiency of a PCR product into the plasmids by preventing re-circularization of the vector and providing a compatible overhang for PCR products generated by the Expand polymerase. It

also contains the region within the alpha-peptide coding region of the enzyme beta-galactosidase. The PCR protocol reaction consist on:

P1. PCR PROTOCOL

1 H, 45 min.

DNA	H_2O	Primers	Deoxynucleotides	Polymerase buffer	Polymerase
[0,01 µg/µl] 0,2 µl	2,9 µl	0,5 µg/µl] 0,2 µl x 2	[2,5 mM] 2 µl	[10X] 2 µl	0,3 µl

Cycles

Temperature at start: 74 ºC

Denaturation: 95 ºC, 20 sec.
Annealing primers: 55 ºC, 30 sec.
Extend primers: 72 ºC, 1 min.
} x 21

Cooling: 4 ºC, ∞

2.1.1.3 Fragment digestion, purification and ligation

cDNA´s are digested for 2 hours at 37 ºC with the adequate restriction enzymes. After neutralization of the digest reaction by addition of 10X loading buffer (Glycerol 50 %, 0,2M EDTA pH 8, bromophenol blue 0,05 %), the different fragments are separated by electrophoresis in a 1% agarose [Agarose Low EEO Ref.: 8008, Laboratorios CONDA, Madrid, Spain] gel (130 ml TBE 1X [1L: 54 g Tris Base, 27,5 g Boric Acid, 20 ml of 0.5 M EDTA] + 1,3 g agarose). A Lambda DNA marker is used as a reference of the weight in pair of bases of the product. The agarose gels are stained with ethidium bromide which acts as an intercalating

agent in between the nucleic acids, and which suffers an almost . Bands corresponding to the vector and fragment respectively are removed from20-fold increase in fluorescence upon binding to DNA. Bands corresponding to the vector and fragment respectively are removed from the gel and purified thanks to the High Pure PCR Product Purification Kit (Ref.: 1173266800, Roche Applied Science, Penzberg, Germany). Once the fragment and the vector are purified, the ligation is performed by using the T4 DNA ligase (Ref.: EL0014, Fermentas, Thermo Fisher Sci. Inc., Rockford, IL, USA) at room temperature overnight.

P2. FRAGMENT DIGEST PROTOCOL
2 H, 37 ºC

DNA	H_2O	Buffer [10X]	BSA [100X]	Enzyme
Vector [1 µg/µl] 2 µl	13,5 µl	2 µl	2 µl	0,5 µl
Fragment [1 µg/µl] 4 µl	11,5 µl	2 µl	2 µl	0,5 µl

P3. PURIFICATION PROTOCOL
25 min

-Cut desired DNA band from gel, cutting the smallest possible gel slice.
-Place excised agarose gel slice in a sterile 1.5 ml microcentrifuge tube.
-Determine gel mass weighting the tube.
-Add 300 µl binding buffer for every 100 mg agarose gel slice to the microcentrifuge tube.
-Vortex the microcentrifuge tube 15-30 sec to resuspend the gel slice in the binding buffer.
-Incubate the suspension for 10 min at 56 ºC.
-Add 150 µl isopropanol for every 100 mg agarose gel slice to the tube.

P3. PURIFICATION PROTOCOL
25 min
continuation

-Centrifuge 30 – 60 sec at maximum speed in a standard table top centrifuge at 15 to 25 ºC.
-Discard the flow through solution.
-Add 30 µl elution buffer and leave for at least 10 min.
-Centrifuge 1 min at maximum speed.
-Reconnect filter tube with the same collection tube.
-Add 500 µl wash buffer to the upper reservoir.
-Centrifuge 1 min at maximum speed.
-Discard the flow through solution.
-Add 200 µl wash buffer.
-Centrifuge 1 min at maximum speed.
-Place the High Pure filter tube with a clean 1.5 ml microcentrifuge tube.

P4. LIGATION PROTOCOL
O/N, RT

DNA Fragment	DNA Vector	Ligase buffer [10X]	Ligase
[1 µg/µl] 1 µl	[1 µg/µl] 1 µl	1 µg/µl] 2 µl	2 µl

2.1.1.4 Bacterial transformation

Already ligated vector and fragment are transformed in an *E. Coli* BSJ strain, which has previously been prepared to be competent. The purpose of this technique is to introduce the foreign plasmid into bacteria and use it to amplify the plasmid in order to make large quantities of it. A number of mechanisms are available to transfer DNA into bacteria, such as electroporation, calcium or heat shock. This one produces competent cells that will uptake DNA after a heat

shock step (Transformation Buffer [TB] 2X: 40 mM $MgCl_2$, 20 mM $CaCl_2$). To help the bacterial cells recover from the heat shock, the cells are briefly incubated with non-selective growth media. Finally, the cells are seeded into LB agar plates with the specific antibiotic such as Kanamycin (Kan^R) or Ampicilin (Amp^R) (1000X solutions: Ampicilin: 100 mg/ml, Kanamycin: 30 mg/ml) at 37 ºC.

P5. TRANSFORMATION PROTOCOL
1 H, 20 min

- Thaw one vial (or more) of cells (100 µl volume) on ice.
- Add 5 µl of ligation reaction or plasmid DNA (10-50 pg) and mix.
- Incubate on ice for 15-30 min.
- Heat shock for 10 min at RT.
- Add 1 ml of LB medium.
- Incubate at 37 ºC for 45 min.
- Give a pulse and remove 950 µl of LB.
- Seed the culture on a 10 cm LB agar plate.
- Incubate the plates inverted at 37 ºC until colonies have grown.
- The plates can be stored, after parafilm sealing, at 4 ºC. The colonies remain viable for up to a week.

2.1.1.5 DNA extraction and quantification

To obtain DNA in small amounts, each colony is grown in 3 ml of LB medium with selection (Amp^R/Kan^R) for 37 ºC at 220 rpm overnight (O/N). Then, 2 ml culture are transferred to a microcentrifuge tube and spin at max speed to pellet cells. The pellet is resuspended in TE 1X (TE 10X: 100 mM Tris-HCl pH 8, 10 mM EDTA), and then lysed with SDS/NaOH (0,2 M NaOH/1 % SDS); SDS denatures proteins and NaOH denatures DNA. Before 1-minute lysis time, neutralization buffer (3 M potassium acetate, 5 M acetic acid) is added and mix immediately. This neutralizes the mixture, allowing plasmid DNA to re-anneal. To

separate lipids from proteins, a solution made of phenol/chloroform (25:24) is added. The aqueous phase is removed and transferred to a new microcentrifuge tube. The DNA precipitation is done using isopropyl alcohol. Finally DNA is washed with 70 % ethanol and resuspended in TE 1X. Between 1-2 μg of DNA is obtained by this procedure.

P6. DNA EXTRACTION PROTOCOL
30 min

- Grow 3 ml O/N culture in LB + selection (Amp^R, Kan^R, etc.).
- Transfer 2 ml O/N culture to microcentrifuge tube. Spin 1 min at maximum speed to pellet cells.
- Discard supernatant and resuspend pellet in 150 μl TE 1X. Make sure pellet is completely resuspended.
- Add 150 μl NaOH/SDS lysis buffer. Mix gently but thoroughly by inverting tube 5-6 times.
- Add 150 μl of neutralization buffer and mix immediately, but gently.
- Add 80 μl of phenol : chloroform.
- Spin 5 min.
- Extract with 400 μl and transfer to a new microcentrifuge tube with 200 μl of isopropyl alcohol.
- Spin 5 min.
- Wash pellet with 70 % EtOH.
- Dry pellet in 37 ºC.
- Dissolve plasmid in 30 μl of TE+RNAse buffer.

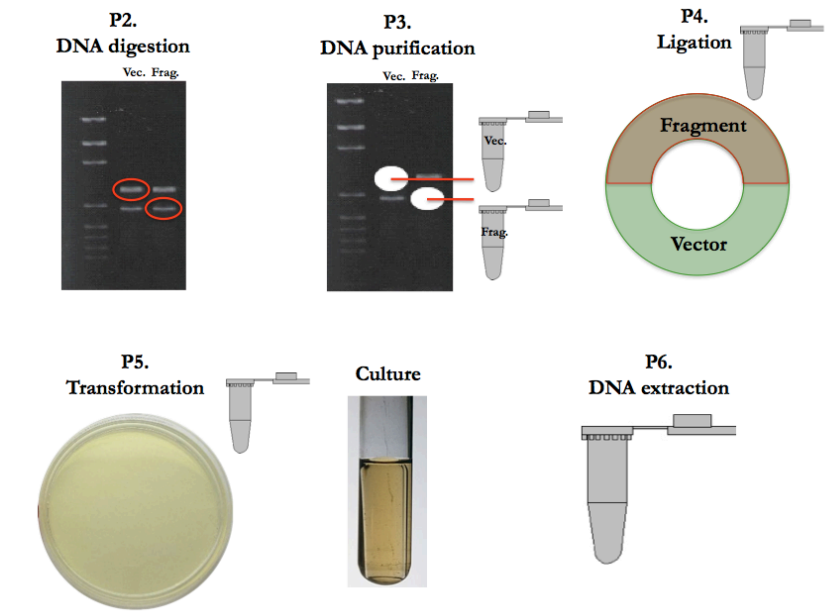

2.1.2 Tags and fluorophores

Tag insertion is useful when no commercial antibodies that directly recognize any extracellular domain of the protein under study are available. In our case, for surface expression assays, K_v7.2 channels were tagged with two epitopes of the protein hemagglutinin (HA) from the flu virus (HA: YPYDVPDYA), between the first and second extracellular loops. With the HA tag, some residues from a chloride channel were inserted to improve the exposure from the epitope and to be recognized by the antibody. Additionally, a variant of the cyan fluorescent protein (CFP), [the cerulean protein (mCer)], with some mutations (S72A, Y145A, H148D and to be monomer A206K) was also inserted, presenting increased fluorescence and being photo-stable (Ex: 433 nm Em: 475 nm) inserted at the N- and at the C-terminus. Fortunately, for the western blot assays the mCerulean protein is recognized by the anti-GFP antibody.

2.1.3 Vector expression

According to the type of experiment, the constructs were subcloned into different plasmids, low expression vectors like pSRC5, manufactured in the laboratory with a ADSV40 promoter and a UTR5´, into one designed for high-level, constitutive expression like pcDNA3, pcDNA3.1, (with Cytomegalovirus (CMV) enhancer-promoter for high-level expression, within other features (Ref.: V790-20, Invitrogen, Life Tech., Carlsbad, CA, USA) or pEGFP, that encodes a red-shifted variant of wild-type GFP which has been optimized for brighter fluorescence and higher expression in mammalian cells. The vector backbone also contains an SV40 origin for replication in mammalian cells expressing the SV40 T-antigen.

2.1.4 Chimeras

2.1.4.1 CD25/Tac-K_v7.2

CD25 or Tac is a transmembrane glycoprotein known as the alpha chain of the Interleukin-2 receptor (UniprotKB/Swiss-Prot: P01589). When transfected into cells, Tac is mainly localized at the plasma membrane. Tac is composed by an extracellular N-terminal domain with two glycosilable residues (240 aa's), a transmembranal segment (19 aa's) and a short C-terminal domain (13 aa's). The protein was subcloned into the pEGFP vector, to be easier for localization once transfected.

2.1.4.2 K_v7.5/K_v7.2

ShineGene Molecular Biotech (ShineGene Molecular Biotech, Shanghai, China) synthesized to our requirements the K_v7.5 N-terminal sequence with two

restriction sites at the beginning and at the end. This way, we could easily subclone it into the K_v7.2 DNA.

2.1.4.3 CD4/K_v7.2

CD4 (cluster of differentiation 4) is a glycoprotein that assists the T cell receptor with an antigen-presenting cell. It is expressed at the membrane of many different cells like monocytes, macrophages and dendritic cells. Two different versions of CD4 were provided by Dr. Blanche Schwappach (Max Planck Institute of Biophysical Chemistry, Göttingen, Germany). CD4-CCAAXX, which contains an artificial tetramerization domain (-CC-) used to assemble Shaker potassium channels into functional channel tetramers in the absence of the T1 domain (Zerangue, 2000), and CD4-AAXX, that contains only the C-terminal dilysine ER localization motif, able to reach the plasma membrane but not to tetramerize. The C-terminus of K_v7.2 channels was fused after the CC domain in order to recover surface expression.

2.2 Mammal cell experimentation techniques

2.2.1 HEK293T cell maintenance

Human embryonic kidney 293 cells, also referred as HEK293, are derived from human embryonic kidney grown in tissue culture. A variant of this cell line is the 293T cell that contains the SV40 large T-antigen that allows for episomal replication of transfected plasmids containing the SV40 origin of replication (pcDNA3.1, pEGFP). This allowed us the amplification of transfected plasmids and extended temporal expression of the desired gene products. The cells grow in a monolayer fashion and are anchorage dependent (adherent cells). HEK293T

cells are maintained at 37 ºC and 5% CO_2 in Dulbecco's Modified Eagle's Medium (Ref.: D0422, Sigma-Aldrich Co., St. Louis, MO, USA), supplemented with non-essential amino acids (Ref.: M7145, Sigma-Aldrich Co., St. Louis, MO, USA) and 10% FBS (Lonza Group Ltd., Basel, Switzerland). When the cells reach around 80-90% confluence, the monolayer is washed with dissociation buffer (Ref.: 13151, Gibco, Life Technologies, Carlsbad, CA, USA) to remove serum traces. Then, a mixture of trypsin-dissociation buffer (Tripsin-EDTA [1X] Ref.: 25300-054, Gibco, Life Technologies, Carlsbad, CA, USA), at a (1:1) is added to detach cells from the flask. After a few minutes in the incubator, DMEM medium is added to resuspend cells and plated into another flask.

P7. CELL PASSAGE
10 min

-Warm medium and trypsin in a water bath at 37 ºC.
-Check cells under the microscope to confirm that the cells are 90 %-100 % confluency.
-Clean hood with ethanol.
-Sterilize all materials, bottles, etc., which are loaded into the hood. Spray hands with ethanol. Jars of liquid need to be sprayed with ethanol. Sterile pipettes may be placed in the hood directly.
-Spray hands with ethanol. Remove flasks from the incubator.
-Connect a Pasteur pipette to the tube attached to the vacuum pump. Turn on the vacuum.
-Using the aspirator, empty liquid media covering cells. Be careful to not touch the pipette to anything outside the flask.
-Add 2 ml dissociation buffer to the flask. Lightly swish buffer on base of the flask. Aspirate.
-Add 1 ml trypsin to the flask. Lightly swish trypsin.
-Place flask into the incubator for 1 min, or until detached.
-While cells are in the incubator, pipette appropriate volume of fresh media into new flasks. Label with name, date, cell type, passage number and passage dilution.
-Check that cells are detached from the surface.
-Add 9 ml of medium to dilute trypsin (the liquid suspension now contains the cells). Carefully resuspend cells.
-Aliquot appropriate cell suspension volumes into freshly prepared flasks with medium.
-Swish media and cells to mix. Place flasks in the incubator.

2.2.2 Cell counting

HEK293T cells are easy to distinguish whether they are alive or not, because of their high refraction to light. From a T75 flask (T75), DMEM+10% FBS is added to detach cells from the surface. 10 µl suspension cells are charged at both sides of the Neubauer chamber (0,1 mm depth BR718905 [Brand GmbH, Wertheim, Germany]) and counted as in Figure 2.1 using a dark-field microscope. Different algorithms have to be followed for the correct calculation of the number of cells per ml.

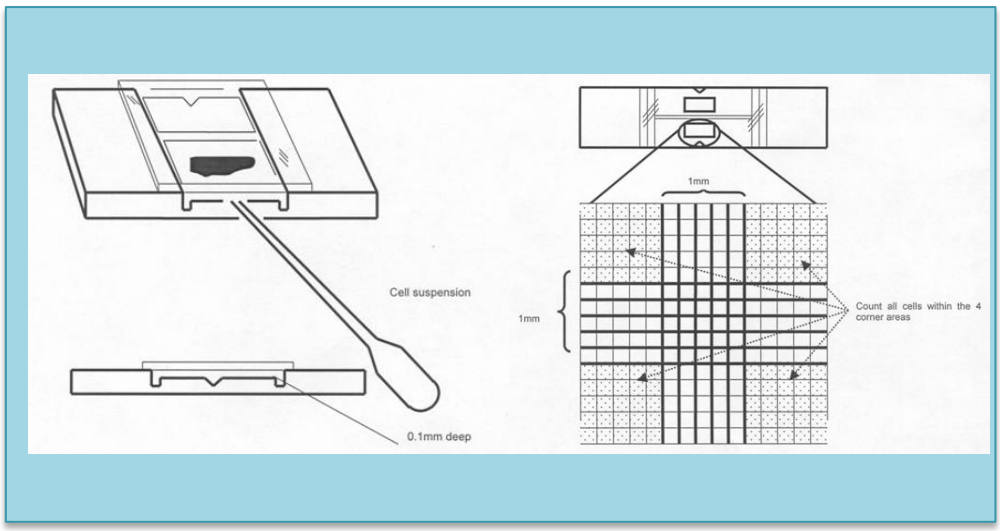

Figure 2.1. Neubauer chamber. Schematic representation of the Neubauer chamber and cell counting procedure.

2.2.3 Cell preservation

For each cryovial, a T75 flask, with fetal bovine serum (FBS) and 10 % DMSO (Ref.: D8418, Sigma-Aldrich Co., St. Louis, MO, USA) is used. Once the cells are in the cryovials, they are immediately place in a frosty minicooler box (Ref.: 5100-

0001, Thermo Fisher Sci. Inc., Rockford, IL, USA) that will allow them to cool down gradually to -80 ºC. To thaw the cells, cryovials are unfreezed at 37 ºC and added to a T75 flask with DMEM medium and 10 % FBS.

P8. CELL PRESERVATION: CELL FREEZING
15 min

-Cells are grown in standard T75 Flask at 70% confluency
-Add 2 ml of dissociation buffer to the flask. Lightly swish buffer on base of the flask. Aspirate
-Add 1 ml trypsin to the flask. Lightly swish trypsin
-Place flask in incubator for 1 min, or until detached
-Add 9 ml of medium to dilute trypsin, (the liquid suspension now contains the cells). Carefully
resuspend cells
-Place cells to 15 ml tubes
-Spin down at 1400 rpm for 5 min at room temperature
-Remove supernatant and add 10 ml DMEM+FBS to the tube
-Repeat step 7
-Resuspend cells into 1 ml of 100 % FBS for each T75 Flask
-Quickly aliquot the cell suspension into three NUNC vials by adding 0,5 ml of cells suspension with 0,5
ml 80 % FBS + 20 % DMSO and immediately place them in a frosty minicooler box
-Place the box in a -70 ºC freezer for 1-2 days, then transfer the individual cryovials into a liquid nitrogen
container for long term storage

P9. CELL PRESERVATION: CELL THAWING
15 min

-Remove cryovial from Liquid Nitrogen and immediately transfer to 37 ºC water bath
-When completely thawed, transfer vial contents to 15 ml test tube containing 3-4 ml of DMEM+10 % FBS.
-Spin down cells at 1400 rpm for 5 min at room temperature.
-Aspirate medium and resuspend pellet in 10 ml of DMEM + 5 % FBS.
-Place into a T75 Flask and incubate at 37 ºC and 5 % CO_2.

CELL MAINTENANCE SOLUTIONS

-Dulbecco´s Modified Eagle´s Medium (DMEM, Ref.: D0422, Sigma-Aldrich Co., St. Louis, MO, USA).
-Non-essential amino acids (Ref.: M7145, Sigma-Aldrich Co., St. Louis, MO, USA).
-10 % Fetal bovine serum (FBS, Lonza Group Ltd., Basel, Switzerland).
-Dissociation Buffer (Ref.: 13151, Gibco, Life Technologies, Carlsbad, CA, USA).
-Trypsin-EDTA (1 x), phenol red (Tripsin-EDTA [1X] Ref.: 25300-054, Gibco, Life Technologies, Carlsbad, CA, USA).
-Dimethyl sulfoxide (Ref.: D8418, Sigma-Aldrich Co., St. Louis, MO, USA).

2.2.4. Cell transfection

All DNA used to transfect cells were purified by alkaline lysis and affinity columns from a 100 ml of bacteria culture (Genopure Plasmid Midi Kit [Ref.: 3143414, Roche Applied Science, Penzberg, Germany]). DNA was quantified in a Cary 3 Bio spectrophotometer (Varian Inc., Agilent Tech., Palo Alto, CA, USA) taking as reference a quartz cuvette with MilliQ water. DNA is measured at λ_{260} (1 O.D. $_{A260}$ <> 50 μg / ml DNA) and at λ_{280} to estimate the amount of protein in the sample. The ratio between $\lambda_{260}/\lambda_{280}$ gives information of the purity of the extracted DNA.

There are various methods of introducing foreign DNA into a eukaryotic cell, but most of the times the calcium phosphate transfection method was used.

2.2.4.1 Calcium phosphate transfection method

The method described here is a modification of some of the original methods (cheaper, simpler, quicker and non toxic) but as well more reliable and consistent. The day before transfection cells must be at least at 30-40 % of confluency. Next morning, 4 hours before transfection, the medium is replaced (DMEM+10 % FBS) and supplemented with gentamycin (Ref.: G1397, Sigma-Aldrich Co., St. Louis, MO, USA). This seems to help the transfection efficiency at least in part by helping boost cell cycle progression and therefore increasing entry into mitosis

where DNA is taken up into the nucleus. Later in the day, cells can be transfected. First, a mixture between DNA and A Solution (250 mM $CaCl_2$) is prepared and added to another tube with HBS solution (50 mM HEPES, 1,5 mM Na_2HPO_4, 140 mM NaCl pH: 7.05). After 1 minute, the mix is added to the cells. After 10-12 hours, the medium is removed and changed with a new one supplemented with gentamycin.

P10. CALCIUM PHOSPHATE TRANFECTION PROTOCOL
4 H, 25 min

-0.15 ml of A Solution is added in a sterile tube.
-Appropriate DNA amount to each tube is added. Mix contents of each tube.
-In a second tube, prepare 0.15 ml of HBS solution.
-Add tube one to tube two. Let sit for at least 1 min.
-Add transfection mixture to flasks in drop wise fashion, mix by rocking back and forth and put in 5 % CO_2 incubator (using a 5 % CO_2 incubator is important).
-Change media next day with fresh DMEM+10 % FBS+ gentamycin.

SOLUTIONS OF CALCIUM PHOSPHATE TRANSFECTION PROTOCOL

Solution A: ($CaCl_2$ solution)

-250 mM $CaCl_2$ (tissue culture grade).
Dissolve in MilliQ water and sterilize by filtration (0.22 µm).

Solution B: (HBS [HEPES buffered saline] solution)

-50 mM HEPES
-1,5 mM Na_2HPO_4
-140 mM NaCl
Dissolve in MilliQ water and adjust pH to 7.05 with NaOH or 1 M HCl. Sterilize by filtration (0.22 µm).
-Gentamycin (Ref.: G1397, Sigma-Aldrich Co., St. Louis, MO, USA)

2.2.4.2. Lipofectamine transfection method

Only used for the electrophysiology experiments, lipofectamine (Lipofectamine 2000, Invitrogen, Life Tech., Carlsbad, CA, USA) is based on liposomes that can be easily merged with the cell membrane since they are both made of a phospholipid bilayer. Lipofectamine generally uses cationic lipids to form an aggregate with the anionic genetic material. The main advantage of Lipofectamine is its high efficiency. The disadvantage is its high price and toxicity.

P11. LIPOFECTAMINE TRANFECTION PROTOCOL
6 H, 25 min

-Prepare 2 tubes:
DNA mixture: dissolve 1.5 µg of DNA in 0,25 ml of DMEM uncompleted.
Lipofectamine mixture: dissolve 10 µl of Lipofectamine in 250 µl of DMEM uncompleted.
-Incubate for 3-5 minutes and then add to the DNA mix.
-Incubate the DNA-Lipofectamine mixture for at least 20 minutes.
-Remove the DMEM medium from cells to transfect, wash once with PBS and add 1,5 ml of DMEM uncompleted.
-Add DNA-Lipofectamine mixture (all the mixture should be 0,5 ml) and incubate for not more than 6 hours.
-Remove DMEM from transfected cells, wash once with PBS and add 2 ml complete DMEM.
-Next day, remove DMEM and add new complete DMEM.

2.2.5. Protein extraction

Protein extraction is performed to observe the transient protein expression in eukaryotic cells. Around 180.000 cells are seeded in each T25 flask and transfected following protocol P7. and P10. After 36 hours of cell transfection, protein extraction is done as follows:

P12. PROTEIN EXTRACTION PROTOCOL
2 H, 25 min

-Media is removed from cells and washed twice with 2 ml phosphate buffered saline buffer (PBS), and then the solution is aspirated.
-1.5 ml of a mixture of trypsin-EDTA/dissociation buffer (1:1) is added to the flask to remove adhered cells.
-After 2-3 min in the incubator, the adhered cells are lifted from the bottom of the plate.
-Detached cells are transferred to 1.5 ml tubes.
-Steps 1-3 are repeated for every treatment plate.
-The 1.5 ml tubes are centrifuged for 15 min at 1.500 rpm and the media supernatants is aspirated from the tubes.
-0.2 ml of lysis buffer (TNE 1X [TNE 10X: 0,5 M Tris-HCl pH 7.5, 50 mM EDTA, 1 M NaCl], 0,5 % NP-40, 1 tablet Protease Inhibitor Cocktail is added to each pellet to lyse cells.
-Cells are left on ice for 30 min and vortexed every 10 min.
-Cell lysates are centrifuged at 2.500 rpm for 15 min at 4 °C to remove nucleus.
-Clear lysate is transferred to clean 1.5 ml tubes.
-Cell lysates are centrifuged at 13.000 rpm for 15 min at 4 °C to remove membranes.
-Clear lysate is transferred to clean 0.5 ml tubes and loading buffer (LB 5X) is added (LB 5X: Tris-HCl 0.25 M pH 6.8, 50 % glycerol, 10 % SDS, 0.0125 % 2- betamercaptoethanol).

PROTEIN EXTRACTION PROTOCOL SOLUTIONS

-Lysis Buffer ([TNE 10X: 0.5 M Tris-HCl pH 7.5, 50 mM EDTA, 1 M NaCl] + 0.5 % NP40).
-Protease Inhibitor Cocktail (cOmplete Mini, EDTA-free, Ref.: 11836170001, 25 Tablets, Roche, Mannhein, Germany).
-Loading buffer (LB 5X: Tris-HCl 0,25 M pH 6.8, 50 % glycerol, 10 % SDS, 0.0125 % 2-betamercaptoethanol).

2.2.6. Western blot

Western blot, discovered by George Stark and given the name by a parallelism to the northern and southern blot, is a technique that allows to determine the molecular weight of a protein and to measure relative amounts of the protein

present in different samples. $K_v7.2$ and $K_v7.3$ subunits as well as Tac chimeras, were resolved in 8 % SDS-PAGE (H_2O, 30 % acrylamide mix (Mini-Protean II Bio-Rad Lab., Hercules, CA, USA), 1.5 M Tris pH 8.8, 10 % SDS, TEMED). Calmodulin was resolved in 15 % SDS-PAGE. The proteins are transferred to PVDF blotting paper (Inmobilon-P [Ref.: IPVH00010, EMD Millipore Corp., Billerica, MA, USA]) previously activated before by using methanol/ethanol, and incubated later with a generic protein (such as milk or BSA, depending on the type of protein) to bind to any remaining sticky places on the PVDF blotting paper. The antibody is then added to the solution, where it binds to its specific protein. After washing the membrane, the secondary antibody is then added, and after an hour washed again with PBS-Tween20 to remove traces of antibody. The secondary antibody has the horseradish peroxidase enzyme (HRP) which allows the reaction that emits light during the enzyme catalyzed decomposition when mixed with the enhanced chemiluminescence (ECL) solutions (Ref. 32106 Pierce ECL Western Blotting Substrate, Thermo Fisher Scientific, Waltham, Massachusetts, USA).

P13. WESTERN BLOT PROTOCOL
28 H

-Run the proteins in an appropriate gel according to their molecular weight until the blue front is at the bottom of the gel (running conditions: 80 V).
-Leave in electro-transfer buffer on shaker for 5 minutes.

Transfer
-Blot onto a PVDF membrane. Pre-wet materials in transfer buffer. Stack in the following order: case (clear side)-sponge-Whatman paper-PVDF membrane-gel-Whatman paper-sponge-case (black side).
-Place in the transfer apparatus with black side facing black; 400 mA x 1 H using an ice pack to cool down the apparatus.

P13. WESTERN BLOT PROTOCOL (Continuation)

Blotting

-Block the membrane overnight in 20 ml 1X PBS + 5 % non-fat dry milk + 0.1 % Tween 20, in a tube of 50 ml on a shaker at 4 ºC.

-Primary antibody: Incubate with primary antibody diluted 1:1000 in 10 ml of 1X PBS + 5% non-fat dry milk + 0.1 % Tween20. Incubate 1 H at RT. The primary antibody mixture can be re-used storing at -20 ºC.

-Wash 3 times for 10 min in 15 ml 1XPBS + 0.1 % Tween20 at RT in a shaker

-Secondary antibody: Incubate with secondary antibody diluted 1:3000 in 10 ml of 1x PBS 0.1 % Tween 20, for 1 H.

-Wash 5 times for 10 min in 15 ml 1X PBS + 0.1 % Tween20 at RT in a shaker.

-Detect protein with ECL kit (2 ml/membrane). In a separate tube, mix black and white ECL solutions.

in a 1:1 ratio. Aliquot solution onto membranes and wait for 1 min. Capture images with the Versadoc.

Imaging System (Ref.: 1708010, Bio-Rad Lab., Hercules, CA, USA).

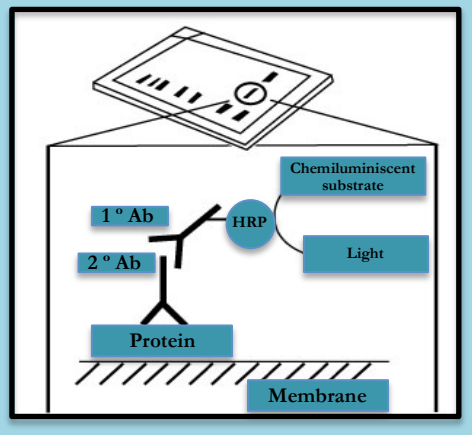

2.2.7. Flow cytometry

This technique is useful as it allows the quantification of cells having surface expression when cotransfected with one of our constructs. The result, once the cells have passed through the cytometer, is an histogram in which we can distinguish cells that have not been transfected (value of relative fluorescence 10^1 in a logarithmic scale), cells transfected but with a low surface expression (value of relative fluorescence 10^1-10^2 in a logarithmic scale) and those transfected and with high surface expression (value of relative fluorescence 10^2 in advance in a logarithmic scale). Fluorophores are typically attached to an antibody that recognizes a target feature on or in the cell.

The detectors are located at the point where the flux of cells passes through the light broad: one in line with the light beam (Forward Scatter or FSC) and several perpendicular to it (Side Scatter or SSC). Each cell passing through the beam scatters the ray, and fluorescent chemicals found in the particle or attached to the particle may be excited, emitting light at a longer wavelength than the light source. This combination of scattered and fluorescent light is picked up by the detectors and, by analyzing fluctuations in brightness at each detector (one for each fluorescent emission peak), it is then possible to derive various types of information about the physical and chemical structure of each individual particle. While FSC correlates with the cell volume, SSC depends on the inner complexity of the particle such as shape. The immunolabeled samples were analyzed in the Gallios Flow Cytometer (Ref.: 775014, Beckman Coulter, Brea, CA, USA), exciting cells at 395 nm (the excitation peak of the GFP) and at 488 nm (the wavelength of the antibody fluorophore). The software of the cytometer allows us to select just the cells that present a reasonable shape and size and also those that

have a minimum cell expression. At least 10.000 cells with those characteristics are captured and afterward analyzed.

The obtained histograms are analyzed with the WinMDI 2.9 free software (www.facs.scripp.edu/software.html), where cells with low expression and those aggregated and/or death can be removed and analyzed the rest. Data is represented using Excel.

P14. FLOW CYTOMETRY PROTOCOL
6 H

Fixation
-Separate a fraction of cells to be analyzed by western blot (250 µl) (See protocol P13.).
-Centrifuge cells at 3.000 rpm for 15 min and aspirate supernatant.
-Resuspend cells in 700 µl PFA 3%/1X PBS and leave at RT in a tube shaker.
-Centrifuge cells at 3.000 rpm for 10 min and aspirate supernatant.

Blocking
-Resuspend cells in 700 µl of BSA 5 %/ 1X PBS and incubate 30 min in a tube shaker.
-Centrifuge cells at 3.000 rpm for 10 min and aspirate supernatant.

Immunostaining
-Resuspend cells in 400 µl of 1:1.000 antibody/ BSA 0,5 %/ 1X PBS.
-Incubate for 1 hour at room temperature.
-Centrifuge cells at 3.000 rpm for 10 min and aspirate supernatant.
-Wash cells for 15-20 min with 500 µl BSA 5 %/ 1X PBS.
-Resuspend cells in 400 µl 488 conjugated secondary antibody, 1:1.000 / BSA 0,5 %/ 1X PBS
-Incubate for 1 H at room temperature.
-Wash cells for 15-20 min with 500 µl BSA 5 %/ 1X PBS.
-Resuspend cells in 500 µl 1X PBS and analyze with the flow cytometer.

2.2.8 Immunoprecipitation (IP)

The immunoprecipitation (IP) is one of the most commonly used methods to analyze the interaction between two proteins. An antibody for the protein of interest is incubated with a cell extract so that the antibody binds the protein in

solution. The antibody/antigen complex will then be pulled out of the sample previously fixed to a in the protein A/G-coupled agarose beads (Protein G Sepharose, Fast Flow Ref: P3296, Sigma-Aldrich Co., St. Louis, MO, USA; Protein A from *Staphylococcus aureus*, Ref: P6031, Sigma-Aldrich Co., St. Louis, MO, USA), depending on the host of the primary antibody. This physically isolates the protein of interest from the rest of the sample. The sample can then be separated by SDS-PAGE for western blot analysis and detected with specific antibodies.

P15.
IMMUNOPRECIPITATION PROTOCOL
72 H

Protein-Sepharose preparation (previous day of IP)
-Protein-sepharose is incubated with H_2O mQ to rehydrate until a final volume of 90 µl/group.
-Protein-sepharose is resuspended in RIPA buffer and transferred to clean 15 ml tubes, leave at 4 ºC overnight with gentle agitation.
-Half of this protein is transferred to new 15 ml tubes and incubated with the specific antibody (1:1.000) at 4 ºC overnight with gentle agitation.

Preparation of lysates
-Remove medium form the flask and wash the cells with PBS.
-Drain the PBS and add 1.5 ml of a mix of trypsin-EDTA/dissociation buffer (1:1).
-Transfer the cell suspension into a 15 ml tube and put then into ice.
-Separate a fraction of cells to be analyzed by western blot (250 µl) (Pre-IP sample) (See protocol P13.).
-Centrifuge 1.500 rpm 15 min at 4 °C.
-Aspirate the supernatant and add 400 µl of RIPA buffer.
-Left tubes on ice for 30 min and vortex every 10 min.
-Cell lysates are centrifuged at 2.500 rpm for 15 min at 4 °C to remove nucleus.
-Clear lysate is transferred to clean 1.5 ml tubes.
-Cell lysates are centrifuged at 13.000 rpm for 15 minutes at 4 °C to remove membranes.
-Clear lysate is transferred to clean 1.5 ml tubes.

Pre-clearing the lysates
-Pre-clearing the lysate help to reduce non-specific binding of proteins to sepharose beads. The end result will be a lowering of background and an improved signal-to-noise ratio.
-Incubate the cell extract with the protein-sepharose without antibody for 1 H at 4 ºC with gentle agitation.
-Spin in centrifuge at 4.000 rpm at 4 °C for 10 min.
-Discard bead pellet and keep supernatant for immunoprecipitation.

P15. IMMUNOPRECIPITATION PROTOCOL, 72 H (Continuation)

Immunoprecipitation

-Wash twice the beads with antibody to remove the excess of it with RIPA buffer.
-Add 400 µl of the protein-sepharose to the supernatant to immunoprecipitate the complex.
-Incubate the lysate-beads mixture at 4 °C under rotary agitation for 24 H.
NOTE: It is advisable to use pipette tips with the end cut off to prevent damage to the beads.

Elution

-Centrifuge the tubes, remove supernatant and wash the beads in RIPA buffer three times (each time centrifuging at 4 °C and removing the supernatant).
-Remove the last supernatant and add 60 µl of 5X loading buffer.
-Boil at 95-100 °C for 5 min to denature the protein.
-Centrifuge at 3.000 rpm and keep the supernatant.
-Run samples on a SDS-PAGE. See P13.

2.2.9 Immunofluorescence

To detect those proteins that are expressing at the membrane is necessary to have antibodies that can recognize extracellular epitopes. Sometimes, the epitopes can be sensible to the fixation process, so, in that cases, it is useful to test different methods to be sure that the cell membrane is not being permeabilized. The extracellular loop of $K_v7.2$ that connects transmembrane domains S1 and S2 is tagged with two HA epitopes. To increase the accessibility, the epitope is flanked with fragments from the extracellular D1-D2 loop of the ClC-5 chloride channel. This insertion changes the sequence between transmembrane domains S1 and S2 to ^{115}KEYEKSSEGSEH**YPYDVPDYAG****YPYDVPDYA**VTFEERDKCPE-WNA^{126}. Images from stain cells are captured using a 60X oil objective on a Nikon Eclipse TE2000-U fluorescence microscope (Nikon Instr., Tokyo, Japan) equipped with a confocal module using a 30 µm pinhole. Image acquisition and analysis are performed blind, with no

previous knowledge of the transfected construct. Fluorophores are excited with a 408 nm laser (Coherent Inc., Santa Clara, CA, USA) for CFP, or a 560 nm laser line (CVI Melles-Griot, Albuquerque, NM, USA) for AlexaFluor 594. The emission filters used are BA 485/40 (Chroma Tech. Corp., Bellows Falls, VT, USA) for CFP and BA593/40 (Nikon Corp., Tokyo, Japan) for AlexaFluor 594.

P16.
IMMUNOFLUORESCENCE PROTOCOL
72 H

Treatment of coated coverslips
-Sterilized each side of the coverslip with U.V light, 10 min.
-Treat coverslips for 30 min with 1 mg/ml poly-L-Lysine/PBS 1X (reusable).
-Wash coverslips with PBS 1X to remove the excess of poly-L-Lysine.

Seed cells
-Cells are grown in standard M6 plates at 40 % confluency with 3 ml of DMEM + 10 % FBS.

Transfection of the cells
-24 H after seeding and 4 H before transfection, the medium is replaced (DMEM+10 % FBS) and supplemented with gentamicine.
-Later, cells are transfected with the calcium phosphate protocol (P10.).
-Next day, medium is replaced (DMEM+10 % FBS) and supplemented with gentamicine.

Immunostaining
-Coverslips are washed twice with PBS 1X.
-Cells are fixed with 3 % paraformaldehyde/PBS for 20 min.
-Coverslips are washed three times with PBS.
-To block cells, coverslips are pre-incubated for 30 min with 5 % BSA/PBS 1X.
-Primary antibody (1:1.000 in 5 % BSA/PBS 1X) is added for 1 H.
-Cells are washed 3 times for 5 min in 5 % BSA/PBS 1X.
-Secondary antibody (1:1.000 AlexaFluor –conjugated in 5 % BSA /PBS 1X) is added for 1 H.
-Cells are washed three times in PBS 1X and mounted with ProLong Antifade reagent.

2.2.10 Electrophysiological recordings

The patch clamp technique was developed as an improvement of the classical voltage-clamp technique (Sakman and Neher, 1983). The principal advantage of this method is the use of a single microelectrode with a relatively large tip opening

(1-2 μm) for stimulation and acquisition of the electrical signals. Measurements of the plasma membrane current were performed with the whole-cell and perforated-patch configurations of the patch clamp technique (Hamill et al., 1981; Horn and Marty, 1988). HEK393T cells were used for whole-cell patch recordings, which were obtained at R.T. (21-25°C) 48 h after transfection using lipofectamine 2000 (Invitrogen, Life Tech., Carlsbad, CA, USA). Cells were bath-perfused with the following solution (in mM): 10 HEPES, 140 NaCl, 4 KCl, 2 $CaCl_2$, 2 $MgCl_2$, 5 D-glucose, adjusted to pH 7.4 with NaOH. Osmolarity was adjusted with mannitol to ~315 mOsm. Pipettes were pulled from borosilicate glass capillaries (Sutter Instruments, USA) with a Narishige micropipette puller using a PC-10 micropipette puller (Narishige Group, Japan). Membrane currents were measured using an EPC-8 amplifier (HEKA Elek., Lambrecht, Germany) with pipette and membrane capacitance cancellation. Pipettes were filled with an internal solution containing (in mM): 10 HEPES, 125 KCl, , 5 $MgCl_2$, 5 EGTA, 5 Na_2ATP, adjusted to pH 7.2 with KOH and osmolarity adjusted to ~300 mOsm with mannitol. The access resistance was typically 2-3 MΩ. The amplitude of the K_v7 current was defined as the peak difference of the current relaxation measured at -30 mV after 1.500 ms pulses to -120 mV (all channels closed) and to +60 mV (all channels opened). The data were acquired and analyzed using pCLAMP software (version 8.2 [Molecular Devices Corp., Sunnyvale, CA, USA]), normalized in Excel (Microsoft Corp., Redmond, WA, USA) and plotted in SigmaPlot (Systat Soft., Chicago, IL, USA). The data is shown as the mean ± S.E.M. (n indicates the number of samples). The differences between the means were evaluated using the unpaired Student's t test and values of $P \leq 0.05$ were considered significant. Those experiments were performed with the help of Dr. Carolina Gomis Perez.

2.2.11 Xenopus oocytes experimentation technique

Xenopus laevis is a popular model system to study aspects related to the structure and the function of potassium channels and their receptors. *Xenopus* oocytes are very large cells (around 1 mm of diameter) which are easy to culture and do not contain many intrinsic channels and receptors. The protein expression process contains different steps, which includes cRNA synthesis, preparation of oocytes and cytoplasmic microinjection of cRNA. These experiments were done under the supervision of Dr. Paloma Aivar Mateo.

2.2.11.1 cRNA synthesis

For functional studies, channel subunits were subcloned into the psrC5 vector that is flanked by the non-coding 5´ region of the globin gene of *Xenopus* and the 3´ polyA of SV40, which are not translated but that increase the stability of the cRNA. After the linearization of the cDNAs with ApaL I, the cRNAs were synthesized *in vitro* with the T7 transcription kit (Ambion, Life Tech., Carlsbad, CA, USA).

P17. cRNA SYNTHESIS PROTOCOL
2 H

-Thaw the frozen reagents and place the RNA polymerase on ice. All reagents should be microfuged briefly before opening to prevent loss and/or contamination of material that may be present around the rim of the tube.
-Assemble transcription reaction at R.T.

Linear DNA	Nuclease free-H_2O	NTP	Reaction buffer	Enzyme mix
1 µg/µl 2 µl	4 µl	2X 10 µl	[10X] 2 µl	2 µl

P17. cRNA SYNTHESIS PROTOCOL
2 H (Continuation)

-Mix thoroughly.
-Incubate at 37 °C, 1 H.
-Stop the reaction and precipitate the RNA by adding 30 µl nuclease-free water and 30 µl LiCl precipitation solution.
-Mix thoroughly. Chill for ≥ 30 min at -20 ºC.
-Centrifuge at 4 °C for 15 min at maximum speed to pellet the RNA.
-Carefully remove the supernatant. Wash the pellet once with ~ 1 ml 70 % ethanol, and re-centrifuge to maximize removal of unincorporated nucleotides.
-Carefully remove the 70 % ethanol, and resuspend the RNA in TE. Determine the RNA concentration by using a spectrophotometer at 260/280 nm.

2.2.11.2 Oocyte preparation and RNA injection

After anesthetizing the frogs, oocytes were extracted and only those in stage V or VI were selected and defolliculated enzymatically with 1 mg/ml collagenase (Ref.: C9891, Sigma-Aldrich Co., St. Louis, MO, USA), in Ca^{2+}-free OR2, n the following buffer (in mM): 5 HEPES, 82.5 NaCl, 2.5 KCl and 1 $MgCl_2$, pH 7.5. Then, oocytes were transferred to a Ca^{2+}-containing solution (ND96) consisting of (in mM): 5 HEPES, 96 NaCl, 2 KCl, 1.8 $CaCl_2$, 1 $MgCl_2$, pH 7.5 and supplemented with 100 units/ml of penicillin, 0,1 mg of streptomycin and 0,25 mg/ml of gentamycin. The oocytes were injected with 50 nl of a solution which approximately contains 20 ng of cRNA and keep for 3 days at 19 ºC before starting with the electrophysiological recordings.

P18. OOCYTE PREPARATION PROTOCOL
1 H

-Anesthetize female frogs by using MS-222 (ethyl 3-aminobenzoate methanesulfonate salt, Ref: A-5040, Sigma-Aldrich Co., St. Louis, MO, USA) for 15-30 min.
-Carefully dislodge the oocytes from the surrounding tissue with a wire loop and treat with type A collagenase (Ref: C-9891, Sigma-Aldrich Co., St. Louis, MO, USA) at 1 mg/ml in OR2 without Ca^{2+}, (in mM): 5 HEPES pH 7.5, 82.5 NaCl, 2.5 KCl, 1 $MgCl_2$.
-Recover oocytes and wash twice in OR2 with Ca^{2+}, (in mM): 5 HEPES pH 7.5, 96 NaCl, 2 KCl, 1 $MgCl_2$, 1.8 $CaCl_2$.
-Media should be supplemented with antibiotics penicillin/streptomycin (0.1 mg/ml).

2.2.11.3 Two-electrode voltage clamp recordings

This technique is used to measure the whole-cell ion channel currents while controlling the membrane potential. It uses two separate electrodes unlike the whole cell patch clamp, one measuring the voltage and the other one injecting the current. The membrane potential is clamped at the desired level (Vh) by injecting current into the oocyte via a second electrode. Any change in membrane current caused by opening or closure of ion channels is immediately followed by a change in the current (equal in amplitude but opposite in sign) at the output of the amplifier (Geneclamp 500B amplifier, [Axon Instr., Molecular Devices Corp., Sunnyvale, CA, USA]) connected to the current electrode. The amplifier output is monitored on a graphic recorder (DIGIDATA 1320A, [Axon Instr., Molecular Devices Corp., Sunnyvale, CA, USA]) that in turn is controlled by the pCLAMP software (version 8.1, Axon Instr. Molecular Devices Corp., Sunnyvale, CA, USA). Electrophysiological recordings were performed 3 days after being microinjected and were perfused continuously in *Xenopus* saline made with (in mM): 5 HEPES 100 NaCl, 2.5 KCl, 1 MgCl2, 2 MnCl2, pH 7.5. All chemicals, except stated otherwise, were from Sigma (Sigma-Aldrich Co., St. Louis, MO, USA). The electrodes were made of borosilicate that were filled with 3 M KCl and

had resistances of 1MΩ. Data were acquired at a sampling rate of 1 KHz and filtered at 100 Hz. Voltage-step protocols and current analysis were performed with the pCLAMP 8.1 software (Axon Instr., Molecular Devices Corp., Sunnyvale, CA, USA). These experiments were performed by Dr. Carolina Gomis Perez. Current values represent the average (±S.E.) of the maximal conductance obtained from the fit of the g–V relationship to the Boltzmann equation:

$$I = I_{max} / [1 + Exp ((V_{1/2} - V_m)/ slope)]$$

where:

I = tail current amplitude in an 800 ms voltage step to – 20 mV

$\mathbf{I_{max}}$ = is the maximal current

$\mathbf{V_{1/2}}$ = membrane potential at which the current is half Imax

Vm = membrane potential (pulse)

S = slope

2.2.11.4 Luminescence assay

To estimate the number of channels located at the surface of the oocyte plasma membrane, the method described by Schwake *et al.* (2000) was followed. All the K_v7 subunits used were tagged with an HA epitope in the extracellular loop that connects transmembrane domains S1 and S2 (kindly provided by Prof. Thomas J. Jentsch, Max-Delbrück-Centrum für Molekulare Medizin, Berlin, Germany). Oocytes were injected with 20 ng cRNA and a 1:1 ratio of the $K_v7.2/K_v7.3$ group. Oocytes without injection were used as the negative control. After 3 days at 19 °C, the oocytes were placed in ND96 with 1 % BSA (ND96/ BSA) at 4 °C for 30 min

to block unspecific binding. Subsequently, the oocytes were incubated in ND96/BSA for 60 min at 4 °C with 1 μg/ml rat monoclonal anti-HA antibody (Ref.: 3F10, Roche Applied Science, Penzberg, Germany), washed with ND96/BSA and incubated in ND96/BSA with HRPcoupled secondary antibody for 60 min (goat anti-rat antigen binding fragments [Jackson ImmunoResearch, West Grove, PA, USA]). Finally, the oocytes were washed thoroughly with ND96/BSA and then with ND96 alone to eliminate the background signal produced by BSA. Individual oocytes were placed in 50 μl power signal ELISA solution (Thermo Fisher Sci. Inc., Rockford, IL, USA) and chemiluminescence was quantificated in a Sirius luminometer (Berthold Tech. GmbH, Pforzheim, Germany).

2.2.12 Drug treatment for degradation assays

Transfected HEK293T cells grown in T25 flasks were treated with cycloheximide (CHX, 75 μg/mL, Ref: C4859, Sigma-Aldrich Co., St. Louis, MO, USA) for distinct times and then analyzed by western blotting. For lysosomal inhibition, cells were treated 10 h with 50 μM chloroquine (Ref: C6628, Sigma-Aldrich Co., St. Louis, MO, USA) (Su *et al.*, 2011) and with 20 μM MG132 (Ref: 474790, Merck KGaA, Darmstadt, Germany) for proteosomal inhibition (Soldovieri *et al.*, 2006). After degradation, the remaining proteins were separated by SDS-PAGE and analyzed by western blotting using anti-Myc or anti-GFP. Anti-tubulin antibody was used in both cases as a loading control.

2.3 Protein purification and fluorescence assays

2.3.1 GST fusion protein purification

The following C-terminal Kv7.2 channel sequences:

- G_{310}-L_{548} (AB wt)
- G_{310}-L_{548}–ΔT_{359}-T_{501} (AB-Δ2)
- G_{310}-L_{548}–ΔT_{359}-T_{501} (ABCD-Δ2)
- G_{310}-L_{548}–ΔT_{359}-T_{501} (AB-Δ2-ST)

were subcloned into the pGEX-3X (AB wt) or pGEX-6P1 GST (AB-Δ2), (ABCD-Δ2) and (AB-Δ2-ST) fusion vectors (Ref.: 27-4803-01 and 27-4597-01, respectively [GE Healthcare, Little Chalfont, UK]) and transformed into BL21-DE3 *E. Coli.*

Cells were grown at 37 °C in LB medium containing 100 μg/ml ampicillin till A_{600} 0.6-0.8. The expression of the fusion proteins was induced with 0.3 mM of IPTG for 3 h at 30 °C. Cells were harvested by centrifugation and suspended in 20 ml of chilled GST buffer [20 mM Tris-HCl (pH 7.4), 100 mM NaCl, 0.5 % Triton X-100, 2 mM D, plus half tablet of Protease Inhibitor Cocktail Roche Applied Science, Penzberg, Germany]. After lysis by sonication, cell debris were removed by centrifugation at 80.000 g for 30 min at 4 °C. Finally, the supernatant (soluble fraction) was transferred to a fresh tube while the insoluble cell lysate (inclusion bodies) was treated separately.

The inclusion bodies isolated by centrifugation were resuspended three times in 10 ml of the same buffer used for sonication and then centrifuged to remove any remaining soluble material. The precipitate was dissolved for 30 min at 4 °C in 5

ml of 20 mM Tris-HCl (pH 7.4), 100 mM NaCl, 2 mM DTT and 6 M urea, mixing occasionally. The solution was centrifuged at 20.000 g for 20 min at 4 °C and the supernatant was diluted to a final concentration of aproximatelly 1 mg/ml. Refolding was done with an "urea concentration gradient dialysis". The solution of denatured protein was dialyzed against 2 L of freshly made 4, 2, 1, 0.5, and 0 M Urea, with 20 mM Tris-HCl (pH 7.4), 100 mM NaCl and 2 mM DTT. For each concentration the protein was dialyzed 10 h at 4 °C.

The soluble fraction and refolded proteins were incubated separately with glutathione-sepharose 4B (Ref.: 17-0756-01, GE Healthcare, Little Chalfont, UK) previously equilibrated with GST buffer. Bound proteins were washed and then eluted with 50 mM Tris-HCl (pH 8.5) and 15 mM of reduced glutathione (Ref.: G4251, Sigma-Aldrich Co., St. Louis, MO, USA). Proteins in various fractions were identified on 10-12 % SDS-PAGE gels, dialyzed, concentrated and stored at -20 °C. The protein concentration was determined using the Bradford method (Bradford, 1976). The initial experiments (see later) were performed with proteins purified from the soluble fraction to ensure that they were properly folded. In latter experiments, fusion proteins were solubilized from inclusion bodies with 6 M urea and then refolded. The results obtained with these proteins were indistinguishable from the soluble material. Additionally, dispersion of the samples was evaluated by dynamic light scattering using a Zetasizer Nano Instrument (Malvern Instr. Ltd., Malvern, Worcestershire, UK) to exclude the presence of aggregates. The correlation function and the polydispersity index (less than 0.2) demonstrated that the proteins were monodispersed, and that no aggregates were present. These experiments were performed under the supervision of Dr. Alessandro Alaimo.

P19. PURIFICATION OF GST FUSION PROTEINS PROTOCOL 5 D

-Grow the cells at 37 °C in 1 L of LB medium containing 100 μg/ml ampicillin until A_{600}= 0.6-0.8. Induce protein expression for 3 h at 30 °C with 0.3 mM IPTG.
-Harvest the cells by centrifugation and resuspend the pellet in 20 ml of chilled GST buffer (20 mM Tris-HCl [pH 7.4], 100 mM NaCl, 0.5 % Triton X-100, 2 mM DTT, half a tablet of the protease inhibitor cocktail "1x Complete" [Roche]). After lysis by sonication, remove the cell debris by centrifugation for 30 min at 80,000 g and 4 °C. Transfer the supernatant (soluble fraction) to a fresh tube while the insoluble cell lysate (inclusion bodies) is treated separately.
-Resuspend the inclusion bodies in 10 ml GST buffer and then centrifuge again to remove any remaining soluble material. Repeat this operation three times. Dissolve the precipitate in 5-10 mL solubilization buffer (20 mM Tris-HCl [pH 7.4], 100 mM NaCl, 2 mM DTT and 6 M urea) for 30 min at 4 °C mixing occasionally. Centrifuge for 20 min at 20,000 g and 4 °C, and dilute the supernatant to a final concentration of ~1 mg/ml. Refold the proteins with urea concentration gradient dialysis. Dialyze the protein against 2 L of freshly made refolding buffer (20 mM Tris-HCl [pH 7.4], 100 mM NaCl and 2 mM DTT), containing 4, 2, 1, 0.5 or 0 M urea. Filter all the buffers before use, gradually reducing the concentration of urea. At each urea concentration, dialyze the proteins for 8-10 h at 4 °C. Centrifuge at 30,000 g for 30 min at 4 °C to remove any aggregates and recover the supernatant.
-Incubate the soluble fraction and refolded proteins separately with Glutathione Sepharose beads previously equilibrated with GST buffer. Wash the resin three times before transferring it to a disposable column and elute the fusion proteins with 10-20 ml of elution buffer (50 mM Tris-HCl [pH 8.5] and 15 mM glutathione reduced).
-Analyze the fractions obtained on 10-15 % SDS-PAGE gels and dialyze to remove the glutathione against a buffer of choice at 4 °C. Concentrate the proteins if needed and store at -20 °C. Determine the protein concentration using the Bradford method.
-Incubate the soluble fraction and refolded proteins separately with Glutathione Sepharose beads previously equilibrated with GST buffer. Wash the resin three times before transferring it to a disposable column, and elute the fusion proteins with 10-20 ml of elution buffer (50 mM Tris-HCl [pH 8.5] and 15 mM glutathione reduced).
-Analyze the fractions obtained on 10-15 % SDS-PAGE gels and dialyze to remove the glutathione against a buffer of choice at 4 °C. Concentrate the proteins if needed and store at -20 °C. Determine the protein concentration using the Bradford method.

2.3.2 Calmodulin purification

The rat CaM gene was transformed into BL21-DE3 *E. Coli* bacteria kindly provided by Dr. Antonio Villalobo Polo ("Instituto de Investigaciones Biomédicas Alberto Sols", Madrid, Spain). CaM gene was cloned into the expression vector pET-14b (Ref.: 69660-3, EMD Millipore Corp., Billerica, MA, USA).

The *E. Coli* transformant cells were grown at 37 °C in LB medium containing 100 μg/ml ampicillin until A_{600} 0.8-1. The expression of the fusion proteins was induced with 0.4 mM of IPTG for 4-6 h at 37 °C. Cells were harvested by centrifugation for 10 min at 5.000 rpm using a JLA-9.1000 rotor (Beckman Coulter Inc., Brea, CA, USA). The bacterial pellet was washed twice in 50 mM Tris–HCl (pH 7.5) containing 2 mM EDTA and 0.2 mM phenylmethanesulfonyl fluoride (PMSF), then resuspended in the same buffer and finally, lysed by sonication twice for 5 min. The sample was subjected to 3 cycles of "freeze/thawing" (dry ice ethanol bath alternating with a water bath at 37 °C). The suspension was centrifuged at 15.000 rpm in a Mikro 20 Hettich centrifuge (Hettlich Lab Tech., Tuttlingen, Germany) at 14.000 rpm for 15 min. The supernatant was heated to 95 °C for 5 min and re-centrifugated at 14.000 rpm for 10 min. The new supernatant was collected, and after addition of 5 mM $CaCl_2$, applied at room temperature into a phenyl–sepharose CL-4B (Ref.: P7892, Sigma-Aldrich Co., St. Louis, MO, USA) column equilibrated with 50 mM Tris–HCl (pH 7.5) containing 5 mM $CaCl_2$ and 0.1 M NaCl. The column was washed with the same buffer containing 0.1 mM $CaCl_2$. Then, the column was washed with the same buffer containing 0.5 M NaCl and finally eluted with 50 mM Tris–HCl (pH 7.5) containing 1 mM EGTA. CaM-containing fractions were identified on 15 % SDS-PAGE (+ 5 mM EGTA) gels, dialyzed, concentrated and stored at -20 °C or

lyophilized. Concentration of CaM was estimated from the absorbance at 276 nm = 1.8 mM (1%, 1 cm).

P20. PURIFICATION OF CaM PROTEIN PROTOCOL 5 D

-Grow the BL21-DE3 cells at 37 °C in 1 L of LB medium containing 100 μg/ml ampicillin to A_{600}= 0.8-1. Induce protein expression with 0.4 mM IPTG for 4-6 h at 37 °C.
-Spin down the cells and wash the pellet twice with 50 ml of fresh lysis buffer (50 mM Tris–HCl [pH 7.5], 2 mM EDTA and 0.2 mM PMSF), resuspending it in the same buffer.
-Store the sample at -20 °C as 10 ml aliquots.
-Thaw an aliquot on ice and sonicate it (3 cycles of 10 s on ice) before performing 3 freeze/thaw cycles using a dry ice ethanol bath and alternating with a 37 °C water bath. Centrifuge the sample in a microcentrifuge at 14,000 g for 15 min, and then heat the supernatant to 95 °C for 5 min before again centrifuging as above. This step takes advantage of CaM elevated thermal stability.
-Add $CaCl_2$ (5 mM final concentration) to the new supernatant and load at room temperature to a Phenyl–Sepharose column equilibrated with CQ buffer (50 mM Tris–HCl [pH 7.5], 100 mM NaCl and 5 mM $CaCl_2$). Wash with 20 volumes of CW buffer (50 mM Tris–HCl [pH 7.5], 100 mM NaCl and 0.1 mM $CaCl_2$), then with 10 volumes of CHSW buffer (50 mM Tris–HCl [pH 7.5], 500 mM NaCl and 0.1 mM $CaCl_2$) and elute with 20 volumes of CE buffer (50 mM Tris–HCl [pH 7.5] and 1 mM EGTA).
-Analyze the fractions containing CaM on 15 % SDS-PAGE (+ 5 mM EGTA) gels, dialyze, concentrate if needed and store at -20 °C or lyophilize. The CaM concentration can be estimated from the absorbance at 276 nm, given that ε276= 3,030 M^{-1} cm^{-1} and ε276, 1%= 1.8 $(g/100\ ml)^{-1}$ cm^{-1}. Alternatively use the Bradford method.

2.3.3 Calmodulin dansylation

CaM (100 μl at 10 mg/ml) was diluted 10-fold in 100 mM Tris-HCl (pH 8.5) and 20 mM $CaCl_2$. Dansyl chloride (Ref.: 39220, Sigma-Aldrich Co., St. Louis, MO, USA) dissolved in acetone (2.17 mg/ml) was added (12.5 μl) to a final concentration of 100 μM. The mixture was incubated at room temperature in the dark for 2 h, vortexing every 20 min. Unincorporated dansyl was eliminated using

a 1 ml G-25 sepharose column (Ref.: G25150, Sigma-Aldrich Co., St. Louis, MO, USA).

2.3.4 Fluorescence spectroscopy assays

Dansyl-calmodulin (D-CaM) and GST-K_v7.2 fusion proteins were dialyzed against 2 L buffer containing 25 mM Tris-HCl (pH 7.4), 120 mM KCl, 5 mM NaCl and 2 mM $MgCl_2$ for 48 h, changing the buffer every 10–12 h. Final concentration of D-CaM used was 12.5 nM. The fluorescence emission spectrum was obtained with an Aminco Bowman Series 2 fluorescence spectrophotometer (SLM Aminco, Rochester, NY, USA) in a final volume of 100 μl (using quartz cuvette) at 25 °C. The excitation wavelength was 340 nm, and emissions were registered from 400 to 660 nm.

For the titration experiment, increasing concentrations of each GST protein were added to a cuvette containing D-CaM alone (in the presence of EGTA 10 mM) or in the presence of excess of calcium (2 μM free Ca^{2+}) in D-CaM binding buffer [25 mM Tris-HCl (pH 7.4), 120 mM KCl, 5 mM NaCl, 2 mM $MgCl_2$, 10 mM EGTA].

Fluorescence enhancements were plotted against GST-fusion/D-CaM ratio or [GST-fusion] in order to obtain concentration-response curves. Data were fitted to the Hill equation by curvilinear regression to estimate EC_{50} values for each curve. Data are shown as an average of ± S.E.M. of at least four independent experiments.

2.4 Antibodies

- Anti-HA (rat) (3F10)
[Ref.: 11867423001, Roche Applied Science, Penzberg, Germany]

-Anti-Tac (mouse)
[Ref.: SM3015P, Acris Antibodies GmbH, Herford, Germany]

- Anti-GFP (mouse) (7.1 and 7.3 clons)
[Ref.: 11814460001, Roche Applied Science, Penzberg, Germany]

- Anti-Calmodulin (mouse) IgG1
[Ref.: 05-173, Upstate, EMD Millipore Corp., Billerica, MA, USA]

- Anti-α Tubulin (mouse) (DM1A clon)
[Ref.: T6199, Sigma-Aldrich Co., St. Louis, MO, USA]

- Anti-CD25 (mouse) (M-A251clon)
[Ref.: 555430, BD Biosciences, Franklin Lakes, NJ, USA]

- Anti-CD4 (mouse) (Q4120 clon)
[Ref.: C-1805, Sigma-Aldrich Co., St. Louis, MO, USA]

- Anti-Myc (mouse) (9E10 clon)
[Ref.: 5546, Sigma-Aldrich Co., St. Louis, MO, USA]

- Anti-rat Alexa Fluor 594 (goat)
[Ref.: A11007, Molecular Probes, Eugene, OR, USA]

- Anti-mouse Alexa Fluor 488 (goat)
[Ref.: A11001, Molecular Probes, Eugene, OR, USA]

- Anti-mouse Alexa Fluor 546 (goat)
[Ref.: A11003, Molecular Probes, Eugene, OR, USA]

- Anti-mouse Alexa Fluor 594 (goat)
[Ref.: A11005, Molecular Probes, Eugene, OR, USA]

- Anti-mouse Alexa Fluor 594 (donkey)

[Ref.: A21203, Molecular Probes, Eugene, OR, USA]

- Anti-mouse HRP (goat)
[Ref.: 170-6516, Bio-Rad Lab., Hercules, CA, USA]

- Anti-rat HRP (goat)
[Ref.: 712-475-153, Jackson Immunoresearch Lab. Inc., West Grove, PA, USA]

2.5 Solutions and reactives

SOLUTIONS FOR THE PCR PROTOCOL

- Expand polymerase (Expand High Fidelity Plus, 03300242001, Roche).
- pGEM-EasyT vector (823893002, Promega).
- Pfu turbo (600250, Stratagene).
- Primers: .synthesized by IDT (Integrated DNA Technologies) and Sigma-Aldrich

SOLUTIONS OF THE DNA EXTRACTION PROTOCOL

TE 10X (Tris-EDTA buffer) pH 8
- 100 mM Tris-HCl pH 8
- 10 mM EDTA
Dissolve in 500 ml MilliQ water

NaOH/SDS lysis buffer
- 5 M NaOH
- 10 % SDS

Neutralization buffer
- 3 M Potassium acetate
- 5 M Acetic acid

Phenol-chloroform solution
- Ratio 25:24

FRAGMENT DIGESTION, PURIFICATION AND LIGATION PROTOCOLS

Tris-borate-EDTA (TBE 10 X Buffer)
- 108 gr Tris base
- 55 gr boric acid
- 9,3 gr EDTA
Dissolve in 1 litter of MilliQ water

- Agarose (Agarose low eeo, cat. nº 8008, Conda).

- Ethidium bromide.
- Enzymes: Fermentas (Thermo Fisher Scientifics, Waltham, Massachusetts, USA).
- DNA Gel Extraction Kit (High Pure PCR Product Purification Kit, Ref.: 1173266800, Roche).

TRANSFORMATION PROTOCOL SOLUTIONS

Transformation 2X Buffer:
- 40 mM $MgCl_2$
- 20 mM $CaCl_2$

Dissolve in 100 ml of MilliQ water

LB medium (pH 7)
- 1 % Peptone
- 2 % Yeast extract
- 1% NaCl

Dissolve in 1 litter of MilliQ water and autoclave

LB- Antibiotic plates
- Peptone 1 %
- Yeast extract 2 %
- NaCl 1 %
- Agar 2 %

Dissolve in 1 litter of MilliQ water and autoclave. Allow medium to cool to 50 ºC and add 1 ml of antibiotic to a 100 µl/ml final concentration

Antibiotics (1000 X stocks) sterilized by filtration
-Ampicillin (in water): 100 mg/ml
-Kanamycin (in ethanol): 35 mg/ml

CHAPTER 3

Surface expression and subunit specific control of steady-state protein levels by the $K_V7.2$ helix A-B linker

Surface expression and subunit specific control of steady-state protein levels by the K_v7.2 helix A-B linker

3.1 Introduction

K_v7 channels are of crucial importance in excitable tissues (Brown and Passmore, 2009; Jentsch, 2000). Although it is known that K_v7.2 acts in the plasma membrane, the majority of this protein is located at the ER and at other intracellular compartments, both in neurons and in cells heterologously expressing the channel (Peretz *et al.*, 2005; Soldovieri *et al.*, 2006). A membrane protein must pass through multiple quality control mechanisms before reaching the plasma surface. It begins with the translation of the protein and involves subunit assembly, ER exit and its transport to the membrane (Deutsch, 2002; Heusser and Schwappach, 2005). Those proteins that fail to do so are disposed of by proteolytic degradation (Lord *et al.*, 2000). These overlapping events (from the nascent protein to its place in the plasma membrane) control ion channel expression at the cell surface and may be coordinated or even cooperate (Deutsch, 2002). However, the mechanisms that control the abundance of K_v7 channels at the membrane are generally poorly understood. As for other membrane proteins, these mechanisms hinge on intrinsic and extrinsic signals. The reentrant loop that forms the pore is the strongest intrinsic signal known to control the surface expression of M-channels (Gomez-Posada *et al.*, 2010). In conjunction with helix D located in the intracellular C-terminus that constitutes the assembly domain

(Schwake *et al.*, 2006; Schwake *et al.*, 2000), this region drives the increase in the number of M-channels observed upon heteromerization. CaM binds to helix A and B of the intracellular C-terminus (Gamper and Shapiro, 2003; Yus-Najera *et al.*, 2002), and some mutations linked to BFNC that are located in helix A (Moulard *et al.*, 2001; Richards *et al.*, 2004) reduce CaM binding, thereby leading to ER retention and the consequent reduction in surface expression (Alaimo *et al.*, 2009; Etxeberria *et al.*, 2008).

Aim of the study

While the mechanisms controlling surface expression of certain membrane proteins are well documented (Heusser and Schwappach, 2005; Ma and Jan, 2002; Mikosch and Homann, 2009), little is known regarding the intrinsic signals that influence the surface expression of K_v7 channels. The present study has been focused in analyzing the amino acid sequence of K_v7.2 to identify intrinsic signals that may control its surface expression. We have seen that removing the interlinker connecting helix A and helix B of the intracellular C-terminus, a large increase in the number of functional channels at the plasma membrane is produced. Moreover, the elimination of this linker increased the steady-state amount of protein, which was not associated with a decrease of protein degradation. The magnitude of this increase was inversely correlated with the number of helix A – helix B linkers present in the tetrameric channel assemblies. In contrast to the remarkable effect on the amount of K_v7.2 protein, removal of the K_v7.2 linker had no detectable impact on the steady-state levels of K_v7.3 protein.

3.2 Results

3.2.1 The linker between helices A and B increases protein yield

In order to understand which could be the factors that are being involved in channel trafficking, the $K_v7.2$ subunit was analyzed trying to identify any intrinsic signal. Thus, we did a systematic evaluation of the $K_v7.2$ C-terminal by producing deletions in which different regions from the distal channel were removed. A hemagglutinin (HA) tag epitope was inserted between the S1 and S2 transmembrane domains with the intention of measuring the surface expression in female *Xenopus* oocytes by chemiluminiscent techniques (Etxeberria *et al.*, 2008; Schwake *et al.*, 2000) (Fig. 3.1).

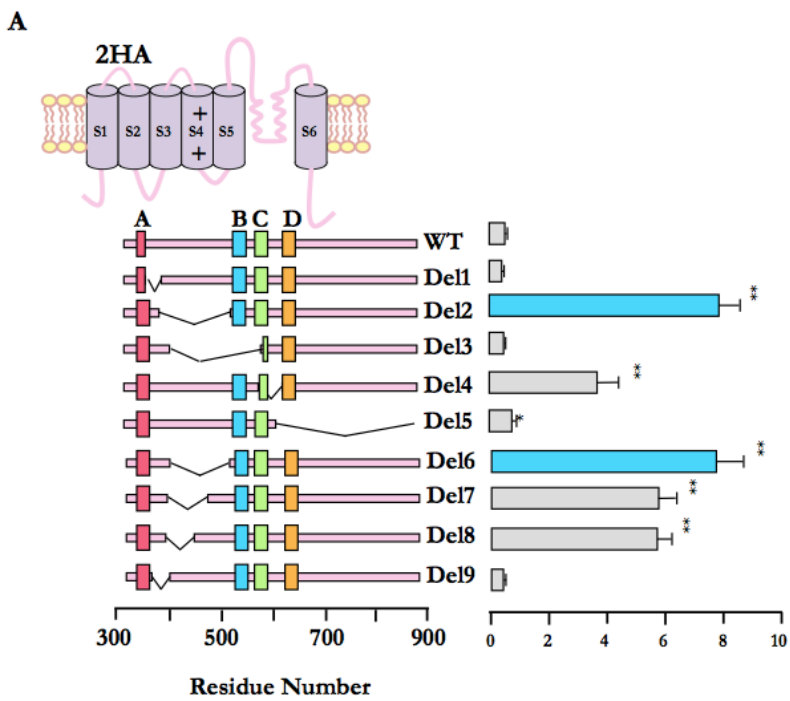

Figure 3.1. Identification of C-terminal regions that influence K_V7.2 surface expression. Schematic representation of the different deletions introduced into the intracellular C-terminus of the K_V7.2 subunit. The boxes along the intracellular C-terminus scheme indicate regions with a high probability of adopting an alpha helix configuration.
On the right, normalized surface expression in female *Xenopus laevis* oocytes of the K_V7.2 subunits tagged with HA at the extracellular S1-S2 loop (n≥12, two batches). The amount of K_V7.2-HA containing channels in the oocyte membrane was quantified using a single whole-oocyte chemiluminiscent assay (see Chapter 2, experimental procedures). The background of uninjected oocytes was subtracted and the values given are the means (±S.E.M) normalized to the values obtained from WT-K_V7.2-HA channels from the same batch. * $P \leq 0.05$; *** $P \leq 0.001$; unpaired Student´s *t* test.

The removal of different regions within the AB linker led to an increased in surface expression and protein production (Fig. 3.2).

In addition to the helix A-B linker, the loop connecting helices C and D exerted an important influence on surface expression (see [K_V7.2-Del2 2HA-ΔT359-T501 (Del2)] and [K_V7.2-Del4 2HA-ΔL548-M591 (Del4)], Fig 3.1). Moreover, truncation after helix C [K_V7.2-Del5 2HA-ΔS590 (Del5)] augmented surface expression, although not to the extent of the deletions between helices A-B or C-D. Among the analyzed deletions, [K_V7.2-Del8 2HA-ΔY372-K408 (Del8)] was the smallest one that augmented surface expression, while [K_V7.2 Del9 2HA-ΔT359-Y372 (Del9)] had no effect on surface expression or total protein signal. Except for Del9, comparable increases in protein yield were observed for the different AB linker deletion mutants (Fig. 3.2) ranging from 2.35 to 3.30 fold. The average pooled increase in protein yield for [K_V7.2 Del6 2HA-ΔY372-K493 (Del6)], [K_V7.2 Del7 2HA-ΔY372-S450 (Del7)] and Del8 was 2.65±0.23 fold (n=10). Unlike deletions of the helix A-B loop (Del2), (Del6) and (Del8), the steady state protein levels were not so obviously affected by removal of the linker between helices C and D (Del4). As the greatest influence on surface expression was observed for

mutants in which the helix A-B linker was removed, we focused our analysis on this region, more specifically, in the Del6 deletion.

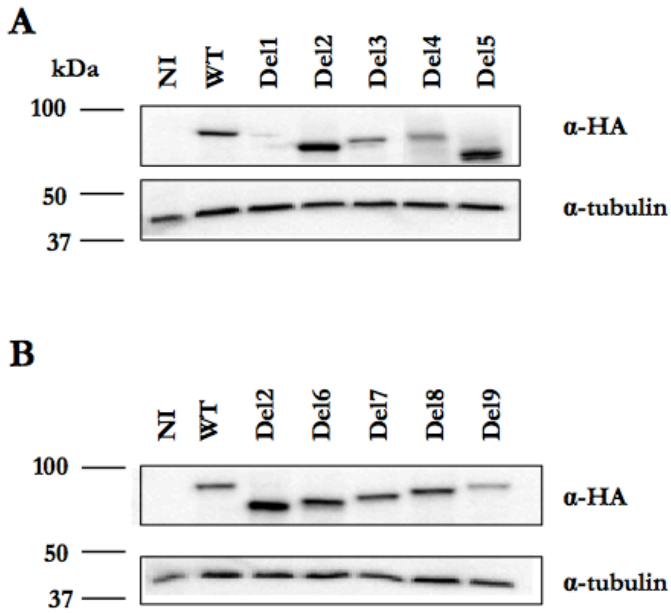

Figure 3.2. Del2, Del6 and Del8 are the identified regions that influence more K_v7.2 surface expression. Proteins from *Xenopus laevis* oocytes injected with the same amount of mRNA expressing the indicated HA-tagged constructs were separated by SDS-PAGE and analyzed by western blotting with anti-HA antibody (n=4).

3.2.2 There is a correlation between CaM binding and channel function

The impact of the linker on CaM binding cannot explain changes in surface expression. CaM binds to helix A and B regulating the exit of K_v7.2 subunits from

the ER (Etxeberria *et al.*, 2008; Wen and Levitan, 2002; Yus-Najera *et al.*, 2002). Corroborating previous findings in the laboratory (Yus-Najera *et al.*, 2002), some coimmunoprecipitation assays demonstrated that CaM interacted with the channels in both presence and absence of the linker (Fig. 3.3).

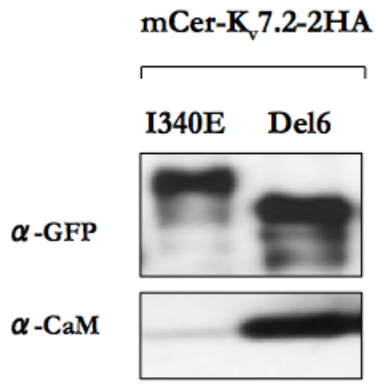

Figure 3.3. **Del6 keeps on binding CaM.** Co-immunorecipitation of CaM and K_V7.2 tagged with mCFP and HA. Proteins from cells expressing the constructs were immnuoprecipitated by using an anti-HA antibody, separated by SDS-PAGE and analyzed by western blotting by using anti-CaM and anti-GFP antibodies. As a negative control, I340E was also co-immunoprecipitated.

Thus, to examine the interaction in more detail, we performed *in vitro* binding assays using a fluorescent derivate of CaM (D-CaM). The D-CaM emission spectrum is enhanced when the environment of the dansyl moiety becomes hydrophobic. This tool has proved useful to detect conformational changes as a consequence of interactions with Ca^{2+}, peptides or proteins (Alaimo *et al.*, 2009). The apparent affinity observed in the dose-response for the CaM-Del6 binding was almost identical to that obtained with the WT binding site, while the maximal fluorescence emission was only slightly but significantly reduced (Fig. 3.4). So, the

impact of the linker on surface expression appears to be unrelated to its interaction with CaM.

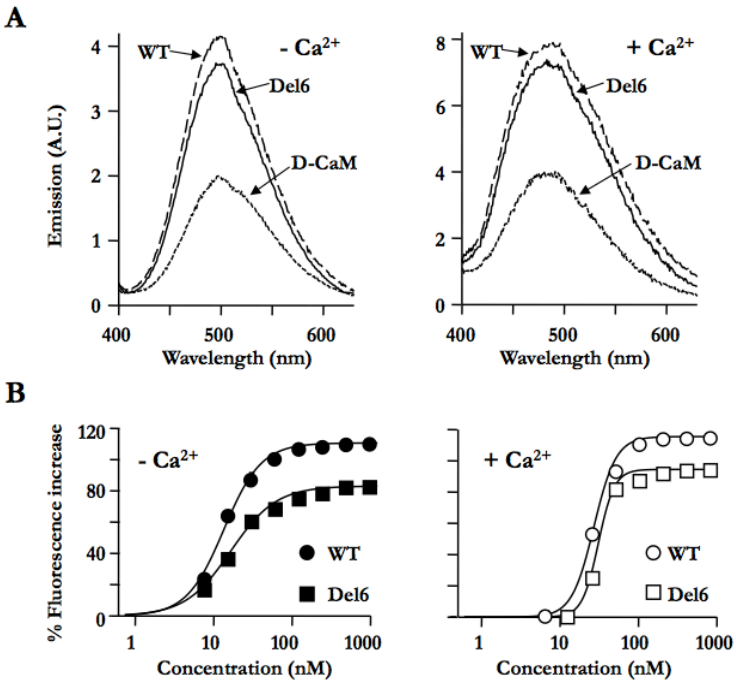

Figure 3.4. Characterization of Del6-CaM interaction.
A. Emission spectra of 12.5 nM D-CaM in the absence (left panel; 10 mM EGTA and no added Ca^{2+}), and in the presence of 2 µM free Ca^{2+} (right panel), as well as in the presence of molar excess of the indicated GST-K_v7.2 fusion proteins (200 nM). Note the difference in the fluorescence emission axis, as well as the shift in the peak emission to the left in the presence of Ca^{2+}.
B. Relative concentration-dependent enhancement of D-CaM fluorescence emission in the absence (left) and presence of 2 µM free Ca^{2+} (right). The parameters used to fit a Hill equation to the data for WT in absence of Ca^{2+} were: Max= 111 ± 1.4, EC_{50}= 11±0.5 nM, h= 1.8 ± 0.2 (n=9). For Del6 in absence of Ca^{2+}: Max= 83 ± 1.3, EC_{50}= 13 ± 0.7 nM, h = 1.5 ± 0.1 (n=5). For WT in the presence of Ca^{2+}: Max= 115 ± 2.2, EC_{50}= 27 ± 1.2 nM, h= 3.1 ± 0.4 (n=9). For Del6 in presence of Ca^{2+}: Max= 95 ± 1.1, EC_{50}= 31 ± 0.8 nM, h = 4.2 ± 0.3 (n=5). The data represent the means ± S.E.M. The error bars are smaller than the symbols.

3.2.3 Removal of the A-B linker increases protein yield in mammalian cells

Protein levels induced by the expression of the WT and Del6 constructs were compared by loading increasing amounts of the sample protein extracts into SDS gels, which were then analyzed by western blotting. To obtain a signal comparable to that seen for the Del6 extracts, approximately fivefold more sample was required from cells expression WT subunits (Fig. 3.5).

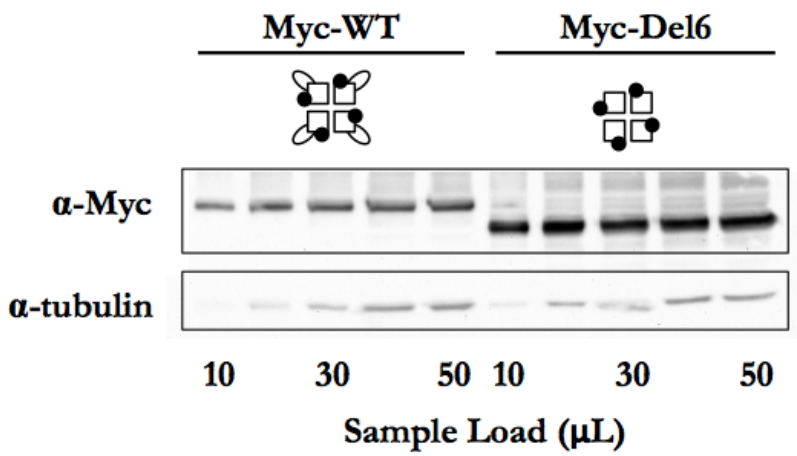

Figure 3.5. The Del6 mutant subunit presents increased K_V7.2 total protein. Western blot of increasing sample load from HEK293T cells extracts expressing the same amount of DNA encoding WT or Del6 -Myc tagged subunits. The optical densities (OD) of the bands were analyzed using ImageJ software. A linear regression fit was obtained from the OD *vs* load relation. From this regression, the amount required to obtain the same OD´s was found to be 4.7 ± 1.22 fold larger (n=5) for WT subunits than for the Del6 mutant K_V7.2 subunits.

In order to determine the effect of Del6 over WT and vice versa, co-expression assays were performed transfecting both subunits in a ratio 1:6 in each case, being each construct tagged with a different epitope (Myc/GFP) (Fig. 3.6A). Thus, only

channels incorporating at least one Myc-tagged subunit could be detected and, due to the greater amount of cDNA encoding non-Myc-tagged subunits (6 fold that of the mutant/WT subunits), the vast majority of the channels detected contained one Myc-tagged mutant subunit and three non-Myc-tagged subunits. The rationale is that, given that assembly of $K_v7.2$ is a random process (Stewart *et al.*, 2012) mass action will favor the assembly of Myc-tagged subunits with the most abundant non-tagged subunits.

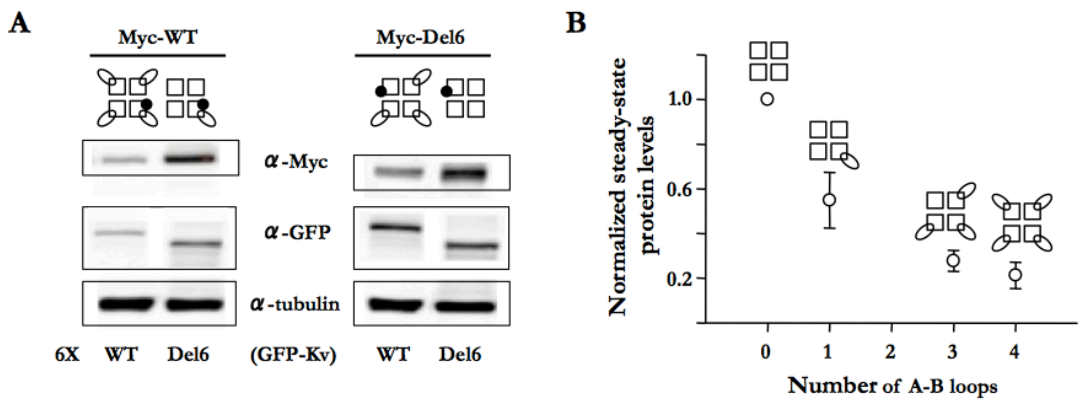

Figure 3.6. Co-expression of Del6/WT constructs.
A.- The steady-state protein levels are inversely proportional to the number of A-B loops present in the tetrameric $K_v7.2$ assemblies. Western blot of protein extracts from HEK293T cells expressing Del6 (right panel) or WT -Myc subunits (left panel) when co-expressed with a six large fold larger amount of plasmid DNA coding the indicate YFP-tagged protein (n=4). Myc tagged WT and Del6 $K_v7.2$ channels were detected using anti-Myc antibody. Del6 protein levels decreased when co-expressed with WT subunits, whereas increased protein levels of WT were detected when co-expressed with Del6. A schematic representation of the theoretical assemblies detected with the anti-Myc antibody is represented at the top. The subunits that were overexpressed and that lack a Myc tag, so they are not detected in the western blot, are indicated at the bottom of each lane.
B.- Normalized quantification of western blot signals as a function of the theoretical number of A-B loops present on the detected channel assemblies. On each western blot, the OD's were normalized to the signal obtained for tubulin. The values were subsequently normalized to those obtained with Del6 or WT -Myc in the same western blot. Data points for 0 (Del6) and 4 (WT) loops were derived from data obtained as in panel A, data points for 1 and 3 loops were obtained from

western blots equivalent to the left and right columns in panel B, respectively. The points represent the means ± S.E.M. (n≥4).

The number of loops present in the tetrameric K_v7.2 channel was inversely correlated with the steady-state protein expression. Indeed, the protein yield in cells expressing loop-less mutant subunits was reduced when were co-expressed with an excess of the WT subunits (Fig. 3.6A, right panel). In this way, these channels contained 3 and 0 loops, respectively, and accordingly, we could plot the relative protein abundance as a function of the number of loops (Fig. 3.6B). Similarly, the relative protein abundance of channels having 4 and 1 loops was examined (Fig. 3.6A, left panel), and the results were incorporated into Figure 3.6B. Given the increase in protein levels and surface expression observed in oocytes expressing different helix A-B linker deletion mutant constructs, these results suggest a causal relationship between protein yield and surface expression.

3.2.4 The presence of the A-B loop does not augment the rate of protein degradation

The increase in protein yield by Del6 may be due to a reduction in the degradation rate or, alternatively, to an increase in the rate of protein synthesis. The sequence connecting helices A and B reveals the existence of three PEST motives (Fig. 3.7). These motives are rich in proline (P), glutamate (E), serine (S) and threonine (T) (Rogers *et al.*, 1986), are often encountered in CaM binding proteins that are susceptible to proteolysis by endogenous neutral proteases such as calpain I and calpain II (Barnes and Gomes, 1995), and have been found to promote the rapid degradation of proteins (Rechsteiner and Rogers, 1996).

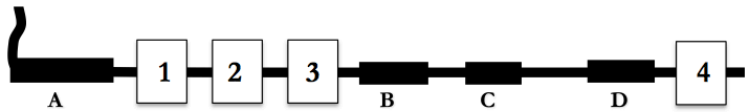

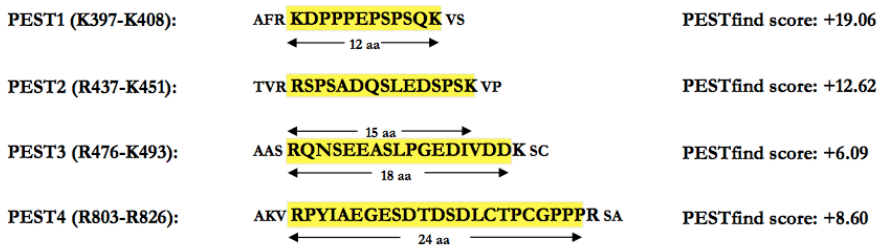

Figure 3.7. Schematic representation of the C-terminal of the K_V7.2 subunit with the PEST sequences.
The boxes in the expanded intracellular C-terminus indicate regions with a high probability of adopting an alpha helix configuration. Squares (numbered 1 to 4) indicate regions with a significant PESTfind score. The PESTfind scores (www.biu.icnet.uk/projects/pest) were 19.06, 12.62, 6.09 and 8.6 for PEST1 ($_{397}$KDPPPEPSPSQK$_{408}$), PEST2 ($_{437}$RSPSADQSLEDSPS$_{451}$), PEST3 ($_{476}$RQNSEEASLPGEDIVDD$_{493}$) and PEST4 ($_{803}$RPYIAEGESDTDSDLCTPCGPPPR$_{826}$), respectively.

Therefore, we tested the impact of the loop on protein degradation. HEK293T cells were treated with the protein synthesis blocker cycloheximide (CHX) for various time periods and the remaining protein levels after degradation were evaluated by western blotting. However, contrary to our expectations, in four independent experiments we did not observe differences in the stability of the protein that could account for the increased protein yield (Fig. 3.8).

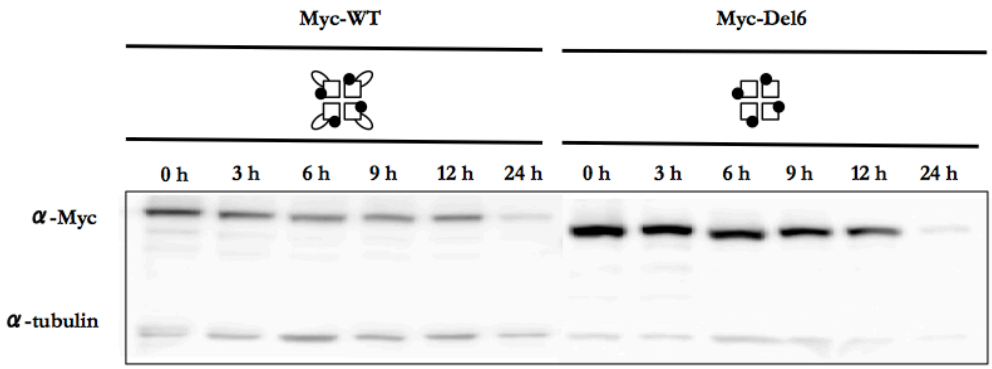

Figure 3.8. HEK293T cells treated with CHX for various time periods.
CHX treatment assay of K_V7.2 subunit in HEK293T cells. Cells were transfected with plasmids WT and Del6 –Myc and treated with protein synthesis inhibitor CHX (cycloheximide, 75 μg/ml) for the indicated time period (0, 3, 6, 9, 12 and 24 H). After degradation, the remaining proteins were separated by SDS-PAGE, and analyzed by western blotting using anti-Myc or anti-tubulin antibody.

We also tested lysosomal and proteasomal inhibitors, such as chloroquine (CQ) and MG132 respectively. No significant differences were observed after 10 h treatment with MG132 (n=3), as (Soldovieri *et al.*, 2006). After 10 h treatment with CQ, the levels of channels that are not carrying the A-B loop tended to be larger (n=3), (Fig. 3.9). However, the differences were modest, and further experiments are required to test the contribution of this pathway.

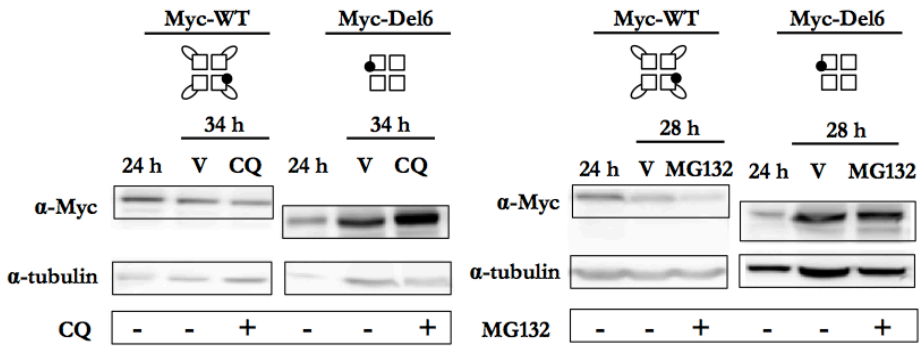

Figure 3.9. Lysosomal and proteasomal inhibitors. Shown is a degradation assay using proteasome (MG132) and lysosome inhibitor, CQ of WT- or Del6 in HEK293T cells. Cells were transfected with plasmids WT and Del6 –Myc and treated with CQ (50 μM) and MG132 (20 μM) for the indicated time periods. Samples were loaded in lanes from the left in the following order: control without any treatment (24 h), vehicle (PBS) for the CQ treatment after 10 hours and (DMSO) for the MG132 treatment after 10 h. After degradation, the protein extracts were separated by SDS-PAGE and analyzed by western blotting using anti-Myc and anti-tubulin antibodies (n=2).

To further test the impact of the loop on the stability of K_v7.2, we performed pulse and chase experiments revealing that the degradation rate was not reduced after loop removal (Fig. 3.10). On the contrary, the removal of the loop apparently led to a faster degradation rate. The simplest explanation, therefore, is that the presence of the loop causes a reduction on the rate of K_v7.2 protein synthesis.

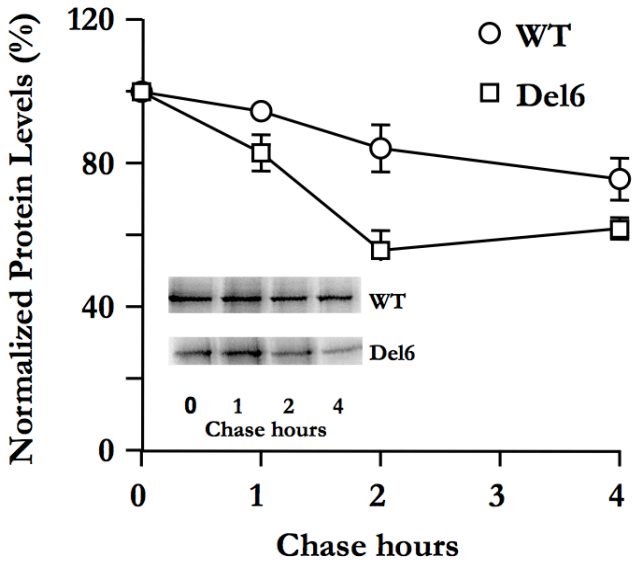

Figure 3.10. The Del6 mutant subunit presents a faster degradation rate. Pulse-chase analysis of WT and Del6 subunit stability. Densitometric quantification of the bands normalized to the value at time 0 (no chase). Each data point is the mean ± S.E.M. calculated from three separate experiments. Inset: representative images of autorradiographic films of experiments in HEK293T cells transfected with the indicated plasmids. Metabolic labeling was performed for 1 H, 36 H post-transfection, followed by chase times of 1, 2 and 4 H.

3.2.5 Removing the linker between helices A-B is compatible with channel function in HEK293T cells

Cells expressing mutant subunits give rise to functional channels (Fig. 3.11). In this set of experiments, we took advantage of the presence of a fluorescent tag on the subunits to select cells with similar levels of protein expression. Thus, differences of the current size cannot be attributed to changes in the total number of channels in the cell. Nevertheless, the averaged current density tended to be

higher in Del6 expressing cells, although due to the data scattering, the difference did not reach statistical significance.

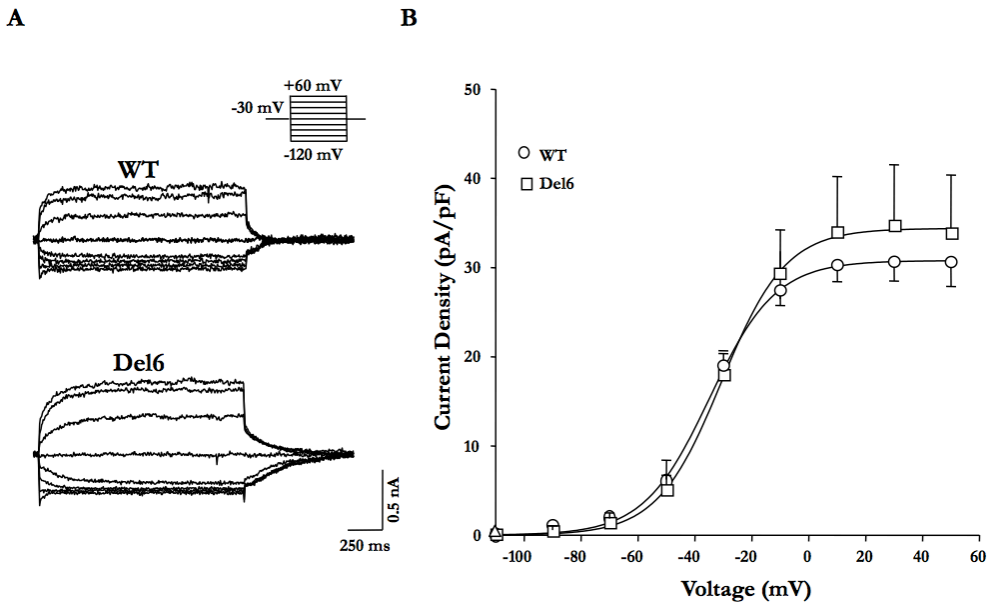

Figure 3.11. Removal of the A-B linker results in functional K_v7.2 channels.
A.- Representative currents recording from HEK293T cells transfected with WT- and Del6-, activated from a holding potential (Vh) = -30 mV after 1,500 ms steps to the indicated voltages.
B.- Current density-voltage relationship from tail currents of WT (n=13) or Del6 (n=15) channels. Each point represents the mean ± S.E.M. A Boltzmann equation D = Dmax/(1+e((V-V1/2)/S)) was fitted to the data. The averaged Boltzmann parameters were: WT: V1/2 = -34.8 ± 1.9 mV, Slope = 11.6 ± 1.7, Dmax = 30.7 ± 0.9 pA/pF; Del6: V1/2 = -30.6 ± 5.1 mV, Slope = 11.2 ± 4.5, Dmax = 34.4 ± 2.6 pA/pF; Del2: V1/2 = -29.6 ± 5.5 mV, Slope = 14.2 ± 4.5, Dmax = 34.1 ± 2.6 pA/pF.

On the other hand, the impact of the deletion on the Boltzmann parameters was not significant (see Fig. 3.11 legend). Of note, we found that there was no correlation between subunit expression based on fluorescent signal and functional electrophysiological detection.

3.2.6 The PIP_2 sensitivity is not reduced after A-B loop removal

It has been shown that the loop between helices A and B has a strong influence on PIP_2 dependent function of $K_v7.2$ subunits (Hernandez *et al.*, 2008). The current view is that PIP_2 binding is essential for K_v7 channel function. Due to the PIP_2 dependence, it can be expected that disruption of the proposed PIP_2 site will lead to a large reduction in functional channels. To test this hypothesis, we evaluated the PIP_2 sensitivity of the channels using a voltage-dependent phosphatase (Murata *et al.*, 2005). The advantage of using this phosphatase is that no other signaling pathways, such as Ca^{2+} or PKC activation, are recruited, simplifying the interpretation of the results. In the experiment shown in Figure 3.12, a current relaxation is evoked by a depolarization step to -20 mV, a voltage at which the phosphatase is not activated. This control pulse reveals the basal current levels. The second pulse to +100 mV activates the phosphatase. In response to this second pulse more channels open, as revealed by the initial current increase. Simultaneously, the levels of PIP_2 decrease, causing, after a delay, a reduction on the current. Providing that the rate of PIP_2 resynthesize is the same, as shown in Fig. 3.12D, the rate of current reduction is related to the affinity for PIP_2, such as the faster the rate, the lower the affinity (Fig. 3.12B). In addition, the final current levels depend on the duration of the test pulse (Fig. 3.12C), and from the relation between pulse duration and current levels, the relative affinity can be evaluated. We found that the rate of current reduction was slower in Del6 channels, but the difference was not statistically significant (Fig. 3.12B). Consistent with this result, the relation between pulse duration and current levels also suggested that the channels without the A-B linker had a higher PIP_2 affinity (Fig. 3.12C). However, the differences did not reach statistical significance due to the scatter of the data from cells expressing Del6 channels.

Taking all these observations together, we can conclude that removal of the A-B linker does not cause a reduction in PIP_2 affinity.

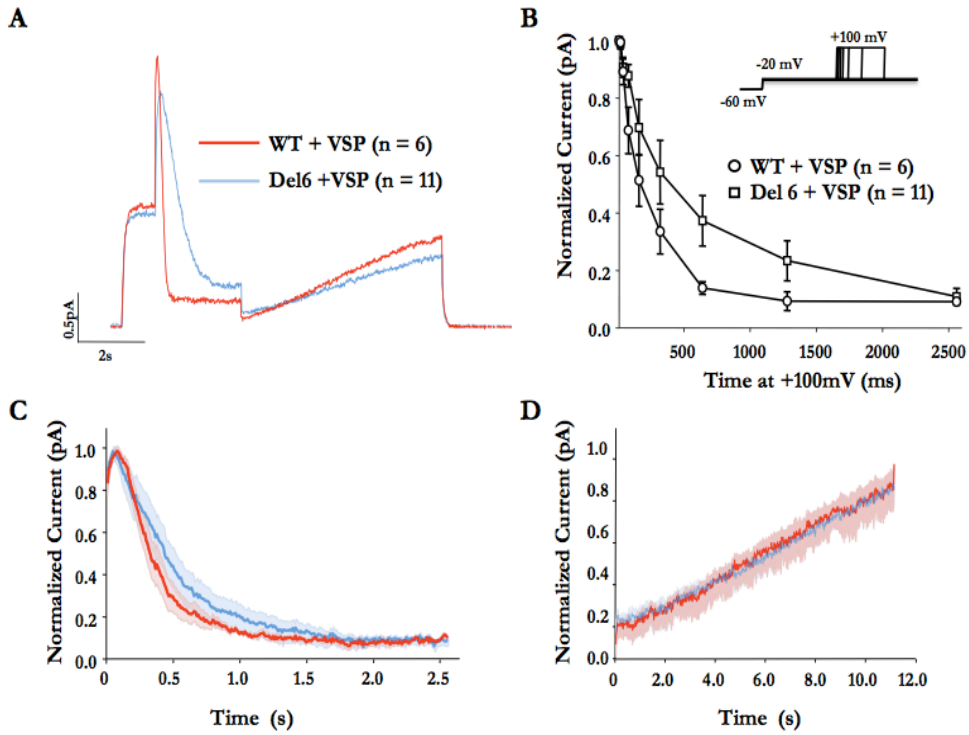

Figure 3.12. Removal of the A-B linker does not decrease PIP_2 affinity.
A.- Current recorded in cells transfected with WT and *Danio rerio* voltage dependent phosphatase (VSP, red) and Del6 + VSP (blue) activated from a holding potential (V_h) = -60 mV. The initial pulse to -20 mV opens the channels without activating VSP. The second pulse to +100 mV opens additional channels faster than VSP is activated, giving rise to an initial current increase, followed by a decline. The decline phase is governed by the reduction on PIP_2 levels at a rate that depends on the PIP_2 affinity of the channels. After a variable period (2.560 ms in this example), voltage is returned to -20 mV, and the relative inhibition can be measured. This protocol is described in detail in (Falkenburger *et al.*, 2010).
B.- Averaged time course of the current decline during 2.560 ms VSP activation at +100 mV in cells transfected with WT + VSP (red; n=6) and Del6 + VSP (blue; n=11) subunits. The shadows represent the mean ± S.E.M.
C.- Normalized current at -20 mV (after/before step to +100 mV) for different durations at +100 mV. Each point represents the mean ± S.E.M. for 6-11 cells.

The data from cells expressing Del6 subunits presented a large scatter, and the differences with the data from WT expressing cells did not reach statistical significance.
D.- Time-course during recovery at -20 mV. The shadows represent the mean ± S.E.M. for data from cells expressing WT (red) or Del6 (blue) channels. The rate of recovery after PIP_2 depletion was indistinguishable.

3.2.7 There is a significant increase in the number of cells displaying surface staining when transfected with Del6

To examine surface expression in mammalian cells, subunits with two extracellular HA epitope between S1-S2 were employed. Transfected non-permeabilized cells were surface immunostained and examined by epifluorescence followed by confocal microscopy. The presence of this extracellular epitope in conjunction with an N-tagged fluorescent protein allowed us to monitor surface and total expression simultaneously. Cells with comparable total fluorescence signal were selected for the analysis. Similar to the whole-cell recording experiments, the variations in surface expression cannot be ascribed to differences in total protein. Of the cells expressing WT subunits, only about 35 % presented a clear surface expression signal, whereas this percentage increased to 60 % in the population expressing the Del6 mutant subunit (Fig. 3.13). Thus, in addition to favoring protein yield, removal of the linker also appears to facilitate the traffic of the channels to the plasma membrane. The inspection of the images revealed that a direct correlation between total protein levels and surface expression did not exist.

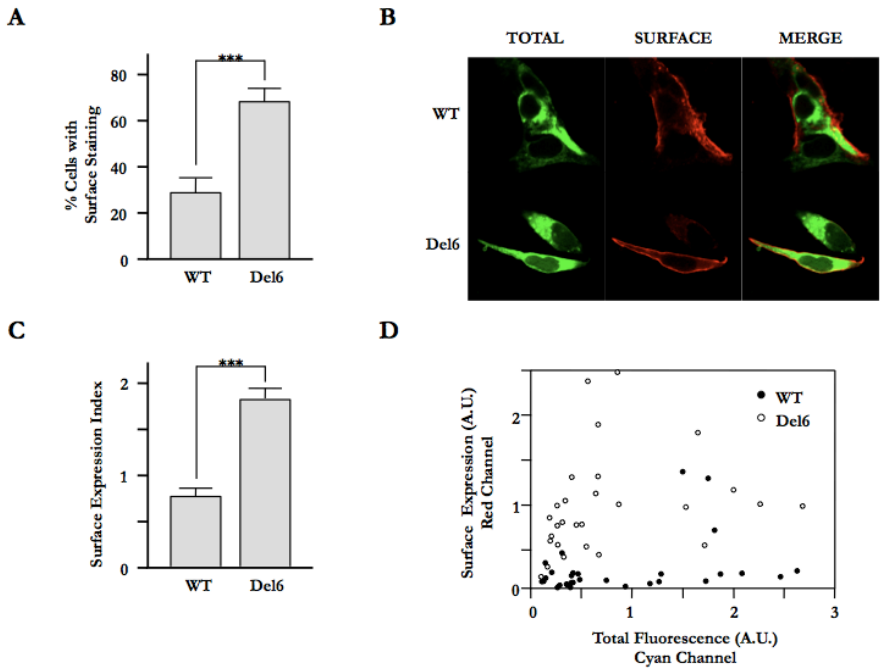

Figure 3.13. Surface expression of WT and Del6 subunits in human HEK293T cells.

Analysis of confocal images of cells expressing the indicated constructs. The subunits have a mCFP tag at the N-terminus (rendered in green) and an extracellular 2xHA tag, allowing simultaneously monitoring total (green) and surface expression (red). The proportion of the cells in confocal images with surface staining was determined in > 40 mCFP positive cells for each construct in three independent experiments.

A.- Grey bars represent mean ± S.E.M. of the percentage of cells expressing the channel at the surface. *** $P \leq 0.001$; unpaired Student's *t* test.

B.- Representative images of cells expressing the indicated subunit.

C.- Ratio of surface/total expression (red fluorescence/cyan fluorescence) from wide field epifluorescence images of cells expressing the indicated $K_v7.2$ subunits. *** $P \leq 0.001$; unpaired Student's *t* test.

D.- Plot of the cyan fluorescence *vs* red fluorescence intensity from wide field epifluorescence images of cells expressing the indicated subunits. There was no correlation between total and surface expression (>90 cells from >5 independent experiments).

Figure 3.13 includes a striking example that illustrates this lack of correlation. The bottom of Figure 3.13B shows a field with two cells with similar protein expression levels. Whereas a robust surface signal is present in one cell, no label is discernible in the other. A similar pattern was found in > 90 % of the fields examined. Quantitation of total and surface expression in wide field epifluorescence images also demonstrated an increase in membrane staining after removal of the A-B linker (Fig. 3.13C). A plot of total *vs.* surface signal from more than 90 cells for each subunit is displayed in Fig. 3.13D, further highlighting the lack of correspondence between these two parameters. These observations are consistent with the functional variability observed in the electrophysiological recordings described previously.

3.2.8 The K_v7.2 A-B linker does not have a major impact on the steady-state protein level of K_v7.3 subunits

K_v7.3 subunits are the main component of the M-current, and facilitate surface expression and function of K_v7.2 subunits. To test whether the K_v7.2 A-B loop affected K_v7.3 protein yield, WT or Del6 were co-expressed with K_v7.3 subunits at a 5:1 ratio, and the intensity of the protein bands were examined by western blotting. The K_v7.3 subunits were tagged with YFP, and revealed with anti-GFP. As a reference, YFP-tagged K_v7.3 subunits were co-expressed with molar excess of K_v7.3 subunits without the YFP tag, which cannot be detected with the anti-GFP antibody. Figure 3.14 and 3.15 show that K_v7.2 subunits caused a significant reduction on K_v7.3 protein signal. However, the impact on K_v7.3 protein yield of WT and Del6 was indistinguishable (Fig. 3.14B).

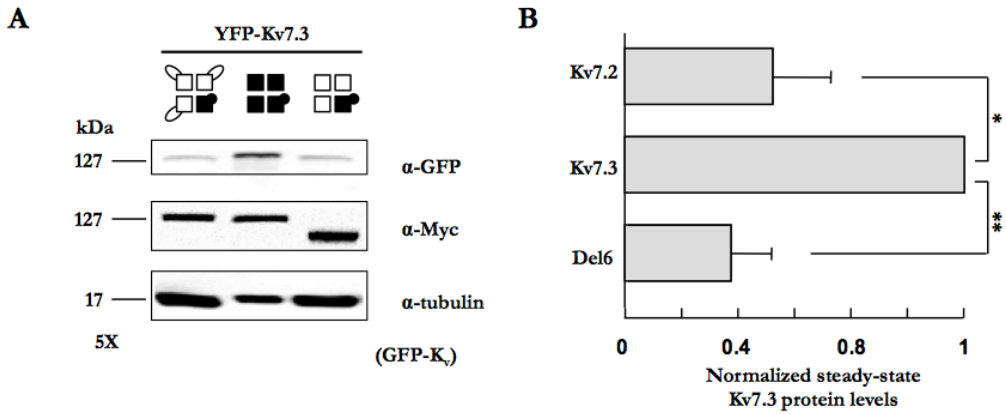

Figure 3.14. The K_v7.2 A-B linker is not critical for K_v7.2 mediated reduction on K_v7.3 protein levels.
A.- Western blot of protein extracts from HEK293T cells transfected with YFP-K_v7.3 and the constructs indicated at the bottom of each column at a 1:5 ratio. The constructs indicated at the bottom did not have a fluorescent protein tag, and were not detected by the anti-GFP antibody.
B.- Densitometric quantification of the band intensity relative to the tubulin signal, normalized to the value obtained for cells overexpressing K_v7.3. Overexpression of WT- or Del6-K_v7.2 caused a significant reduction in the signal of YFP-K_v7.3, and the extent reduction was not statistically different. Bars represent mean ± S.E.M. from 5 experiments. ** $P \leq 0.01$; * $P \leq 0.05$; paired Student's *t* test.

Similarly, the protein levels of WT and Del6 channels were not affected by the overexpression of K_v7.3 subunits (Figs. 3.15A and B).

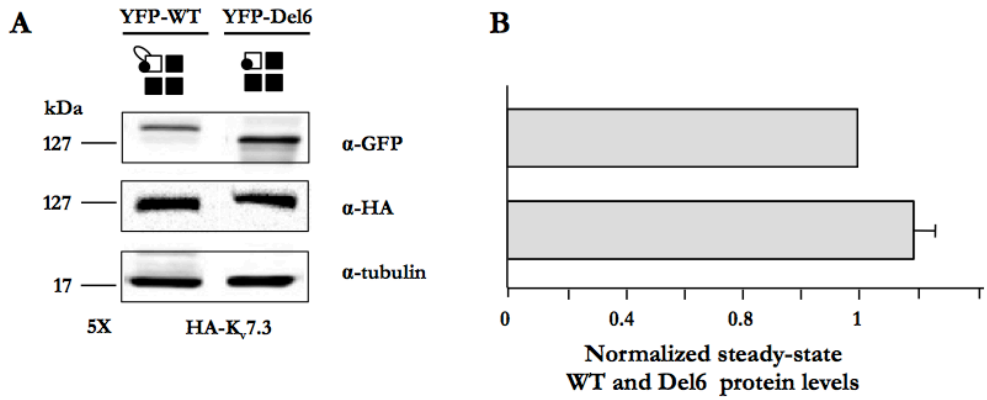

Figure 3.15. The K_V7.3 is not being affected by both WT and Del6 subunits.
A.- Western blot of protein extracts from HEK293T cells cotransfected with YFP-WT and Del6 subunits and the HA-K_V7.3 construct at a 1:5 ratio. The construct indicated at the bottom did not have a fluorescent protein tag, and was not detected by the anti-GFP antibody.
B.- Densitometric quantification of the band intensity relative to the tubulin signal, normalized to the value obtained for cells overexpressing K_V7.2. No significant differences were observed on the relative abundance of WT or Del6 subunits upon K_V7.3 overexpression.

The functional impact of the linker on heteromers was next examined. As previously shown in oocytes (Etxeberria *et al.*, 2004; Schwake *et al.*, 2000), HEK293 cells expressing heteromers channels displayed larger currents (Fig. 3.16B) and an increased surface expression (Fig. 3.17A and 3.17B).

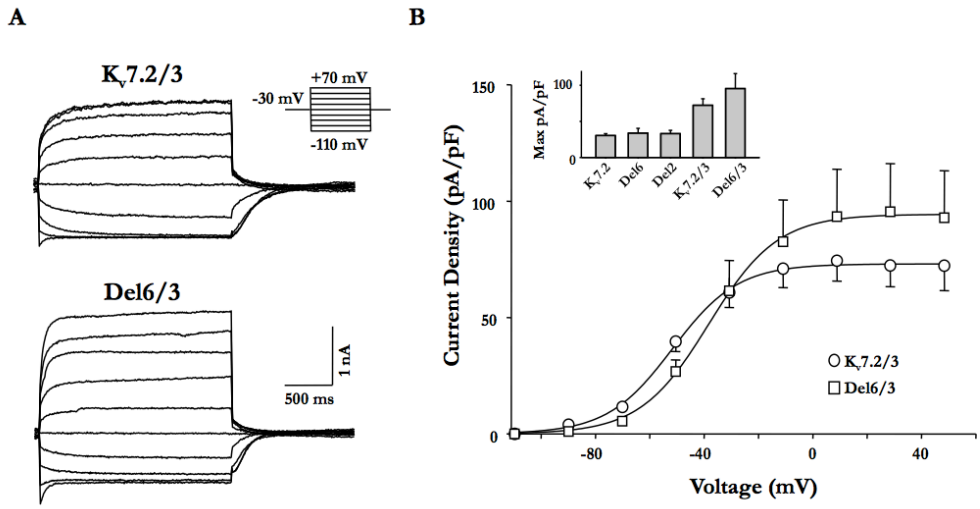

Figure 3.16. K_v7.3/Del6 heteromers displayed larger currents
A.- Representative current recording from HEK293T cells transfected with K_v7.3 and WT or Del6, activated from a holding potential (V_h) = -30 mV after 1,500 ms steps to the indicated voltages.
B.- Current density-voltage relationship from tail currents of K_v7.3 co-expressed with WT or Del6 (n=7) K_v7.2 subunits. Each point represents the mean ± S.E.M. The averaged Boltzmann parameters were: K_v7.2/3: $V_{1/2}$ = -38.2 ± 8.5 mV, Slope = 12.6 ± 5.1, Dmax = 73.0 ± 3.4 pA/pF; Del6/3: $V_{1/2}$ = -51.6± 3.5 mV, Slope = 12.0 ± 3.1, Dmax = 94.3 ± 8.4 pA/pF. Inset: Maximal current density from cells expressing the indicated subunits. * $P \leq 0.05$ for maximal density; unpaired Student's *t* test.

According to the results obtained on protein abundance, the linker had no significant influence on current density, although there was a tendency for Del6/K_v7.3 heteromers to yield larger currents (Fig. 3.16B). However, K_v7.3 had a significant influence on the surface expression of K_v7.2-WT, and while the surface expression of this subunit almost is tripled, that observed by the Del6 is nearly quadrupled (Fig. 3.17). Taken together, these data indicate that removal of the linker favors surface expression of K_v7.2/3 heteromers.

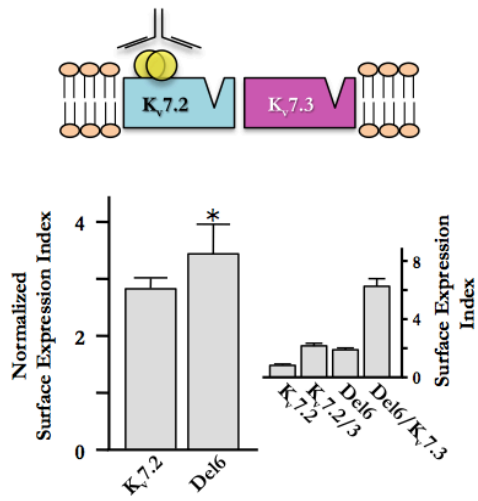

Figure 3.17. Influence of K_V7.3 in surface expression of WT and Del6 subunits. On the top, cartoon representing the scheme of the experiment, indicating that only K_V7.2 subunits are detected at the surface due to the presence of the 2HA tag. Middle, bar graph of the surface expression index normalized to the same index obtained without K_V7.3. The relative increase in surface expression caused by K_V7.3 was significantly larger for Del6 subunits. * $P \leq 0.05$; unpaired Student's *t* test.

CHAPTER 4

Effect of tetramerization in calmodulin binding and surface expression in $K_V7.2$ subunits

Effect of tetramerization in calmodulin binding and surface expression of K_v7.2 subunits

4.1 Introduction

The molecular mechanisms that direct the specific assembly of K_v7 channels are not well understood. The distal C-terminal half contains two tandemly arranged coiled-coils that are supposed to direct the oligomerization: helix C, that forms dimers, and subsequently helix D, that form tetramers (Haitin and Attali, 2008). This region, also called the A-domain, appears to carry all the information for directing the subtype-specific assembly determinants (Haitin and Attali, 2008; Howard *et al.*, 2007). Helices A and B form the binding site for CaM, whose association is required for proper channel assembly and function (Gamper and Shapiro, 2003; Ghosh *et al.*, 2006; Shamgar *et al.*, 2006; Wen and Levitan, 2002; Yus-Najera *et al.*, 2002). In K_v7 channels has been shown that LQT mutations that perturb or significantly weaken the CaM interaction, result in little channel expression in living cells (Ghosh *et al.*, 2006; Shamgar *et al.*, 2006).

Hence, CaM binding seems to be critical for ion channels, whose number and composition at the cell surface determines how cells respond to different stimulus (Gomez-Posada *et al.*, 2011).

Aim of the study

While helices A and B encode the CaM binding domain of K_v7 subunits, helices C and D are responsible for the K_v7 channel assembly. In the present chapter we aim to determine the relationships between CaM binding and tetramerization in order to elucidate the factors that define the trafficking of $K_v7.2$ subunits to the plasma membrane. In this chapter, it is shown that tetramerization favors CaM binding and we have identified a residue that is involved in channel trafficking.

4.2 Results

4.2.1 Del2 mutant does not prevent channel function

Continuing with the deletions performed along the C-terminal of $K_v7.2$ channel (Chapter 3, Fig. 3.1), and once known that Del2 mutant increased protein yield in oocytes (Fig. 3.1, 3.2), the next step was to elucidate the impact of this construct on channel function.

Experiments of patch clamp in whole-cell configuration were performed in HEK293T cells transfected with Del2 subunits. Strikingly, Del2 mutant subunits had an electrophysiological behavior indistinguishable from that of cells expressing the WT subunits (Fig. 4.1). In addition, the impact of the deletion on the Boltzmann parameters was not significant. Of note, as in Del6, there was no correlation between subunit expression (based on fluorescent signal) and functional electrophysiological detection.

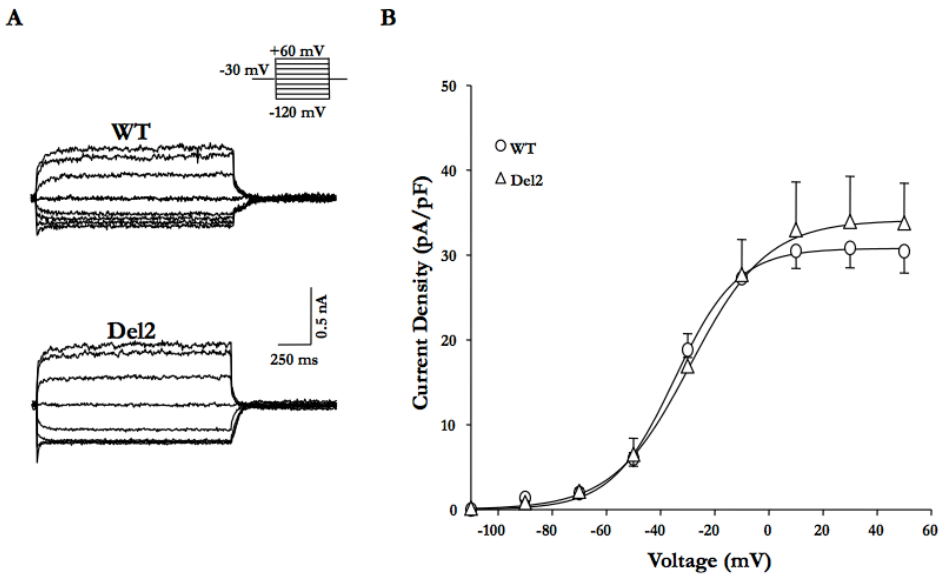

Figure 4.1. Del2 mutant currents are indistinguishable to those obtained for the WT in HEK293T cells.
A.- Representative current recordings from HEK293T cells transfected with WT- or Del2-K_v7.2, activated from a holding potential (V_h) = -30 mV after 1,500 ms steps to the indicated voltages.
B.- Current density-voltage relationship from tail currents of WT (n = 13) channels. Each point represents the mean ± S.E.M. A Boltzmann equation $D = Dmax/(1+e^{((V-V_{1/2})/S)})$ was fitted to the data. The averaged Boltzmann parameters were: WT: $V_{1/2}$ = -34.8 ± 1.9 mV, Slope = 11.6 ± 1.7, Dmax = 30.7 ± 0.9 pA/pF; Del2: $V_{1/2}$ = -29.6 ± 5.5 mV, Slope = 14.2 ± 4.5, Dmax = 34.1 ± 2.6 pA/pF.

4.2.2 Del2 mutant retains the ability of binding calmodulin

To examine the ability of the Del2 and the Del6 subunit mutants to bind CaM, co-immunoprecipitation assays were performed. The results were compared to those obtained with the I340E mutant, a mutation that disrupts CaM binding preventing its surface expression (Etxeberria *et al.*, 2008). Those experiments revealed that CaM interacted with the deleted constructs (Fig. 4.2).

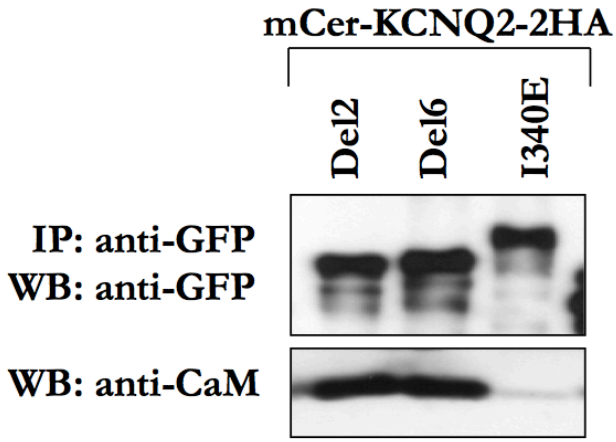

Figure 4.2. Del2 and Del6 mutant subunits bind CaM. Co-immunoprecipitation of full-length mCer-2HA-tagged $K_v7.2$ channels. Proteins from HEK293T cells expressing the constructs indicated were immunoprecipitated with the anti-GFP antibody, separated by SDS-PAGE and analyzed by western blot probed with anti-CaM or anti-GFP antibodies.

4.2.3 $K_v7.2$ helices A-B Del2 fused to Tac do not bind CaM and present reduced glycosylation levels

Previously in the laboratory the trafficking reporter protein Tac has been used to identify determinants of surface expression and it has been observed that the CaM binding site controls the trafficking when is transferred to the Tac protein (Etxeberria *et al.*, 2008). It contains an extracellular N-terminus, a single transmembrane domain and a short C-terminal tail, being constitutively expressed on the cell surface in its native state (Standley *et al.*, 2000). Tac is synthesized as a precursor of 48 kDa, and after being glycosylated in the Golgi it acquires its mature state of 55 kDa. So, to study the influence of the Del2 subunit on trafficking, we designed chimeras composed by Tac, the C-terminus of the K_v7 channel and to

facilitate the detection, a mCFP fluorescent protein was fused at the end of the C-terminal of the channel.

Flow cytometry experiments allow us to record the fluorescent signal from each individual cell. By using the Tac protein reporter (which is mainly expressed at the cell surface) we were able to detect those proteins that are surface stained because cells are not permeabilized. After computational analysis, the result obtained for the experiment will be a histogram that informs about the intensity of fluorescence that each cell has.

Flow cytometry and western blotting assays performed in the past in the laboratory showed that fusion of helices A and B of the $K_v7.2$ subunit does not affect the surface expression when inserted in the Tac monomeric protein. The trafficking parameters obtained for the construct containing the helices A and B were almost equal as for the Tac-CFP (Etxeberria *et al.*, 2008). As expected, the negative control I340E mutant almost completely suppressed surface expression. Glycosylation levels were in agreeing with flow cytometry results, where a reduction on the high molecular weight band was observed for the I340E mutant (Fig. 4.3C, D).

The next step was to further analyze the effects of Del2 and Del6 in Tac (Tac-AB-Del2-CFP, Tac-AB-Del6-CFP).

Flow cytometry analysis of the Del2 mutant gave a remarkably distinct pattern as compared to both the WT and the Del6 construct. As it can be observed in Fig. 4.3A, the obtained histogram reflects a highly heterogeneous sample, Del2 cells expressing a wide range of fluorescent intensities. In contrast, both the WT and the Del6 construct showed the generation of rather uniform fluorescent-enriched cell populations, reflecting an efficient surface expression. The statistical analysis of the flow cytometry data strengthens the disparity of the obtained results (Fig. 4.3 B).

The index of surface expression obtained by the Del2 construct is less than the half of the Del6 construct, (37.9 % *vs.* 100,7 %), while the glycosylation index is 116 % *vs.* 198 % respectively. As results show, there is a correlation between surface expression and glycosylation in both constructs, meaning that both are leaving the ER and reaching the Golgi apparatus although Del6 is better surface expressed (Fig. 4.3).

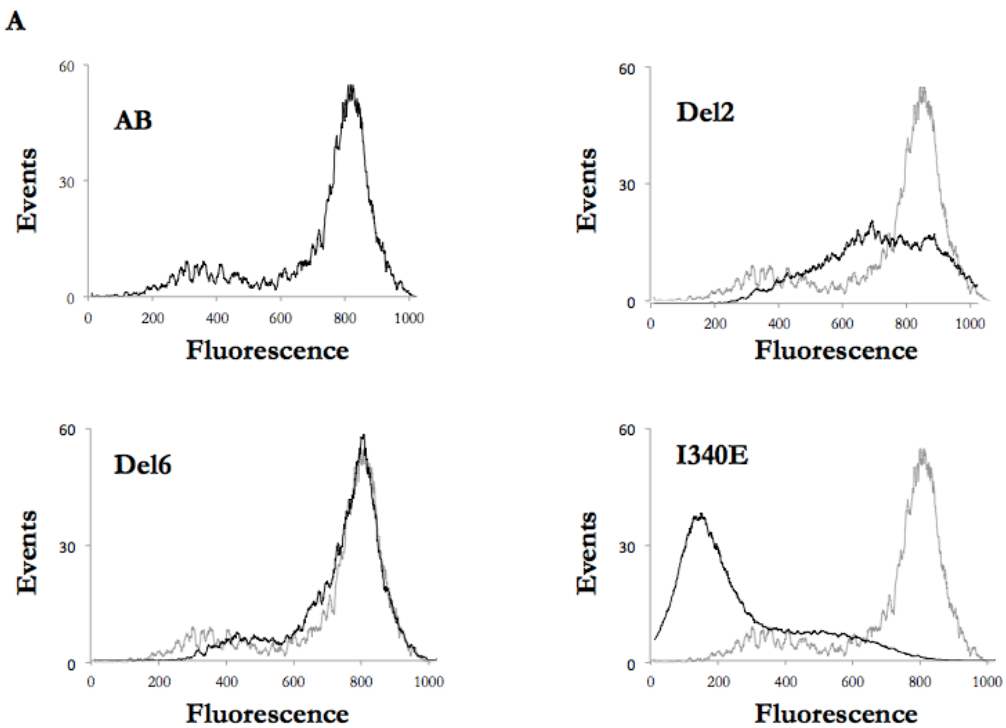

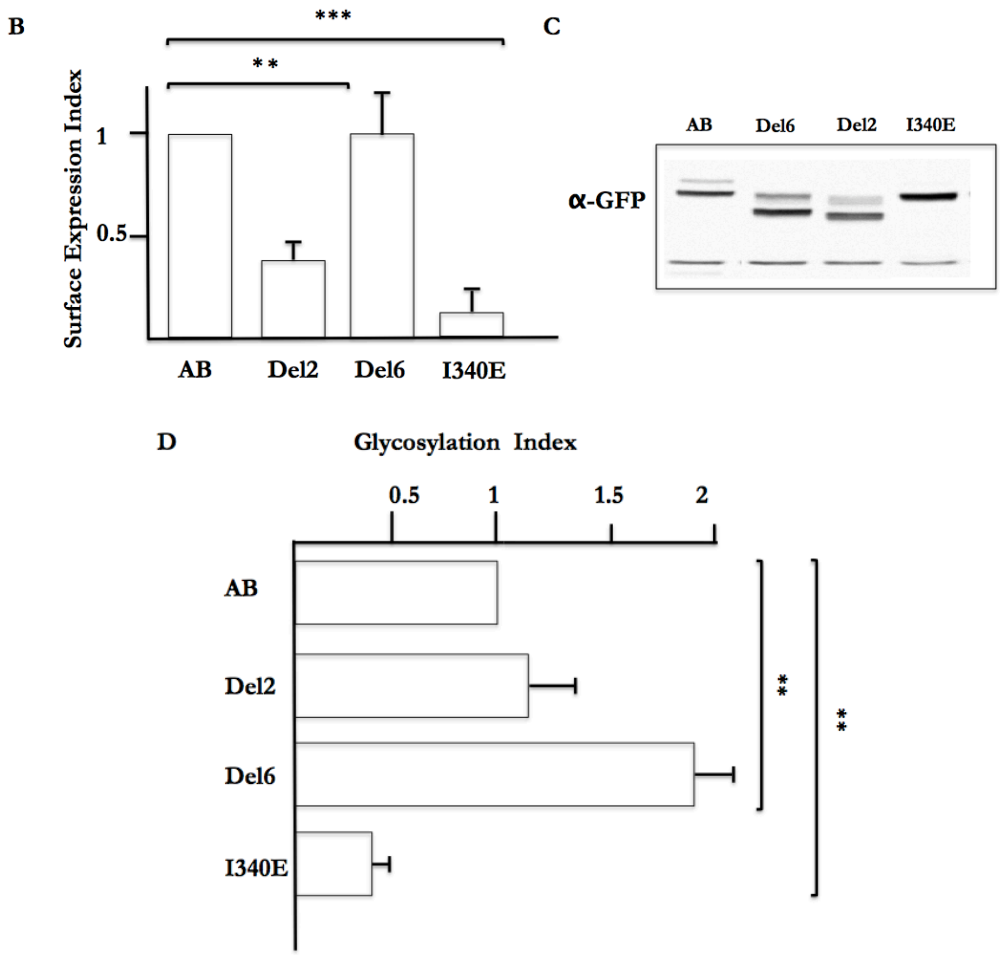

Figure 4.3. Del2 in the Tac protein displays a reduction in the surface expression

A.- Flow cytometry histograms representing the fluorescence of 10,000 cells (events). All histograms are overlapped with the one obtained with the AB construct. It is observed that AB and Del6 are efficiently expressed in the surface comparing to the I340E construct.

B.- The normalized sum of the product of the number of events and fluorescence intensity from the flow cytometry histogram distribution is plotted as surface expression index. Tac-AB-CFP= 100 % (n=4), Tac-AB-Del6-CFP= 100.7 % (n=4), Tac-AB-Del2-CFP= 37.9 % ($p \leq 0.01$** n=4) and Tac-AB-I340E-CFP ($p \leq 0.001$***, n=4).

C.- Protein extracts from HEK293T cells expressing the indicated constructs by using anti-GFP antibody. The upper and the lower band correspond to the mature and the immature band respectively.

D.- The glycosylation of the Del6 construct was larger than that of the AB and Del2 constructs and significantly different. Del2 construct was larger than AB but not significantly different. Tac-AB-CFP= 100 % (n=3), Tac-AB-Del6-CFP= 198 % ($p \leq 0.01$ **) Tac-AB-Del2-CFP= 116 % and Tac-AB-I340E-CFP= 38 % ($p \leq 0.01$***), n=3, paired Student´s *t* test.

4.2.4 Trafficking and CaM binding

To further analyze the relationship between trafficking and CaM binding, Del6 and Del2 constructs were co-immunoprecipitated from solubilized membranes of transiently transfected HEK293T cells. Strikingly, in this set of experiments, not much CaM appeared to be associated with any of the constructs without helices C and D (Tac-AB-CFP, Tac-AB-Del2-CFP, Tac-AB-Del6-CFP) comparing to the full channel configuration (Fig. 4.2), being the Del2 mutant the one with the less CaM bound (Fig. 4.4B). However, previous experiments performed in the laboratory by Dr. Paloma Aivar showed that no CaM appeared to be associated with the Del2 subunit compared to the Del6 construct (Fig. 4.4A). Those differences between the experiments could be associated with problems regarding the effectiveness of the different antibodies. In any case, the Del2 mutant shows a decrease on the intensity of the CaM band compared to the Del6 construct in both cases.

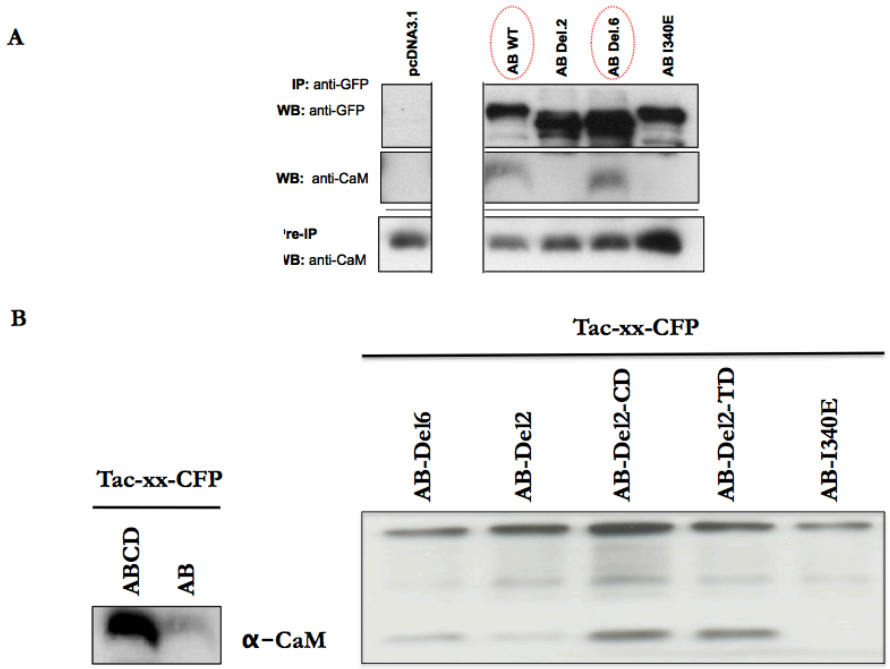

Figure 4.4. CaM binding is impaired in the Del2 mutation.
A.- Figure extracted from Dr. Paloma Aivar´s Thesis were it is shown that Del2 impairs CaM binding.
B.- Protein complexes from HEK293T cells expressing Tac-K_v7.2-C-terminus subunits were immunoprecipitated with anti-GFP antibody, separated by SDS-PAGE and analyzed by western blotting. In the picture are represented the K_v7.2 subunits and immunoprecipitated endogenous CaM detected with anti-GFP and anti-CaM antibodies, respectively.

4.2.5 Tetramerization and trafficking

To further analyze the impact of the tetramerization domain over the WT and the Del2 subunits, helices C and D were fused. Remarkably, CaM binding was recovered (Fig. 4.4B).

However, flow cytometry experiments revealed that the trafficking of the constructs was affected when helices C and D were fused, as Dr. Paloma Aivar

showed before in the laboratory as well as glycosylation (Fig. 4.5). Since CaM binding is recovered when helices C and D are fused, it would be expected a recovery in the trafficking but however, those prevent the trafficking of the constructs to the membrane.

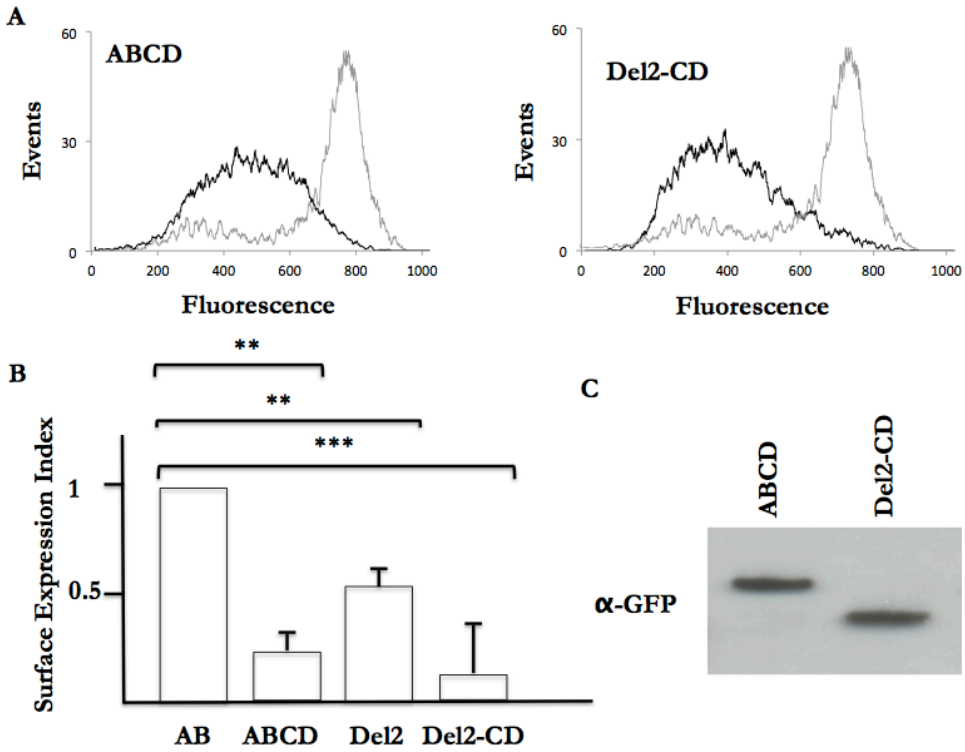

Figure 4.5. Flow cytometry analysis of the chimeras
A.- Flow cytometry histograms. It is observed that Tac-ABCD-CFP and Tac-AB-Del2-CD-CFP are not efficiently expressed in the surface comparing to the AB construct. All histograms are overlapped with the one obtained with the AB construct.
B.- The normalized sum of the product of the number of events and fluorescence intensity from the flow cytometry histogram distribution is plotted as surface expression index. Tac-AB-CFP= 100 % (n=4), Tac-ABCD-CFP= 22.52 % ($p=0.006^{**}$ n=3), Tac-Del2-CD-CFP= 11.67 % ($p\leq0.001^{***}$ n=3).
C.- Glycosylation levels are reduced when helices CD are inserted. Western blot probed with an anti-GFP antibody of HEK293T cell extracts expressing Tac-CFP constructs carrying the indicated mutations.

4.2.6 Is tetramerization playing a role in CaM binding?

Something interesting is the fact that the Del2 construct when expressed in HEK293T cells in the full channel configuration (mCer-K_v7.2-Del2-2HA) behaves in the same way as the WT, in terms of functionality, CaM binding and surface expression. However, when Del2 is transposed to Tac, and helices C and D are deleted (Tac-AB-Del2-CFP), CaM binding is reduced as well as surface expression is. Indeed, when helices C and D are fused to Tac-AB-Del2-CFP (Tac-ABCD-Del2-CFP) and Tac-AB-CFP (Tac-ABCD-CFP), CaM binding is recovered (Fig. 4.4).

Helices C and D are known to help in the assembly and tetramerization of the K_v7.2 channels, but, as well, they could be involved in more functions. In order to characterize the tetramerization and assembly of K_v7.2 channels, an artificial tetramerization domain [TD, a mutated version of the GCN4 leucine zipper, pLI (Harbury *et al.*, 1993; Yuan *et al.*, 2003)] was fused to the Tac-AB-Del2-CFP construct, resulting in Tac-AB-Del2-TD-CFP. Co-immunoprecipitation from solubilized membranes of transiently transfected HEK293T cells revealed that this construct was now able to bind CaM, confirming that tetramerization helps CaM binding (Fig. 4.4).

However, flow cytometry experiments revealed that surface expression was not recovered in any of the constructs analyzed (Fig. 4.6A). Actually, all constructs to which the TD was fused presented a similar flow cytometry pattern, as well as the glycosylation pattern, which revealed a reduction on the high molecular weight band, consistent with the results obtained by flow cytometry (Fig. 4.6B).

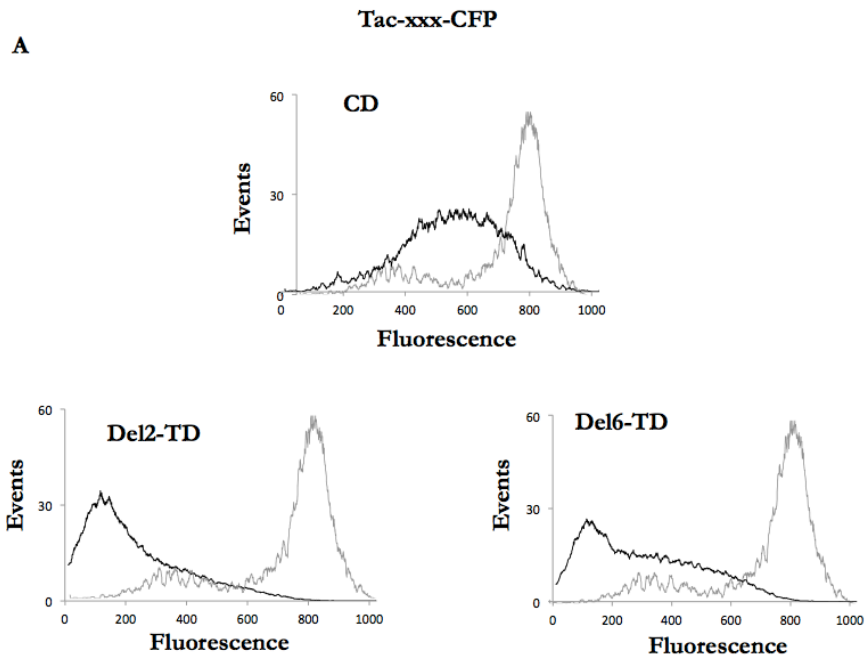
A
Tac-xxx-CFP
CD
Events
Fluorescence
Del2-TD
Del6-TD
0
30
60
200
400
600
800
1000

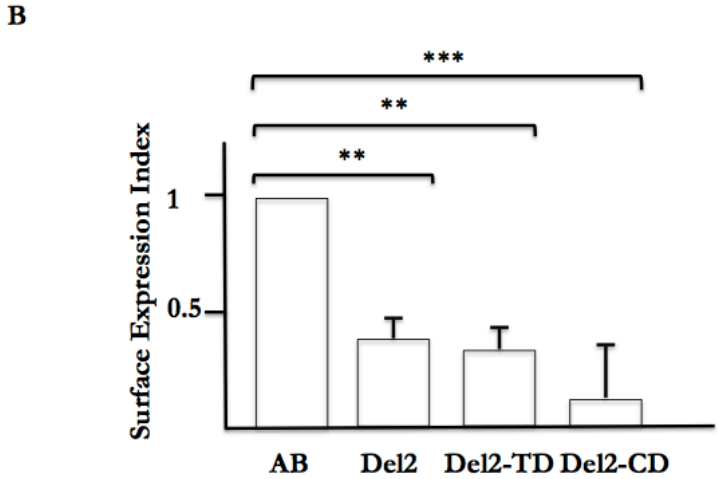
B
***
**
**
Surface Expression Index
1
0.5
AB
Del2
Del2-TD
Del2-CD

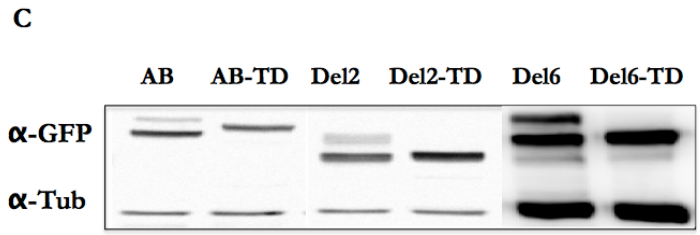

Figure 4.6. Surface expression is abolished when TD is fused to the C-terminus of K_v7.2 subunits.
A.- Flow cytometry histograms where it is observed that Del2-TD and Del6-TD are not efficiently expressed in the surface comparing to the AB construct.
B.- The normalized sum of the product of the number of events and fluorescence intensity from the flow cytometry histogram distribution is plotted as surface expression index. Tac-AB-CFP= 100 % (n=4), Tac-Del2-TD-CFP= 12,08 % (p=0.006** n=3), Tac-Del2-CD-CFP= 6.48 % (p≤0.001*** n=3).
C.- Glycosylation levels are reduced when TD is inserted. Western blot probed with an anti-GFP antibody of HEK293T cell extracts expressing Tac-CFP constructs carrying the indicated mutations. Tubulin is detected as a loading control.

In view of the results obtained, we analyzed the TD in the Tac protein to observe how it affects to its trafficking. Singularly, the construct was not surface expressed, suggesting that Tac is not compatible with signals related to multimerization.

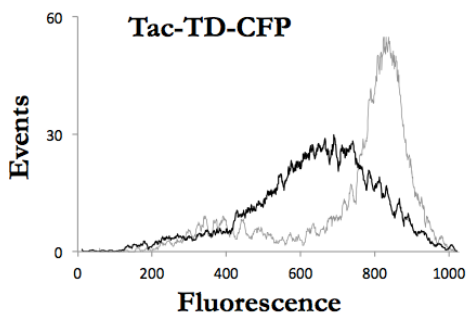

Figure 4.7. The TD abolishes surface expression when fused to Tac protein. Flow cytometry histogram where it is observed that TD is not efficiently expressed in the surface comparing to the AB construct.

To examine the interaction in more detail, we performed binding assays as in Chapter 3. As it can be observed in Figure 4.8, there is an increase in the fluorescence emission of the D-CaM when Del2-TD is added, both in the presence and absence of Ca^{2+}, indicating a conformational change upon binding to CaM. On the contrary, no change on the fluorescence emission was observed in the case of Del2. So, the presence of the TD is affecting CaM binding.

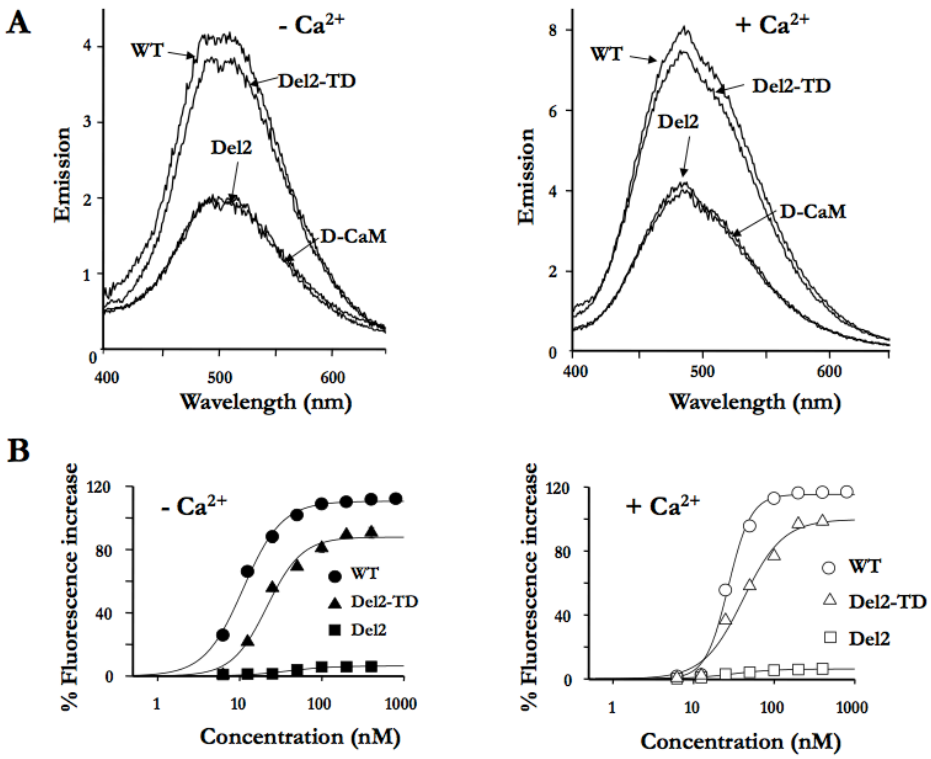

Figure 4.8. Characterization of Del2-TD interaction with CaM.
A.- Emission spectra of 12.5 nM D-CaM in the absence (left panel; 10 mM EGTA and no added Ca^{2+}), and in the presence of 2 μM free Ca^{2+} (right panel), as well as in the presence of molar excess of the indicated GST-K_v7.2 fusion proteins (200 nM). Note the difference in the fluorescence emission axis, as well as the shift in the peak emission to the left in the presence of Ca^{2+}.
B.- Relative concentration-dependent enhancement of D-CaM fluorescence emission in the absence (left) and presence of 2 μM free Ca^{2+} (right). The parameters used to fit a Hill equation to the data for WT in the absence of

Ca^{2+}were: Max = 111 ± 1.4, EC_{50} = 11 ± 0.5 nM, h = 1.8 ± 0.2 (n = 9). For Del2 in the absence of Ca^{2+}: Max = 6.4 ± 0.5, EC_{50} = ND., h = ND. (n = 4). For Del2-TD in absence of Ca^{2+}: Max = 88 ± 3.3, EC_{50} = 21 ± 2.1 nM, h = 2.1 ± 0.3 (n = 4). For WT in the presence of Ca^{2+}: Max = 115 ± 2.2, EC_{50} = 27 ± 1.2 nM, h = 3.1 ± 0.4 (n = 9). For Del2 in the presence of Ca^{2+}: Max = 6.3 ± 0.3, EC_{50} = ND., h = ND. (n = 4). For Del2-TD in the presence of Ca^{2+}: Max = 100 ± 5.9, EC_{50} = 42 ± 5.7 nM, h = 1.7 ± 0.3 (n = 4). The data represent the means ± standard error from four independent experiments. The error bars are smaller than the symbols. N.D.: Not determined.

4.2.7 Identification of relevant residues in the Del2 construct

In order to determine which are the aminoacids involved in the phenomena, a systematic evaluation of the Del2 was performed, adding three by three aminoacids each time, reducing the deletion until T368-T501, three aminoacids before the Del6 construct starts (Fig. 4.9).

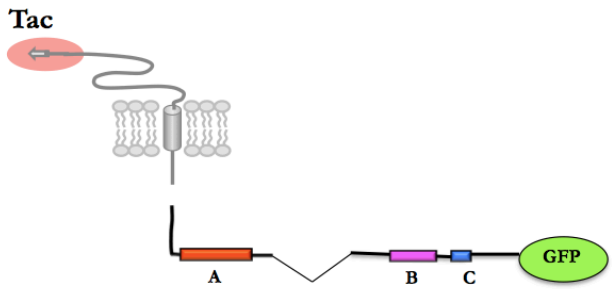


```
Del2: T359-T501 - DLHST--------------TEDLTPG
      Y362-T501 - DLHSTWQY-----------TEDLTPG
      R365-T501 - DLHSTWQYYER--------TEDLTPG
      T368-T501 - DLHSTWQYYERTVT-----TEDLTPG
Del6: Y372-K493 - DLHSTWQYYERTVTVPMY-
```

Figure 4.9. Schematic representation of the deletions done. Sequence alignment of the deletions performed done adding three by three aminoacids to further analyzed the surface expression of the constructs by flow cytometry. Deletions were performed by PCR following the protocol described in the Experimental Procedures chapter (P1).

Surprisingly, we observed by flow cytometry that just adding the following three aminoacids (WQY) to Del2, surface expression was recovered. In the same way, the glycosylation experiments showed an increase on the intensity of the high molecular band, confirming the results obtained by flow cytometry (Fig. 4.10).

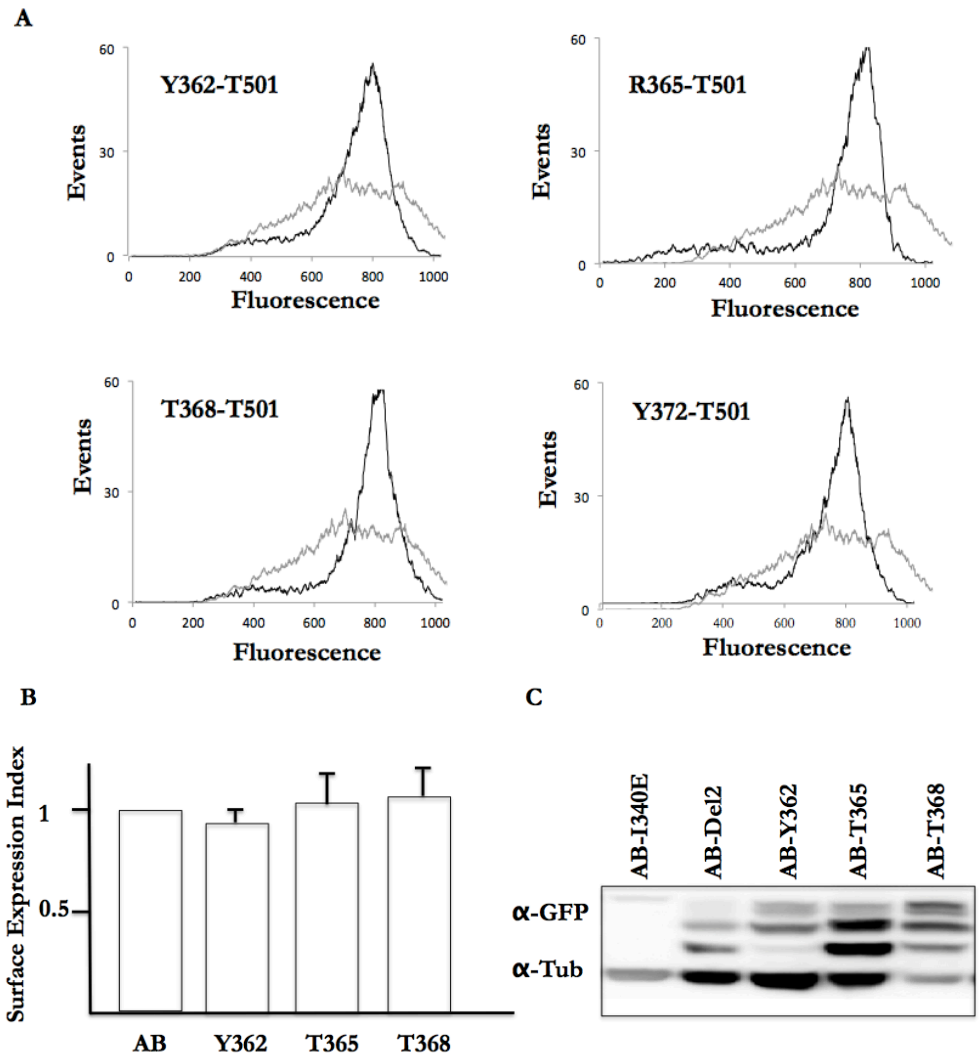

Figure 4.10. Surface expression is recovered when next 3 aminoacids after Del2 are included.
A.- All histograms are overlapped with the one obtained with the Del2 construct. It is observed that all of the constructs are efficiently surface expressed. All histograms are overlapped with the one obtained with the Del2 construct.
B.- The normalized sum of the product of the number of events and fluorescence intensity from the flow cytometry histogram distribution is plotted as surface expression index. Tac-AB, Tac-AB-Y362-T501, Tac-AB-Y362-T501 and Tac-AB-T368-T501 constructs. There is no significance difference between the groups (n=4).
C.- Glycosylation levels are recovered when next three aminoacids are added. Western blot probed with an anti-GFP antibody of HEK293T cell extracts expressing Tac-CFP constructs carrying the indicated mutations. There are not significant differences between the groups.

Some new deletions were performed in which these first two aminoacids were eliminated one by one (Fig. 4.11). These new constructs were again analyzed by flow cytometry.

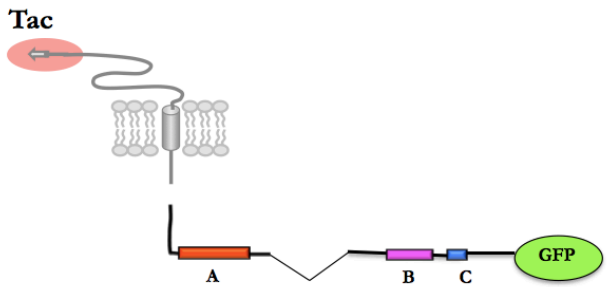


```
Del2: T359-T501 - DLHST----------TEDLTPG
      W360-T501 - DLHSTW---------TEDLTPG
      Q361-T501 - DLHSTWQ--------TEDLTPG
      Y362-T501 - DLHSTWQY-------TEDLTPG
```

Figure 4.11. Sequence alignment of the different K_v7 mutants. Three by three aminoacids were added to further analyze the surface expression of the constructs by flow cytometry. Deletions were performed by PCR following the protocol described in the Experimental Procedures chapter (P1).

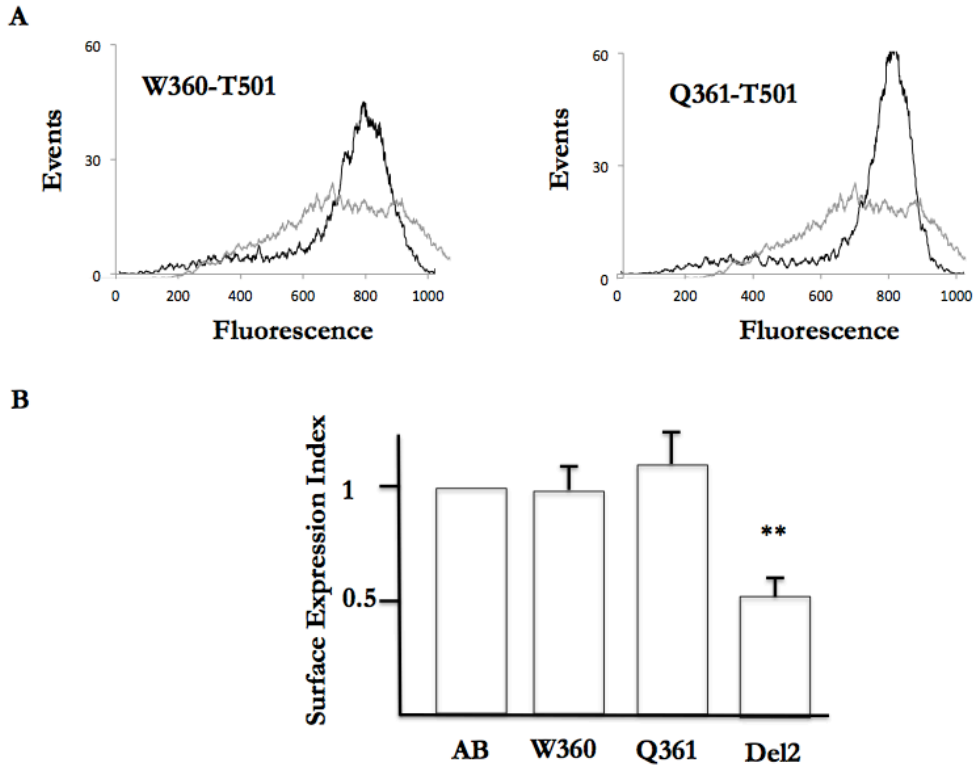

Figure 4.12. Analysis of the Tac-chimeras.
A.- Flow cytometry histograms where all the constructs are efficiently surface expressed. All histograms are overlapped with the one obtained with the Del2 construct.
B.- The normalized sum of the product of the number of events and fluorescence intensity from the flow cytometry histogram distribution is plotted as surface expression index. There are no significance differences between the groups (n=3).

This time by adding only one aminoacid to the Del2 construct (W) surface expression was recovered (Fig. 4.12). It can be concluded that in the absence of the W, trafficking regulation is lost, and probably this residue is also involved in CaM binding, although more experiments should be performed to further corroborate this.

4.2.7 CD4 and its artificial tetramerization domain as a new tool

So far, our results suggest that when tetramerization is restored CaM binding is recovered. Therefore, we used the same domain that has been used to assemble the Shaker potassium channel in the absence of the T1 domain (it mediates the tetrameric assembly of this channel) (Zerangue *et al.*, 2000) subcloned into CD4. Yuan and collaborators used this construct to characterize an arginine-based ER localization signal comparing different surface expression levels (Yuan *et al.*, 2003). As they showed, CD4 both in the presence and the absence of the TD domain were well surface expressed, so, the aim was to subclon the different C-terminal constructs in order to restore surface expression.

Nevertheless, initial attempts did not give good enough results. In order to find the optimal conditions that could make CD4 to behave in a similar way as Yuan and collaborators observed, further experiments would be required. This way, we could verify the potential connection between tetramerization, CaM binding and surface expression.

CHAPTER 5

DISCUSSION

General discussion

Ion channels are broadly expressed throughout the body and they are implicated in a large variety of diseases. Since the discovery of the first ion-channel-related disease, the cystic fibrosis in 1989, the number of known neurological channelopathies is increasing. Some of them have been already identified and characterized, teaching us important lessons about the molecules and the cellular processes that underlie electrical excitability and excitability disorders. In almost 29 different ion channel genes, mutations have been identified which develop in monogenic diseases. Channelopathies affect almost all areas of neurological practice, including epileptology movement disorders, headache, peripheral nerve, pain and myology (Kullmann and Waxman, 2010). Potassium channels, the largest ion channel group, contribute nearly to all the cellular electric signaling events, being the main suspect of epilepsy one-quarter century ago. As most genetic diseases, ion channel mutations are early manifested in life, being sometimes restricted only to the developmental interval as neonatal seizures. Most known channelopathies are dominantly inherited, some of them being only partially penetrant or having highly diverse manifestations (Kullmann, 2010).

K_v7 channels exhibit some structural and functional characteristics that make them different from other potassium channels. The C-terminus with its structural domains includes coiled-coil and amphipathic α helices that contain calmodulin-binding motifs and basic amino-acid clusters. The distal C-terminus of $K_v7.2$ channels plays an important role in channel trafficking, gating and assembly, being

indeed a multimodular structure that also serves as the binding module for a variety of molecules such as CaM and PIP_2 (Haitin and Attali, 2008; Howard *et al.*, 2007).

The data shown in this thesis demonstrates that the linker connecting helices A and B is not essential for channel function. Instead, cells that are expressing linker-less subunits yield more protein and allow the flow of similar current intensities than those of cells expressing WT subunits. The data suggest that the linker does not have a major impact on the maximal current, but it does almost double the channel probability to reach the plasma membrane.

From these results, it can be inferred that if the currents are similar but there are twice as many channels at the membrane, removal of the linker does indeed reduce channel function. The basis of this reduction is unknown, but it is probably not due to a reduction on PIP_2 affinity because there are no significant differences between WT and Del6. In addition to PIP_2, other regulators such as PKC or CaM converge in the CaM binding site, causing a reduction in the channel activity (Haitin and Attali, 2008). Presumably, the removal of the linker causes a restructuration of the CaM binding domain leading to a reduction on the channel probability to be opened.

The rules that govern the trafficking of K_v7 channels to the membrane are poorly understood. The pore, the assembly domain and CaM have been shown to play important roles (Alaimo *et al.*, 2009; Etxeberria *et al.*, 2004; Gomez-Posada *et al.*, 2010; Schwake *et al.*, 2000). The surface expression analysis on human HEK293T cells revealed a remarkable lack of correlation between total and surface expression. In other words, an increase in protein production does not necessarily lead to an increase in surface expression and function. This lack of correlation between protein amounts and function point to the existence of unknown

underlying variables within the cell that may play a major role on the trafficking. But, which is the nature of these variables? Given its implication on the trafficking, CaM is a likely candidate. However, in preliminary experiments overexpressing CaM we still observe a great degree of variability, suggesting that other factors apart from CaM are involved. Although CaM binds to helices A-B, we have found that removal of the linker has a small impact on the interaction and, based on the analysis of a series of CaM-binding perturbing mutants, the *in vitro* results would predict a reduction in surface expression (Alaimo *et al.*, 2009). Thus, the results of the binding assays suggest that CaM is not playing an important role in the linker-mediated effects.

We have found that the protein yield depends on the number of loops present in the channel, such that cells expressing channels with four loops have much lower steady-state levels than cells expressing loop-less channels. What is the mechanism for this loop-dependent decrease in protein production? The simplest explanation for the observed results is that the loop promotes protein degradation, and the more loops are present, the faster the degradation rate. However, we did not obtain any evidence supporting this view. On the contrary, the degradation rate of loop-less subunits appeared to be slightly faster than that of four loop containing channels. If the degradation rate is not increased, we are immediately forced to propose that the synthesis rate is reduced as a function of the number of loops present in the tetrameric assembly.

Little is known regarding protein rate synthesis regulation in eukaryotes. It is well documented that nascent peptide-dependent translation arrest is crucial for the quality control of eukaryotic gene expression. Along the ribosomal exit tunnel, pausing due to charge-specific interactions between the tunnel and the nascent peptide has been inferred (Lu and Deutsch, 2008). Although *in vitro* elongation is a

relatively uniform process, some heterogeneity has been observed *in vivo*, leading to the hypothesis that elongation of nascent chains may be the target of biological regulation (Cruz-Vera *et al.*, 2011; Fahraeus, 2005; Ito *et al.*, 2010; Tenson and Ehrenberg, 2002). Because the loops in one K_v7 subunit affect the yield of a different subunit, the lack of effect on the degradation rate implies that the synthesis of the subunits may be coupled. In other words, if the rate synthesis of one subunit is very slow (because it has a loop), that will cause slowing down the synthesis of another subunits. How can this occur? One possibility is that the subunit assembly is completed before the synthesis is completed so the loop in one subunit affects the fate of the whole complex. In fact, studies carried out with $K_v1.3$ potassium channels, which have an N-terminal tetramerization domain called T1, have demonstrated that T1 tetramers form between neighbouring subunits while the nascent channel peptides are still attached to the ribosomes, perhaps before the monomer is completely synthesized (Lu *et al.*, 2001). In K_v7 channels, the A-B loop is located after the transmembrane domain, which in some channels is sufficient for tetramerization. The fact that the effect of the loop is subunit-specific suggests that helices C and D, which have been implicated in K_v7 subunit-specific assembly (Maljevic *et al.*, 2003; Schwake *et al.*, 2006), may play a role on the process. However, these two helices are located downstream the A-B linker. This theory implies that the loop will influence the synthesis rate even after it has been fully read by the ribosome. It has been proposed that channels with a C-terminal assembly domain may be held in the translocon and released into the bilayer in a coupled event with C-terminal tetramerization (Deutsch, 2003). However, the temporal and spatial sequence of events for the assembly and for the K_v7 channel translocation is completely unknown.

Another puzzling observation from the present thesis is that the $K_v7.2$ loop did not affect the production of $K_v7.3$ subunits, and that the presence of $K_v7.3$ did

not affect the relative total protein levels of $K_v7.2$ with and without the loop. What is the basis for this specificity? One possibility is that the synthesis rate of $K_v7.3/K_v7.2$ is so slow that further delays caused by the $K_v7.2$ loop are inconsequential. Alternatively, the loop may function in conjunction with other determinants that are not present in $K_v7.3$, or there are maybe other regions on $K_v7.3$ that neutralize the effect of the loop. By differentially affecting the synthesis rate of homomers and heteromers, the loop will favor the production of one species over the others. This differential effect has potentially important physiological consequences. Co-expression of $K_v7.2$ and $K_v7.3$ leads to greater surface expression and the generation of much larger currents than when either subunit is expressed alone (Etxeberria *et al.*, 2004; Maljevic *et al.*, 2003; Wang *et al.*, 1998). Additionally, channels produced following $K_v7.2/K_v7.3$ co-expression have ionic permeation and conductive properties distinct from those produced by individual expression of $K_v7.2$ or $K_v7.3$ (Prole and Marrion, 2004). Neurons contain a diverse repertoire of ion channel complexes, and the cell must ensure that associating subunits co-exist spatially and temporally. The differential effect of the A-B loop on $K_v7.2$ homomers and $K_v7.2/3$ heteromers could therefore influence the formation of different subunit combinations, probably favoring the formations of heteromers.

Previous studies in the laboratory have shown that the Ca^{2+}-CaM interaction appears to be critical for the correct of $K_v7.2$ channel activity, discerning a strong correlation between CaM binding and surface expression, as it controls channel exit from the ER. Through Chapter 4, we have further characterized the role played of Del2 construct based on biochemical and electrophysiological approaches. It has been observed that deletions located around the IQ motif do not affect neither channel assembly nor CaM binding (Del2/Del6). Moreover, $K_v7.2$ subunits are efficiently transported to the surface of the plasma membrane.

However, when the region under study was deeply analyzed by means of the Tac system, this effect was not observed. In that case, the assembly, CaM binding and subsequently trafficking was negatively affected when the assembly domain was removed.

5.3.1 Tetramerization and trafficking are inter-related processes

It has been shown that improper or abolished tetramerization of potassium ion channels leads to channel retention at the ER (Steele *et al.*, 2007). Here, we have demonstrated a role of CaM in channel assembly and trafficking by deleting the linkers between helices A and B (where the IQ domain is supposed to be) and helices C and D (assembly domain) in the Tac system, Tac-AB-Del2.

While helices A and B bind CaM in the absence of helices C and D (Yus-Najera *et al.*, 2002), helices C and D assemble in a tetrameric fashion independently. (Wiener *et al.*, 2008). To study the effect of the assembly domain in CaM binding, we choose the Tac protein and the tetrameric domain of the GCN4 leucine zipper (TD). Although it has been shown that the fussion of this domain is compatible with an efficient membrane protein exit from the ER (Yuan *et al.*, 2003), it prevented surface expression of the Tac protein. A possibility to explain this, is the fact that Tac multimers do not exit the ER, do not fold correctly or maybe, they are exposing cryptic retention signals that make Tac be retrieved to the ER when exposed due to an improperly assembled complex as a result of a multimeric assembly. Although Tac has been shown to be constitutively expressed on the cell surface in its native state (Bonifacino *et al.*, 1990), it seems that multimers are not compatible with trafficking. In any case, little is known regarding the specific trafficking parameters that make the Tac protein be expressed in the membrane.

In any case, when the TD was fused to Tac, the CaM binding was recovered, suggesting that both mechanisms, (CaM binding and assembly) are independent but inter-related. Future experiments would determine whether CD4 is able to recover surface expression due to its tetramer-forming ability.

5.3.2 BFNC-linked mutations

The effect of tryptophan is remarkable for channel trafficking. It has been observed that this aminoacid is implicated in trafficking regulation and probably in CaM binding. This is somehow surprising as W is not exactly located in the IQ motif. We performed an alignment of the different K_v7 isoforms ($K_v7.1$-$K_v7.5$) (www.ebi.ac.uk/Tools/msa/clustalw2) (Fig. 5.1), showing that T and W are well conserved within all K_v7 family members. In this regard, there is a mutation that has been linked to this region that causes neonatal convulsions (Volkers *et al.*, 2009). The C-terminal mutation T359K was detected in a family who suffered from BFNC (Volkers *et al.*, 2009). Moreover, some functional studies have demonstrated that, although this mutant is expressed at the cell surface in HEK293T, heterozygously expressed mutants with $K_v7.2$ caused a 75-80 % reduction in the M-current as compared to WT-$K_v7.2$/$K_v7.3$ channels. More experiments are required to assess the precise effect of this specific mutation in CaM binding.

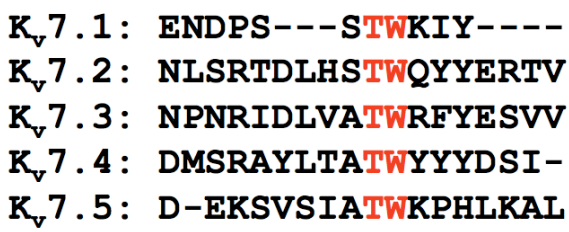

Figure 5.1 Sequence alignment of the different K_v7 subunits. Alignment of the C-terminus starting from helix A and the linker between helix A and B of the different K_v7 subunits. In red are the conserved aminoacids within the different K_v7 isoforms.

A deeper analysis of the biochemical and functional consequences of specific deletions and/or mutations affecting K^+ channels, will provide additional clues on our understanding of ion channel function and their association with diseases of actual importance.

CONCLUSIONS

Conclusions

1.- The absence of the linker between helices A and B of K_v7.2 channels increases protein yield, facilitates channel trafficking to the plasma membrane and is not associated with a decrease of protein degradation. However, there is no correlation between the amount of protein and its function, as they flow similar current intensities than the WT.

2.- The tetramerization domain favours calmodulin binding in K_v7.2 channels.

3.- The W360 residue, which is well conserved among the K_v7 family, is involved in channel trafficking and may play an important role in CaM binding of K_v7 channels.

BIBLIOGRAPHY

Bibliography

Adams PR, Brown DA and Constanti A (1982). M-currents and other potassium currents in bullfrog sympathetic neurones. *J Physiol*, 330, 537-572.

Alaimo A, Gomez-Posada JC, Aivar P, Etxeberria A, Rodriguez-Alfaro JA, Areso P and Villarroel A (2009). Calmodulin activation limits the rate of KCNQ2 K+ channel exit from the endoplasmic reticulum. *J Biol Chem*, 284, 20668-20675.

Bakke O and Dobberstein B (1990). MHC class II-associated invariant chain contains a sorting signal for endosomal compartments. *Cell*, 63, 707-716.

Barnes JA and Gomes AV (1995). PEST sequences in calmodulin-binding proteins. *Mol Cell Biochem*, 149-150, 17-27.

Benham C, Gunthorpe,M. J., Davis, J. (2003). TRPV channels as temperature sensors. *Cell Calcium*, 33, (2003) 2479–2487.

Berridge MJ (1993). Inositol trisphosphate and calcium signalling. *Nature*, 361, 315-325.

Biervert C, Schroeder BC, Kubisch C, Berkovic SF, Propping P, Jentsch TJ and Steinlein OK (1998). A potassium channel mutation in neonatal human epilepsy. *Science*, 279, 403-406.

Biervert C and Steinlein OK (1999). Structural and mutational analysis of KCNQ2, the major gene locus for benign familial neonatal convulsions. *Hum Genet*, 104, 234-240.

Bofill-Cardona E, Vartian N, Nanoff C, Freissmuth M and Boehm S (2000). Two different signaling mechanisms involved in the excitation of rat sympathetic neurons by uridine nucleotides. *Mol Pharmacol*, 57, 1165-1172.

Bonifacino JS, Cosson P and Klausner RD (1990). Colocalized transmembrane determinants for ER degradation and subunit assembly explain the intracellular fate of TCR chains. *Cell*, 63, 503-513.

Borgatti R, Zucca C, Cavallini A, Ferrario M, Panzeri C, Castaldo P, Soldovieri MV, Baschirotto C, Bresolin N, Dalla Bernardina B, Taglialatela M and Bassi MT (2004). A novel mutation in KCNQ2 associated with BFNC, drug resistant epilepsy, and mental retardation. *Neurology*, 63, 57-65.

Bradford MM (1976). A rapid and sensitive method for the quantitation of microgram quantities of protein utilizing the principle of protein-dye binding. *Anal Biochem*, 72, 248-254.

Brodsky JL and Skach WR (2011). Protein folding and quality control in the endoplasmic reticulum: Recent lessons from yeast and mammalian cell systems. *Curr Opin Cell Biol*, 23, 464-475.

Brown DA and Adams PR (1980). Muscarinic suppression of a novel voltage-sensitive K+ current in a vertebrate neurone. *Nature*, 283, 673-676.

Brown DA, Constanti A and Adams PR (1981). Slow cholinergic and peptidergic transmission in sympathetic ganglia. *Fed Proc*, 40, 2625-2630.

Brown DA, Hughes SA, Marsh SJ and Tinker A (2007). Regulation of M(Kv7.2/7.3) channels in neurons by PIP(2) and products of PIP(2) hydrolysis: significance for receptor-mediated inhibition. *J Physiol*, 582, 917-925.

Brown DA and Passmore GM (2009). Neural KCNQ (Kv7) channels. *Br J Pharmacol*, 156, 1185-1195.

Castaldo P, del Giudice EM, Coppola G, Pascotto A, Annunziato L and Taglialatela M (2002). Benign familial neonatal convulsions caused by altered gating of KCNQ2/KCNQ3 potassium channels. *J Neurosci*, 22, RC199.

Charlier C, Singh NA, Ryan SG, Lewis TB, Reus BE, Leach RJ and Leppert M (1998). A pore mutation in a novel KQT-like potassium channel gene in an idiopathic epilepsy family. *Nat Genet*, 18, 53-55.

Chevet E, Cameron PH, Pelletier MF, Thomas DY and Bergeron JJ (2001). The endoplasmic reticulum: integration of protein folding, quality control, signaling and degradation. *Curr Opin Struct Biol*, 11, 120-124.

Clapham DE (2003). TRP channels as cellular sensors. *Nature*, 426, 517-524.

Cooper EC, Aldape KD, Abosch A, Barbaro NM, Berger MS, Peacock WS, Jan YN and Jan LY (2000). Colocalization and coassembly of two human brain M-type potassium channel subunits that are mutated in epilepsy. *Proc Natl Acad Sci U S A*, 97, 4914-4919.

Cooper EC and Jan LY (2003). M-channels: neurological diseases, neuromodulation, and drug development. *Arch Neurol*, 60, 496-500.

Cosens DJ and Manning A (1969). Abnormal electroretinogram from a Drosophila mutant. *Nature*, 224, 285-287.

Cruzblanca H, Koh DS and Hille B (1998). Bradykinin inhibits M current via phospholipase C and Ca2+ release from IP3-sensitive Ca2+ stores in rat sympathetic neurons. *Proc Natl Acad Sci U S A*, 95, 7151-7156.

Cruz-Vera LR, Sachs MS, Squires CL and Yanofsky C (2011). Nascent polypeptide sequences that influence ribosome function. *Curr Opin Microbiol*, 14, 160-166.

Czech MP (2000). PIP2 and PIP3: complex roles at the cell surface. *Cell*, 100, 603-606.

Das B, Chattopadhyay S, Bera AK and Dasgupta C (1996). In vitro protein folding by ribosomes from Escherichia coli, wheat germ and rat liver: the role of the 50S particle and its 23S rRNA. *Eur J Biochem*, 235, 613-621.

Dedek K, Kunath B, Kananura C, Reuner U, Jentsch TJ and Steinlein OK (2001). Myokymia and neonatal epilepsy caused by a mutation in the voltage sensor of the KCNQ2 K+ channel. *Proc Natl Acad Sci U S A*, 98, 12272-12277.

Delmas P and Brown DA (2005). Pathways modulating neural KCNQ/M (Kv7) potassium channels. *Nat Rev Neurosci*, 6, 850-862.

Delmas P, Wanaverbecq N, Abogadie FC, Mistry M and Brown DA (2002). Signaling microdomains define the specificity of receptor-mediated InsP(3) pathways in neurons. *Neuron*, 34, 209-220.

Deutsch C (2002). Potassium channel ontogeny. *Annu Rev Physiol*, 64, 19-46.

Deutsch C (2003). The birth of a channel. *Neuron*, 40, 265-276.

Doyle DA, Morais Cabral J, Pfuetzner RA, Kuo A, Gulbis JM, Cohen SL, Chait BT and MacKinnon R (1998). The structure of the potassium channel: molecular basis of K+ conduction and selectivity. *Science*, 280, 69-77.

Ellgaard L and Helenius A (2003). Quality control in the endoplasmic reticulum. *Nat Rev Mol Cell Biol*, 4, 181-191.

Ellgaard L, Molinari M and Helenius A (1999). Setting the standards: quality control in the secretory pathway. *Science*, 286, 1882-1888.

Etxeberria A, Aivar P, Rodriguez-Alfaro JA, Alaimo A, Villace P, Gomez-Posada JC, Areso P and Villarroel A (2008). Calmodulin regulates the trafficking of KCNQ2 potassium channels. *FASEB J*, 22, 1135-1143.

Etxeberria A, Santana-Castro I, Regalado MP, Aivar P and Villarroel A (2004). Three mechanisms underlie KCNQ2/3 heteromeric potassium M-channel potentiation. *J Neurosci*, 24, 9146-9152.

Etzioni A, Siloni S, Chikvashvilli D, Strulovich R, Sachyani D, Regev N, Greitzer-Antes D, Hirsch JA and Lotan I (2011). Regulation of neuronal M-channel gating in an isoform-specific manner: functional interplay between calmodulin and syntaxin 1A. *J Neurosci*, 31, 14158-14171.

Fahraeus R (2005). Do peptides control their own birth and death? *Nat Rev Mol Cell Biol*, 6, 263-267.

Falkenburger BH, Jensen JB and Hille B (2010). Kinetics of PIP2 metabolism and KCNQ2/3 channel regulation studied with a voltage-sensitive phosphatase in living cells. *J Gen Physiol*, 135, 99-114.

Filippov AK, Webb TE, Barnard EA and Brown DA (1998). P2Y2 nucleotide receptors expressed heterologously in sympathetic neurons inhibit both N-type Ca2+ and M-type K+ currents. *J Neurosci*, 18, 5170-5179.

Gamper N and Shapiro MS (2003). Calmodulin mediates Ca2+-dependent modulation of M-type K+ channels. *J Gen Physiol*, 122, 17-31.

Gamper N and Shapiro MS (2007). Target-specific PIP(2) signalling: how might it work? *J Physiol*, 582, 967-975.

Gamper N, Stockand JD and Shapiro MS (2003). Subunit-specific modulation of KCNQ potassium channels by Src tyrosine kinase. *J Neurosci*, 23, 84-95.

Gamper N, Zaika O, Li Y, Martin P, Hernandez CC, Perez MR, Wang AY, Jaffe DB and Shapiro MS (2006). Oxidative modification of M-type K(+) channels as a mechanism of cytoprotective neuronal silencing. *EMBO J*, 25, 4996-5004.

Gao T, Bunemann M, Gerhardstein BL, Ma H and Hosey MM (2000). Role of the C terminus of the alpha 1C (CaV1.2) subunit in membrane targeting of cardiac L-type calcium channels. *J Biol Chem*, 275, 25436-25444.

Garrido JJ, Fernandes F, Giraud P, Mouret I, Pasqualini E, Fache MP, Jullien F and Dargent B (2001). Identification of an axonal determinant in the C-terminus of the sodium channel Na(v)1.2. *EMBO J*, 20, 5950-5961.

Garrido JJ, Giraud P, Carlier E, Fernandes F, Moussif A, Fache MP, Debanne D and Dargent B (2003). A targeting motif involved in sodium channel clustering at the axonal initial segment. *Science*, 300, 2091-2094.

Ghosh S, Nunziato DA and Pitt GS (2006). KCNQ1 assembly and function is blocked by long-QT syndrome mutations that disrupt interaction with calmodulin. *Circ Res*, 98, 1048-1054.

Gomez-Posada JC, Aivar P, Alberdi A, Alaimo A, Etxeberria A, Fernandez-Orth J, Zamalloa T, Roura-Ferrer M, Villace P, Areso P, Casis O and Villarroel A (2011). Kv7 channels can function without constitutive calmodulin tethering. *PLoS One*, 6, e25508.

Gomez-Posada JC, Etxeberria A, Roura-Ferrer M, Areso P, Masin M, Murrell-Lagnado RD and Villarroel A (2010). A pore residue of the KCNQ3 potassium M-channel subunit controls surface expression. *J Neurosci*, 30, 9316-9323.

Gubitosi-Klug RA, Mancuso DJ and Gross RW (2005). The human Kv1.1 channel is palmitoylated, modulating voltage sensing: Identification of a palmitoylation consensus sequence. *Proc Natl Acad Sci U S A*, 102, 5964-5968.

Gutman GA, Chandy KG, Grissmer S, Lazdunski M, McKinnon D, Pardo LA, Robertson GA, Rudy B, Sanguinetti MC, Stuhmer W and Wang X (2005). International Union of Pharmacology. LIII. Nomenclature and molecular relationships of voltage-gated potassium channels. *Pharmacol Rev*, 57, 473-508.

Hadley JK, Noda M, Selyanko AA, Wood IC, Abogadie FC and Brown DA (2000). Differential tetraethylammonium sensitivity of KCNQ1-4 potassium channels. *Br J Pharmacol*, 129, 413-415.

Haitin Y and Attali B (2008). The C-terminus of Kv7 channels: a multifunctional module. *J Physiol*, 586, 1803-1810.

Hamill OP, Marty A, Neher E, Sakmann B and Sigworth FJ (1981). Improved patch-clamp techniques for high-resolution current recording from cells and cell-free membrane patches. *Pflugers Arch*, 391, 85-100.

Harbury PB, Zhang T, Kim PS and Alber T (1993). A switch between two-, three-, and four-stranded coiled coils in GCN4 leucine zipper mutants. *Science*, 262, 1401-1407.

Harper JF, Cheung WY, Wallace RW, Huang HL, Levine SN and Steiner AL (1980). Localization of calmodulin in rat tissues. *Proc Natl Acad Sci U S A*, 77, 366-370.

Heidenreich M, Lechner SG, Vardanyan V, Wetzel C, Cremers CW, De Leenheer EM, Aranguez G, Moreno-Pelayo MA, Jentsch TJ and Lewin GR (2012). KCNQ4 K(+) channels tune mechanoreceptors for normal touch sensation in mouse and man. *Nat Neurosci*, 15, 138-145.

Henke G, Maier G, Wallisch S, Boehmer C and Lang F (2004). Regulation of the voltage gated K+ channel Kv1.3 by the ubiquitin ligase Nedd4-2 and the serum and glucocorticoid inducible kinase SGK1. *J Cell Physiol*, 199, 194-199.

Hernandez CC, Zaika O, Tolstykh GP and Shapiro MS (2008). Regulation of neural KCNQ channels: signalling pathways, structural motifs and functional implications. *J Physiol*, 586, 1811-1821.

Heusser K and Schwappach B (2005). Trafficking of potassium channels. *Curr Opin Neurobiol*, 15, 364-369.

Hille B, Armstrong CM and MacKinnon R (1999). Ion channels: from idea to reality. *Nat Med*, 5, 1105-1109.

Hirose S, Zenri F, Akiyoshi H, Fukuma G, Iwata H, Inoue T, Yonetani M, Tsutsumi M, Muranaka H, Kurokawa T, Hanai T, Wada K, Kaneko S and Mitsudome A (2000). A novel mutation of KCNQ3 (c.925T-->C) in a Japanese family with benign familial neonatal convulsions. *Ann Neurol*, 47, 822-826.

Horn R and Marty A (1988). Muscarinic activation of ionic currents measured by a new whole-cell recording method. *J Gen Physiol*, 92, 145-159.

Houdusse A and Cohen C (1995). Target sequence recognition by the calmodulin superfamily: implications from light chain binding to the regulatory domain of scallop myosin. *Proc Natl Acad Sci U S A*, 92, 10644-10647.

Houdusse A, Silver M and Cohen C (1996). A model of Ca(2+)-free calmodulin binding to unconventional myosins reveals how calmodulin acts as a regulatory switch. *Structure*, 4, 1475-1490.

Howard RJ, Clark KA, Holton JM and Minor DL, Jr. (2007). Structural insight into KCNQ (Kv7) channel assembly and channelopathy. *Neuron*, 53, 663-675.

Ito K, Chiba S and Pogliano K (2010). Divergent stalling sequences sense and control cellular physiology. *Biochem Biophys Res Commun*, 393, 1-5.

Jacob TC, Moss SJ and Jurd R (2008). GABA(A) receptor trafficking and its role in the dynamic modulation of neuronal inhibition. *Nat Rev Neurosci*, 9, 331-343.

Jenke M, Sanchez A, Monje F, Stuhmer W, Weseloh RM and Pardo LA (2003). C-terminal domains implicated in the functional surface expression of potassium channels. *EMBO J*, 22, 395-403.

Jenkins SM and Bennett V (2001). Ankyrin-G coordinates assembly of the spectrin-based membrane skeleton, voltage-gated sodium channels, and L1 CAMs at Purkinje neuron initial segments. *J Cell Biol*, 155, 739-746.

Jentsch TJ (2000). Neuronal KCNQ potassium channels: physiology and role in disease. *Nat Rev Neurosci*, 1, 21-30.

Jentsch TJ, Hubner CA and Fuhrmann JC (2004). Ion channels: function unravelled by dysfunction. *Nat Cell Biol*, 6, 1039-1047.

Jerng HH, Pfaffinger PJ and Covarrubias M (2004). Molecular physiology and modulation of somatodendritic A-type potassium channels. *Mol Cell Neurosci*, 27, 343-369.

Jespersen T, Grunnet M and Olesen SP (2005). The KCNQ1 potassium channel: from gene to physiological function. *Physiology (Bethesda)*, 20, 408-416.

Jia Q, Jia Z, Zhao Z, Liu B, Liang H and Zhang H (2007). Activation of epidermal growth factor receptor inhibits KCNQ2/3 current through two distinct pathways: membrane PtdIns(4,5)P2 hydrolysis and channel phosphorylation. *J Neurosci*, 27, 2503-2512.

Joiner WJ, Khanna R, Schlichter LC and Kaczmarek LK (2001). Calmodulin regulates assembly and trafficking of SK4/IK1 Ca2+-activated K+ channels. *J Biol Chem*, 276, 37980-37985.

Jurado LA, Chockalingam PS and Jarrett HW (1999). Apocalmodulin. *Physiol Rev*, 79, 661-682.

Kaupp UB and Seifert R (2002). Cyclic nucleotide-gated ion channels. *Physiol Rev*, 82, 769-824.

Kleizen B and Braakman I (2004). Protein folding and quality control in the endoplasmic reticulum. *Curr Opin Cell Biol*, 16, 343-349.

Kosolapov A and Deutsch C (2003). Folding of the voltage-gated K+ channel T1 recognition domain. *J Biol Chem*, 278, 4305-4313.

Krumerman A, Gao X, Bian JS, Melman YF, Kagan A and McDonald TV (2004). An LQT mutant minK alters KvLQT1 trafficking. *Am J Physiol Cell Physiol*, 286, C1453-1463.

Kubisch C, Schroeder BC, Friedrich T, Lutjohann B, El-Amraoui A, Marlin S, Petit C and Jentsch TJ (1999). KCNQ4, a novel potassium channel expressed in sensory outer hair cells, is mutated in dominant deafness. *Cell*, 96, 437-446.

Kullmann DM (2010). Neurological channelopathies. *Annu Rev Neurosci*, 33, 151-172.

Kullmann DM and Waxman SG (2010). Neurological channelopathies: new insights into disease mechanisms and ion channel function. *J Physiol*, 588, 1823-1827.

Leppert M, Anderson VE, Quattlebaum T, Stauffer D, O'Connell P, Nakamura Y, Lalouel JM and White R (1989). Benign familial neonatal convulsions linked to genetic markers on chromosome 20. *Nature*, 337, 647-648.

Lerche C, Scherer CR, Seebohm G, Derst C, Wei AD, Busch AE and Steinmeyer K (2000). Molecular cloning and functional expression of KCNQ5, a potassium channel subunit that may

contribute to neuronal M-current diversity. *J Biol Chem*, 275, 22395-22400.

Lerche H, Biervert C, Alekov AK, Schleithoff L, Lindner M, Klinger W, Bretschneider F, Mitrovic N, Jurkat-Rott K, Bode H, Lehmann-Horn F and Steinlein OK (1999). A reduced K+ current due to a novel mutation in KCNQ2 causes neonatal convulsions. *Ann Neurol*, 46, 305-312.

Li M, Jan YN and Jan LY (1992). Specification of subunit assembly by the hydrophilic amino-terminal domain of the Shaker potassium channel. *Science*, 257, 1225-1230.

Loew LM (2007). Where does all the PIP2 come from? *J Physiol*, 582, 945-951.

Lord JM, Davey J, Frigerio L and Roberts LM (2000). Endoplasmic reticulum-associated protein degradation. *Semin Cell Dev Biol*, 11, 159-164.

Lu J, Robinson JM, Edwards D and Deutsch C (2001). T1-T1 interactions occur in ER membranes while nascent Kv peptides are still attached to ribosomes. *Biochemistry*, 40, 10934-10946.

Lu J and Deutsch C (2008). Electrostatics in the ribosomal tunnel modulate chain elongation rates. *J Mol Biol*, 384, 73-86.

Lupas A (1996). Prediction and analysis of coiled-coil structures. *Methods Enzymol*, 266, 513-525.

Ma D and Jan LY (2002). ER transport signals and trafficking of potassium channels and receptors. *Curr Opin Neurobiol*, 12, 287-292.

Maljevic S, Lerche C, Seebohm G, Alekov AK, Busch AE and Lerche H (2003). C-terminal interaction of KCNQ2 and KCNQ3 K+ channels. *J Physiol*, 548, 353-360.

Maljevic S, Wuttke TV, Seebohm G and Lerche H (2010). KV7 channelopathies. *Pflugers Arch*, 460, 277-288.

Margeta-Mitrovic M, Mitrovic I, Riley RC, Jan LY and Basbaum AI (1999). Immunohistochemical localization of GABA(B) receptors in the rat central nervous system. *J Comp Neurol*, 405, 299-321.

Marrion NV (1997). Control of M-current. *Annu Rev Physiol*, 59, 483-504.

Marx SO, Kurokawa J, Reiken S, Motoike H, D'Armiento J, Marks AR and Kass RS (2002). Requirement of a macromolecular signaling complex for beta adrenergic receptor modulation of the KCNQ1-KCNE1 potassium channel. *Science*, 295, 496-499.

McClellan AJ, Tam S, Kaganovich D and Frydman J (2005). Protein quality control: chaperones culling corrupt conformations. *Nat Cell Biol*, 7, 736-741.

Michelsen K, Mrowiec T, Duderstadt KE, Frey S, Minor DL, Mayer MP and Schwappach B (2006). A multimeric membrane protein reveals 14-3-3 isoform specificity in forward transport in yeast. *Traffic*, 7, 903-916.

Michelsen K, Yuan H and Schwappach B (2005). Hide and run. Arginine-based endoplasmic-reticulum-sorting motifs in the assembly of heteromultimeric membrane proteins. *EMBO Rep*, 6, 717-722.

Mikosch M and Homann U (2009). How do ER export motifs work on ion channel trafficking? *Curr Opin Plant Biol*, 12, 685-689

Moore SD, Madamba SG, Joels M and Siggins GR (1988). Somatostatin augments the M-current in hippocampal neurons. *Science*, 239, 278-280.

Moulard B, Picard F, le Hellard S, Agulhon C, Weiland S, Favre I, Bertrand S, Malafosse A and Bertrand D (2001). Ion channel variation causes epilepsies. *Brain Res Brain Res Rev*, 36, 275-284.

Munns CH and Caterina MJ (2012). Tune in to KCNQ. *Nat Neurosci*, 15, 8-10.

Murata Y, Iwasaki H, Sasaki M, Inaba K and Okamura Y (2005). Phosphoinositide phosphatase activity coupled to an intrinsic voltage sensor. *Nature*, 435, 1239-1243.

Nakamura M, Watanabe H, Kubo Y, Yokoyama M, Matsumoto T, Sasai H and Nishi Y (1998). KQT2, a new putative potassium channel family produced by alternative splicing. Isolation, genomic structure, and alternative splicing of the putative potassium channels. *Receptors Channels*, 5, 255-271.

Netzer WJ and Hartl FU (1997). Recombination of protein domains facilitated by co-translational folding in eukaryotes. *Nature*, 388, 343-349.

Nissen P, Hansen J, Ban N, Moore PB and Steitz TA (2000). The structural basis of ribosome activity in peptide bond synthesis. *Science*, 289, 920-930.

Pan Z, Kao T, Horvath Z, Lemos J, Sul JY, Cranstoun SD, Bennett V, Scherer SS and Cooper EC (2006). A common ankyrin-

G-based mechanism retains KCNQ and NaV channels at electrically active domains of the axon. *J Neurosci*, 26, 2599-2613.

Pan Z, Selyanko AA, Hadley JK, Brown DA, Dixon JE and McKinnon D (2001). Alternative splicing of KCNQ2 potassium channel transcripts contributes to the functional diversity of M-currents. *J Physiol*, 531, 347-358.

Papazian DM (1999). Potassium channels: some assembly required. *Neuron*, 23, 7-10.

Papazian DM, Schwarz TL, Tempel BL, Jan YN and Jan LY (1987). Cloning of genomic and complementary DNA from Shaker, a putative potassium channel gene from Drosophila. *Science*, 237, 749-753.

Park KH, Piron J, Dahimene S, Merot J, Baro I, Escande D and Loussouarn G (2005). Impaired KCNQ1-KCNE1 and phosphatidylinositol-4,5-bisphosphate interaction underlies the long QT syndrome. *Circ Res*, 96, 730-739.

Peretz A, Degani N, Nachman R, Uziyel Y, Gibor G, Shabat D and Attali B (2005). Meclofenamic acid and diclofenac, novel templates of KCNQ2/Q3 potassium channel openers, depress cortical neuron activity and exhibit anticonvulsant properties. *Mol Pharmacol*, 67, 1053-1066.

Powell K and Zeitlin PL (2002). Therapeutic approaches to repair defects in deltaF508 CFTR folding and cellular targeting. *Adv Drug Deliv Rev*, 54, 1395-1408.

Prole DL and Marrion NV (2004). Ionic permeation and conduction properties of neuronal KCNQ2/KCNQ3 potassium channels. *Biophys J*, 86, 1454-1469.

Rechsteiner M and Rogers SW (1996). PEST sequences and regulation by proteolysis. *Trends Biochem Sci*, 21, 267-271.

Richards MC, Heron SE, Spendlove HE, Scheffer IE, Grinton B, Berkovic SF, Mulley JC and Davy A (2004). Novel mutations in the KCNQ2 gene link epilepsy to a dysfunction of the KCNQ2-calmodulin interaction. *J Med Genet*, 41, e35.

Robbins J (2001). KCNQ potassium channels: physiology, pathophysiology, and pharmacology. *Pharmacol Ther*, 90, 1-19.

Rogers S, Wells R and Rechsteiner M (1986). Amino acid sequences common to rapidly degraded proteins: the PEST hypothesis. *Science*, 234, 364-368.

Ronen GM, Rosales TO, Connolly M, Anderson VE and Leppert M (1993). Seizure characteristics in chromosome 20 benign familial neonatal convulsions. *Neurology*, 43, 1355-1360.

Roura-Ferrer M, Sole L, Martinez-Marmol R, Villalonga N and Felipe A (2008). Skeletal muscle Kv7 (KCNQ) channels in myoblast differentiation and proliferation. *Biochem Biophys Res Commun*, 369, 1094-1097.

Saimi Y and Kung C (2002). Calmodulin as an ion channel subunit. *Annu Rev Physiol*, 64, 289-311.

Sakmann B, Hamill OP and Bormann J (1983). Patch-clamp measurements of elementary chloride currents activated by the putative inhibitory transmitter GABA and glycine in mammalian spinal neurons. *J Neural Transm Suppl*, 18, 83-95.

Schmitt N, Schwarz M, Peretz A, Abitbol I, Attali B and Pongs O (2000). A recessive C-terminal Jervell and Lange-Nielsen mutation

of the KCNQ1 channel impairs subunit assembly. *EMBO J*, 19, 332-340.

Schroeder BC, Hechenberger M, Weinreich F, Kubisch C and Jentsch TJ (2000). KCNQ5, a novel potassium channel broadly expressed in brain, mediates M-type currents. *J Biol Chem*, 275, 24089-24095.

Schroeder BC, Kubisch C, Stein V and Jentsch TJ (1998). Moderate loss of function of cyclic-AMP-modulated KCNQ2/KCNQ3 K+ channels causes epilepsy. *Nature*, 396, 687-690.

Schwake M, Athanasiadu D, Beimgraben C, Blanz J, Beck C, Jentsch TJ, Saftig P and Friedrich T (2006). Structural determinants of M-type KCNQ (Kv7) K+ channel assembly. *J Neurosci*, 26, 3757-3766.

Schwake M, Jentsch TJ and Friedrich T (2003). A carboxy-terminal domain determines the subunit specificity of KCNQ K+ channel assembly. *EMBO Rep*, 4, 76-81.

Schwake M, Pusch M, Kharkovets T and Jentsch TJ (2000). Surface expression and single channel properties of KCNQ2/KCNQ3, M-type K+ channels involved in epilepsy. *J Biol Chem*, 275, 13343-13348.

Schweitzer P, Madamba S, Champagnat J and Siggins GR (1993). Somatostatin inhibition of hippocampal CA1 pyramidal neurons: mediation by arachidonic acid and its metabolites. *J Neurosci*, 13, 2033-2049.

Schweitzer P, Madamba S and Siggins GR (1990). Arachidonic acid metabolites as mediators of somatostatin-induced increase of neuronal M-current. *Nature*, 346, 464-467.

Scott DB, Blanpied TA, Swanson GT, Zhang C and Ehlers MD (2001). An NMDA receptor ER retention signal regulated by phosphorylation and alternative splicing. *J Neurosci*, 21, 3063-3072.

Scott DB, Michailidis I, Mu Y, Logothetis D and Ehlers MD (2004). Endocytosis and degradative sorting of NMDA receptors by conserved membrane-proximal signals. *J Neurosci*, 24, 7096-7109.

Selyanko AA, Hadley JK, Wood IC, Abogadie FC, Jentsch TJ and Brown DA (2000). Inhibition of KCNQ1-4 potassium channels expressed in mammalian cells via M1 muscarinic acetylcholine receptors. *J Physiol*, 522 Pt 3, 349-355.

Shamgar L, Ma L, Schmitt N, Haitin Y, Peretz A, Wiener R, Hirsch J, Pongs O and Attali B (2006). Calmodulin is essential for cardiac IKS channel gating and assembly: impaired function in long-QT mutations. *Circ Res*, 98, 1055-1063.

Shieh CC, Coghlan M, Sullivan JP and Gopalakrishnan M (2000). Potassium channels: molecular defects, diseases, and therapeutic opportunities. *Pharmacol Rev*, 52, 557-594.

Singh NA, Charlier C, Stauffer D, DuPont BR, Leach RJ, Melis R, Ronen GM, Bjerre I, Quattlebaum T, Murphy JV, McHarg ML, Gagnon D, Rosales TO, Peiffer A, Anderson VE and Leppert M (1998). A novel potassium channel gene, KCNQ2, is mutated in an inherited epilepsy of newborns. *Nat Genet*, 18, 25-29.

Sivaprasadarao A, Taneja TK, Mankouri J and Smith AJ (2007). Trafficking of ATP-sensitive potassium channels in health and disease. *Biochem Soc Trans*, 35, 1055-1059.

Smith JS, Iannotti CA, Dargis P, Christian EP and Aiyar J (2001). Differential expression of kcnq2 splice variants: implications to m

current function during neuronal development. *J Neurosci*, 21, 1096-1103.

Soldovieri MV, Castaldo P, Iodice L, Miceli F, Barrese V, Bellini G, Miraglia del Giudice E, Pascotto A, Bonatti S, Annunziato L and Taglialatela M (2006). Decreased subunit stability as a novel mechanism for potassium current impairment by a KCNQ2 C terminus mutation causing benign familial neonatal convulsions. *J Biol Chem*, 281, 418-428.

Srinivasan Y, Lewallen M and Angelides KJ (1992). Mapping the binding site on ankyrin for the voltage-dependent sodium channel from brain. *J Biol Chem*, 267, 7483-7489.

Standley S, Roche KW, McCallum J, Sans N and Wenthold RJ (2000). PDZ domain suppression of an ER retention signal in NMDA receptor NR1 splice variants. *Neuron*, 28, 887-898.

Steele DF, Eldstrom J and Fedida D (2007). Mechanisms of cardiac potassium channel trafficking. *J Physiol*, 582, 17-26.

Stewart AP, Gomez-Posada JC, McGeorge J, Rouhani MJ, Villarroel A, Murrell-Lagnado RD and Edwardson JM (2012). The Kv7.2/Kv7.3 heterotetramer assembles with a random subunit arrangement. *J Biol Chem*.

Su J, Cao X and Wang K (2011). A novel degradation signal derived from distal C-terminal frameshift mutations of KCNQ2 protein which cause neonatal epilepsy. *J Biol Chem*, 286, 42949-42958.

Suh BC and Hille B (2002). Recovery from muscarinic modulation of M current channels requires phosphatidylinositol 4,5-bisphosphate synthesis. *Neuron*, 35, 507-520.

Suh BC and Hille B (2007). Regulation of KCNQ channels by manipulation of phosphoinositides. *J Physiol*, 582, 911-916.

Teasdale RD and Jackson MR (1996). Signal-mediated sorting of membrane proteins between the endoplasmic reticulum and the golgi apparatus. *Annu Rev Cell Dev Biol*, 12, 27-54.

Telezhkin V, Reilly JM, Thomas AM, Tinker A and Brown DA (2012). Structural requirements of membrane phospholipids for M-type potassium channel activation and binding. *J Biol Chem*.

Tenson T and Ehrenberg M (2002). Regulatory nascent peptides in the ribosomal tunnel. *Cell*, 108, 591-594.

Tinel N, Diochot S, Lauritzen I, Barhanin J, Lazdunski M and Borsotto M (2000). M-type KCNQ2-KCNQ3 potassium channels are modulated by the KCNE2 subunit. *FEBS Lett*, 480, 137-141.

Tinel N, Lauritzen I, Chouabe C, Lazdunski M and Borsotto M (1998). The KCNQ2 potassium channel: splice variants, functional and developmental expression. Brain localization and comparison with KCNQ3. *FEBS Lett*, 438, 171-176.

Tran QK, Black DJ and Persechini A (2003). Intracellular coupling via limiting calmodulin. *J Biol Chem*, 278, 24247-24250.

Tsui LC (1992). The spectrum of cystic fibrosis mutations. *Trends Genet*, 8, 392-398.

Tu L and Deutsch C (1999). Evidence for dimerization of dimers in K+ channel assembly. *Biophys J*, 76, 2004-2017.

Ullrich S, Su J, Ranta F, Wittekindt OH, Ris F, Rosler M, Gerlach U, Heitzmann D, Warth R and Lang F (2005). Effects of I(Ks) channel inhibitors in insulin-secreting INS-1 cells. *Pflugers Arch*, 451, 428-436.

Unoki H, Takahashi A, Kawaguchi T, Hara K, Horikoshi M, Andersen G, Ng DP, Holmkvist J, Borch-Johnsen K, Jorgensen T, Sandbaek A, Lauritzen T, Hansen T, Nurbaya S, Tsunoda T, Kubo M, Babazono T, Hirose H, Hayashi M, Iwamoto Y, Kashiwagi A, Kaku K, Kawamori R, Tai ES, Pedersen O, Kamatani N, Kadowaki T, Kikkawa R, Nakamura Y and Maeda S (2008). SNPs in KCNQ1 are associated with susceptibility to type 2 diabetes in East Asian and European populations. *Nat Genet*, 40, 1098-1102.

Volkers L, Rook MB, Das JH, Verbeek NE, Groenewegen WA, van Kempen MJ, Lindhout D and Koeleman BP (2009). Functional analysis of novel KCNQ2 mutations found in patients with Benign Familial Neonatal Convulsions. *Neurosci Lett*, 462, 24-29.

Wang HS, Pan Z, Shi W, Brown BS, Wymore RS, Cohen IS, Dixon JE and McKinnon D (1998). KCNQ2 and KCNQ3 potassium channel subunits: molecular correlates of the M-channel. *Science*, 282, 1890-1893.

Wang Q, Curran ME, Splawski I, Burn TC, Millholland JM, VanRaay TJ, Shen J, Timothy KW, Vincent GM, de Jager T, Schwartz PJ, Toubin JA, Moss AJ, Atkinson DL, Landes GM, Connors TD and Keating MT (1996). Positional cloning of a novel potassium channel gene: KVLQT1 mutations cause cardiac arrhythmias. *Nat Genet*, 12, 17-23.

Watanabe H, Nagata E, Kosakai A, Nakamura M, Yokoyama M, Tanaka K and Sasai H (2000). Disruption of the epilepsy KCNQ2 gene results in neural hyperexcitability. *J Neurochem*, 75, 28-33.

Wehling C, Beimgraben C, Gelhaus C, Friedrich T, Saftig P, Grotzinger J and Schwake M (2007). Self-assembly of the isolated KCNQ2 subunit interaction domain. *FEBS Lett*, 581, 1594-1598.

Wen H and Levitan IB (2002). Calmodulin is an auxiliary subunit of KCNQ2/3 potassium channels. *J Neurosci*, 22, 7991-8001.

Wiener R, Haitin Y, Shamgar L, Fernandez-Alonso MC, Martos A, Chomsky-Hecht O, Rivas G, Attali B and Hirsch JA (2008). The KCNQ1 (Kv7.1) COOH terminus, a multitiered scaffold for subunit assembly and protein interaction. *J Biol Chem*, 283, 5815-5830.

Wittig I, Braun HP and Schagger H (2006). Blue native PAGE. *Nat Protoc*, 1, 418-428.

Wuttke TV, Jurkat-Rott K, Paulus W, Garncarek M, Lehmann-Horn F and Lerche H (2007). Peripheral nerve hyperexcitability due to dominant-negative KCNQ2 mutations. *Neurology*, 69, 2045-2053.

Wuttke TV, Penzien J, Fauler M, Seebohm G, Lehmann-Horn F, Lerche H and Jurkat-Rott K (2008). Neutralization of a negative charge in the S1-S2 region of the KV7.2 (KCNQ2) channel affects voltage-dependent activation in neonatal epilepsy. *J Physiol*, 586, 545-555.

Yang WP, Levesque PC, Little WA, Conder ML, Ramakrishnan P, Neubauer MG and Blanar MA (1998). Functional expression of two KvLQT1-related potassium channels responsible for an inherited idiopathic epilepsy. *J Biol Chem*, 273, 19419-19423.

Yuan H, Michelsen K and Schwappach B (2003). 14-3-3 dimers probe the assembly status of multimeric membrane proteins. *Curr Biol*, 13, 638-646.

Yus-Najera E, Santana-Castro I and Villarroel A (2002). The identification and characterization of a noncontinuous calmodulin-binding site in noninactivating voltage-dependent KCNQ potassium channels. *J Biol Chem*, 277, 28545-28553.

Zaczek R, Chorvat RJ, Saye JA, Pierdomenico ME, Maciag CM, Logue AR, Fisher BN, Rominger DH and Earl RA (1998). Two new potent neurotransmitter release enhancers, 10,10-bis(4-pyridinylmethyl)-9(10H)-anthracenone and 10,10-bis(2-fluoro-4-pyridinylmethyl)-9(10H)-anthracenone: comparison to linopirdine. *J Pharmacol Exp Ther*, 285, 724-730.

Zaika O, Lara LS, Gamper N, Hilgemann DW, Jaffe DB and Shapiro MS (2006). Angiotensin II regulates neuronal excitability via phosphatidylinositol 4,5-bisphosphate-dependent modulation of Kv7 (M-type) K+ channels. *J Physiol*, 575, 49-67.

Zerangue N, Jan YN and Jan LY (2000). An artificial tetramerization domain restores efficient assembly of functional Shaker channels lacking T1. *Proc Natl Acad Sci U S A*, 97, 3591-3595.

Zerangue N, Malan MJ, Fried SR, Dazin PF, Jan YN, Jan LY and Schwappach B (2001). Analysis of endoplasmic reticulum trafficking signals by combinatorial screening in mammalian cells. *Proc Natl Acad Sci U S A*, 98, 2431-2436.

Zhang H, Craciun LC, Mirshahi T, Rohacs T, Lopes CM, Jin T and Logothetis DE (2003). PIP(2) activates KCNQ channels, and its hydrolysis underlies receptor-mediated inhibition of M currents. *Neuron*, 37, 963-975.

Zhu J, Watanabe I, Gomez B and Thornhill WB (2001). Determinants involved in Kv1 potassium channel folding in the endoplasmic reticulum, glycosylation in the Golgi, and cell surface expression. *J Biol Chem*, 276, 39419-39427.

PUBLICATIONS

Publications

Gómez-Posada JC, Aivar P, Alberdi A, Alaimo A, Etxeberria A, **Fernández-Orth J**, Zamalloa T, Roura-Ferrer M, Villace P, Areso P, Casis O and Villarroel A (2011). Kv7 channels can function without constitutive calmodulin tethering. *PLoS One*, 6, e25508.

In press

Aivar P*, **Fernández-Orth J***, Gomis-Perez C, Alberdi A, Alaimo A, Rodríguez MS, Giraldez T, Miranda P, Areso P and Villarroel A. (2012). Surface expression and subunit specific control of steady-state protein levels by the Kv7.2 Helix A-B linker. *PLoS One.*

* These authors contributed equally to this work.

Submitted

Alaimo A*, Alberdi A*, Gomis-Perez C*, **Fernández-Orth J**, Gómez-Posada JC, Areso P and Villarroel A. Cooperativity between calmodulin binding sites in Kv7.2 channels.

* These authors contributed equally to this work.

APPENDIX

Appendix

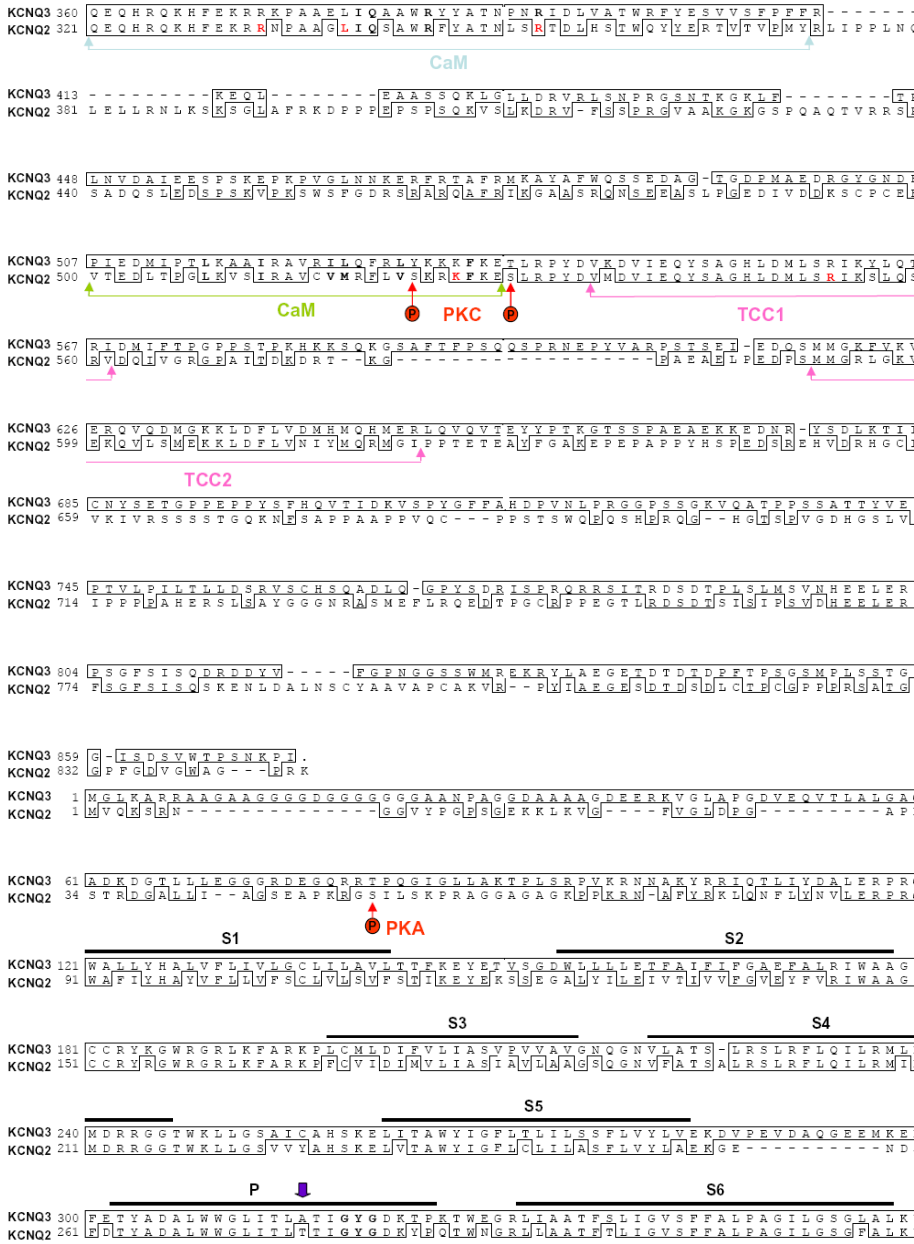

pGEM- Easy T

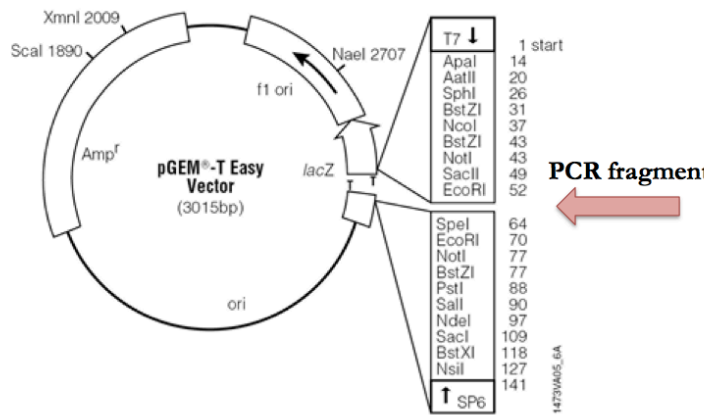

KCNQ2-HA en pSRC5

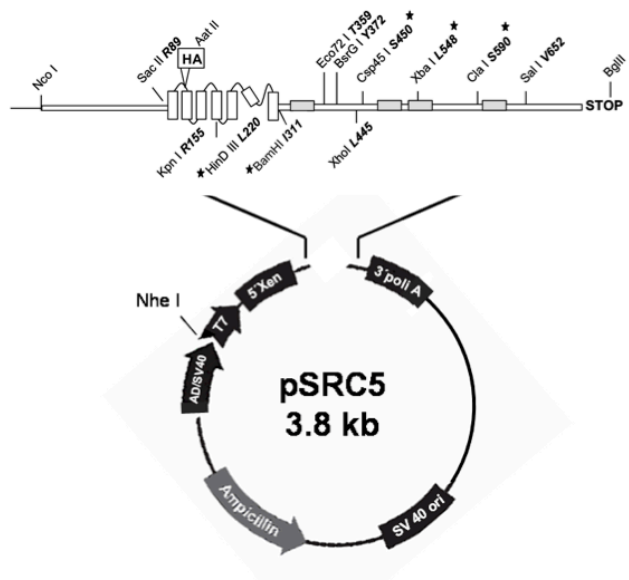

mCer-KCNQ2-2HA en pcDNA3.1

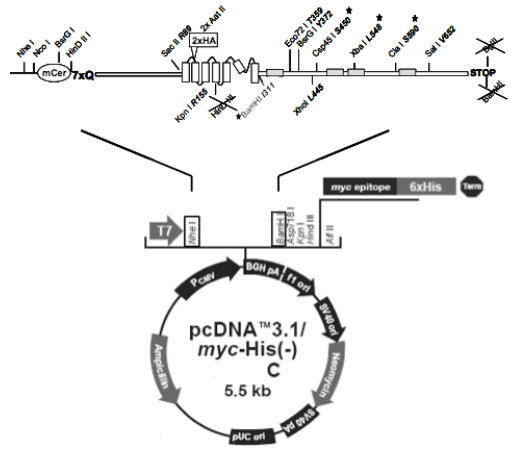

Tac-CFP

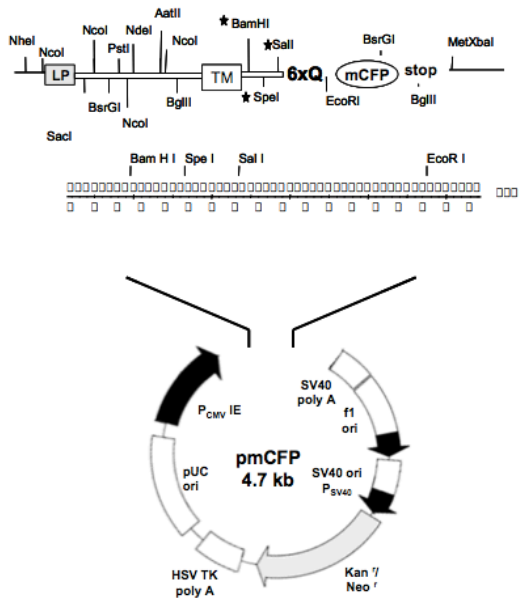
NheI
NcoI
NcoI
NdeI
PstI
AatII
NcoI
BamHI
SalI
BsrGI
MetXbaI
LP
TM
6xQ
mCFP
stop
BsrGI
EcoRI
BglII
SpeI
BglII
NcoI
SacI
Bam H I
Spe I
Sal I
EcoR I
SV40
poly A
f1
ori
P CMV IE
pmCFP
4.7 kb
pUC
ori
SV40 ori
P SV40
HSV TK
poly A
Kan r/
Neo r